



UNIVERSITEIT•STELLENBOSCH•UNIVERSITY
jou kennisvenoot • your knowledge partner

Modelling, simulation and optimization of a solarised combined cycle with storage (SUNSPOT) with a focus on the configuration and control strategy.

Jan-Louis Janse van Vuuren

Assignment presented in partial fulfilment of the requirements for the degree of
Master of Engineering (Mechanical) in the Faculty of Engineering at
Stellenbosch University

Supervisor: Prof F. Dinter

Co-Supervisor: Prof T.W. von Backström

March 2018



Departement Meganiese en Megatroniese Ingenieurswese
Department of Mechanical and Mechatronic Engineering



DECLARATION

By submitting this assignment electronically, I declare that the entirety of the work contained therein is my own, original work, that I am the sole author thereof (save to the extent explicitly otherwise stated), that reproduction and publication thereof by Stellenbosch University will not infringe any third-party rights and that I have not previously in its entirety or in part submitted it for obtaining any qualification.

Date: 2017/11/24

A handwritten signature in black ink, appearing to be 'J. van der Merwe', written in a cursive style.

Copyright © 2018 Stellenbosch University

All rights reserved



UNIVERSITEIT • STELLENBOSCH • UNIVERSITY
jou kennisvennoot • your knowledge partner

Plagiaatverklaring / Plagiarism Declaration

- 1 Plagiaat is die oorneem en gebruik van die idees, materiaal en ander intellektuele eiendom van ander persone asof dit jou eie werk is.
Plagiarism is the use of ideas, material and other intellectual property of another's work and to present it as my own.
- 2 Ek erken dat die pleeg van plagiaat 'n strafbare oortreding is aangesien dit 'n vorm van diefstal is.
I agree that plagiarism is a punishable offence because it constitutes theft.
- 3 Ek verstaan ook dat direkte vertalings plagiaat is.
I also understand that direct translations are plagiarism.
- 4 Dienooreenkomstig is alle aanhalings en bydraes vanuit enige bron (ingesluit die internet) volledig verwys (erken). Ek erken dat die woordelike aanhaal van teks sonder aanhalingstekens (selfs al word die bron volledig erken) plagiaat is.
Accordingly, all quotations and contributions from any source whatsoever (including the internet) have been cited fully. I understand that the reproduction of text without quotation marks (even when the source is cited) is plagiarism.
- 5 Ek verklaar dat die werk in hierdie skryfstuk vervat, behalwe waar anders aangedui, my eie oorspronklike werk is en dat ek dit nie vantevore in die geheel of gedeeltelik ingehandig het vir bepunting in hierdie module/werkstuk of 'n ander module/werkstuk nie.
I declare that the work contained in this assignment, except where otherwise stated, is my original work and that I have not previously (in its entirety or in part) submitted it for grading in this module/assignment or another module/assignment.

16988477	
Studentenommer / Student number	Handtekening / Signature
J Janse van Vuuren	2017/11/24
Voorletters en van / Initials and surname	Datum / Date

Abstract

The Stellenbosch University Solar Power Thermodynamic (SUNSPOT) cycle is regarded as a viable solution to the current energy demand in South Africa. Solarised combined cycles with thermal energy storage results in lower carbon intensive energy production and a greater electricity dispatch ability. This study shows how the SUNSPOT cycle improves on conventional combined cycle technology. This is done by modelling and analysing the components individually and considering how the configuration of the SUNSPOT elements affect the resulting energy output and associated costs of implementation.

Two 4.6 MW Mercury 50TM gas turbines are combined with the 6 MW SST-060TM steam turbine to form the base combined cycle with which the SUNSPOT is compared. Analytical formulations are implemented for off-design operation and validated using the results from other simulation tools. The combined cycle thermal efficiency with these two components at design point is low (41.3 %). This is explained by the lack of optimisation and low design point thermal efficiencies of both the gas and steam turbines. The solar receivers applicable are researched and modelled along with the typical solar resource, optics and collection analysis. Validated high-level models for the high-pressure central air receiver and thermal rock bed storage are used to determine the design point parameters and performance. Annual transient simulations showed that the addition of thermal storage not only changed the way the plant is operated, but also increased the thermal efficiency of the plant. This is due to the steam turbine operation throughout the cooler parts of the day resulting in lower condensing pressures. When comparing the SUNSPOT cycle with the solar retrofitted combined cycle the thermal efficiency increased with 0.67 %. The SUNSPOT cycle showed up to 40 % drop in fuel consumption when compared with the combined cycle. A solar multiple of two gives a high solar fraction and fuel efficiency while maintaining the annual solar efficiency above 20 %. The cycles are compared on a thermo-economic basis. It is found that the operational expenditure of the SUNSPOT cycle did not decrease as much as expected. Even though the fuel consumption dropped significantly it is shown that the SUNSPOT cycle requires more technicians in the field and control operators therefore increasing the annual operational costs. At a solar multiple of two the SUNSPOT cycle resulted in a levelized cost of electricity of 2.12 R/kWh which compares well with other concentrated solar power technologies as given in the revised Integrated Resource Plan of 2016.

The research in this study showed that the SUNSPOT cycle could provide a competitive edge in the energy market given the maturation of components such as the thermal rock bed storage, central receiver systems, high-pressure air receivers and solarised gas turbines. It is also recommended that the SUNSPOT cycle should be modelled on a larger scale to make use of higher combined cycle efficiencies and to make a fair comparison between the SUNSPOT cycle and current operational concentrated solar power technologies.

Uittreksel

Die “Stellenbosch University Solar Power Thermodynamic” (SUNSPOT) kringloop word beskou as ‘n lewensvatbare oplossing vir die huidige energie tekort in Suid-Afrika. Hierdie studie wys hoe die SUNSPOT kringloop op die gewone gekombineerde kringloop verbeter. Die benutting van sonkrag en ‘n termiese warmtestoor lei tot ‘n laer koolstof energie produksie en hoër elektrisiteits versendings vermoë. Die individuele komponente is gemodelleer en analiseer om sodoende die gesamentlike effek van die SUNSPOT kringloop te bepaal op ‘n energie uitset basis sowel as die kostes verbonde aan implimentering.

Die vergelykende gekombineerde kringloop bestaan uit twee 4.6 MW Mercury 50TM gasturbines en ‘n 6 MW SST-060TM stoomturbine. Analitiese modelle word gebruik om hierdie komponente se gedrag oor ‘n reeks van toestande te simuleer. Die modelle is geverifieer met behulp van data beskikbaar vanaf ander simulasië programme. Die termiese doeltreffendheid van die gekombineerde kringloop met hierdie spesifieke komponente is redelik laag (41.3 %). Dit is as gevolg van ‘n lae ontwerp punt doeltreffendheid van beide komponente en ‘n ongeoptimaliseerde ontwerp. Die verskeie warmte ontvangers, straal versamelaars en die optiese toepassing van sonkrag is nagevors en gemodelleer. Om die ontwerp punt parameters en optrede te bepaal is hoë vlak modelle vir die hoë druk sentrale lug ontvanger en termiese rots warmtestoor gebruik. Jaarlikse verbygaande simulasië het gewys dat die warmtestoor gebruik kan word om die operasionele strategie te verander en het so ook tot hoër termiese doeltreffendheid gelei. Dit is as gevolg van die stoomturbine wat deur die kouer dele van die dag krag opwek en sodoende van ‘n laer kondenseringsdruk gebruik maak. In vergelyking met die gekombineerde kringloop wat slegs uitgele is met sonkrag het die SUNSPOT kringloop ook gewys om termiese doeltreffendheid met 0.67 % te lig. Die SUNSPOT kringloop gebruik 40 % minder brandstof as die gekombineerde kringloop alleen. ‘n Sonkrag veelvoud van twee lewer die hoogste sonkrag breuk en brandstof doeltreffendheid sonder dat die sonkrag doeltreffendheid onder 20 % val. ‘n Termiese-ekonomiese ondersoek is uitgevoer op die stelsels. Daar is gevind dat die SUNSPOT kringloop nie die operasionele kostes bestendig verlaag het nie. Na verdere analise is gesien dat bykomende kostes vir tegniese personeel die kostes van brandstof gespaar versag. Die SUNSPOT kringloop met ‘n sonkrag veelvoud van twee lei tot ‘n gelykmakende koste van elektrisiteit van 2.12 R/kWh. In vergelyking met die hersiene “Integrated Resource Plan” (2016) is daar gevind dat die SUNSPOT egter kan kompeteer met huidige gekonsentreerde sonkrag tegnologie in Suid-Afrika.

Dit is dus gevind dat die SUNSPOT kringloop ‘n kompeterende oplossing in die huidige energie mark kan wees indien die komponente soos die termiese rots stoor, sentrale ontvanger sisteme, hoë druk lug ontvangers en sonkrag gasturbines tot volwassenheid ontwikkel. Daar word voorgestel dat die SUNSPOT kringloop op ‘n groter skaal gemodelleer word sodat billike vergelykings gemaak kan word met die gekonsentreerde sonkrag wat huidig in Suid-Afrika toegepas word.

Acknowledgements

I would like to honour the following individuals and organisations for their sacrifices and support throughout the course of my research:

Prof Frank Dinter, my supervisor, for his wisdom, guidance and ever open door,

Prof Theo von Backström, my co-supervisor, for his advice, technical knowledge and professional writing guidance,

Prof Wikus van Niekerk and the Centre for Renewable and Sustainable Energy Studies for funding my entire master's program,

Prof Hanno Reuter for initialising this study and all the inspiring conversations during the first parts of it,

Dr Matti Lubkoll, Dr Lukas Heller, Henk Laubscher, JC Nel and the rest of K419 for helpful discussions and solutions,

The Solar Thermal Energy Research Group for the networking opportunities and academic support,

My family and friends for their sacrificial love, endless encouragement and unfaltering faith,

Louis Karsten for his friendship, accountability and resolve as my desk partner,

and Jesus Christ, my Lord and Saviour, through Whom all things are possible.

Dedication

*Again Jesus spoke to them, saying, “I am the **light** of the world. Whoever follows me will not walk in darkness, but will have the light of life.” John 8:12 (ESV®)*

Table of contents

	Page
Abstract	iii
Uittreksel	iv
Dedication	vi
Acknowledgements	v
Table of contents	vii
List of figures	x
List of tables	xii
Nomenclature	xiii
1 Introduction	1
1.1 Background	1
1.2 The SUNSPOT cycle	2
1.3 Objectives.....	3
1.3.1 Modelling and simulation of a combined cycle power plant	3
1.3.2 Modelling and simulation of the solar components and thermal storage.....	3
1.3.3 Analysis of various application approaches to represent the SUNSPOT cycle or its variations	3
1.4 Methodology	4
1.4.1 Literature study.....	4
1.4.2 Model, simulate and validate the combined cycle, solar and thermal storage components	4
1.4.3 Integration from combined cycle to sunspot cycle.....	4
1.4.4 Final evaluation and documentation of findings	5
1.5 Motivation	5
1.5.1 The case for solar thermal energy and the SUNSPOT cycle.....	5
1.5.2 CSP: Peaking and load following solution.....	5
1.5.3 The motivation for a high-level model of the SUNSPOT cycle ..	6
2 Solarised combined cycles	7
3 Conventional combined cycle plant	11
3.1 Concepts and selection criteria.....	12
3.2 Rankine cycle	13

3.2.1	Steam turbine.....	14
3.2.2	Deaerator and condenser	15
3.2.3	Pump	17
3.2.4	Heat recovery steam generator	17
3.3	Brayton cycle.....	19
3.3.1	Compressor.....	20
3.3.2	Combustor	21
3.3.3	Turbine	23
3.3.4	Generator	26
3.3.5	Recuperator.....	26
3.3.6	Characteristic curves for the compressor/turbine combination	27
4	Model description of solar components and thermal storage.....	30
4.1	General solar resource, optics and collection principles	30
4.1.1	Energy available from the sun	30
4.1.2	Solar angles	31
4.1.3	Other collection principles and challenges.....	33
4.2	Collector: Heliostat field and tower	35
4.3	Central receiver system: Pressurised air receiver.....	36
4.4	Thermal storage: Packed rock-bed storage	38
5	Thermo-economic considerations.....	40
5.1	CAPEX.....	40
5.2	OPEX	42
5.2.1	Power block and equipment repair costs	42
5.2.2	Labour costs.....	42
5.2.3	Fuel costs	43
5.2.4	Water usage	43
6	Design criteria and validation of components.....	44
6.1	Site selection	44
6.2	Power block selection and integration	45
6.2.1	Validation of gas turbine model	46
6.2.2	Validation of steam turbine and HRSG models	47
6.3	Central receiver	48
6.4	Rock bed thermal storage	49
7	Off-design considerations.....	50
8	Configuration and dynamic simulation criteria for SUNSPOT cycle	53
8.1	Configuration details	53
8.2	Transient simulation details.....	53
8.2.1	Thermal inertia of steam turbine	53
8.2.2	Thermal inertia of gas turbine	53

8.2.3	Thermal inertia of receiver and piping system	54
8.2.4	Operating strategy	54
8.2.5	Balance over solar receiver	54
9	Results and discussion	55
9.1	Steady state models	55
9.2	Dynamic simulations	55
9.2.1	Solar multiple of SUNSPOT cycle system evaluation	56
9.2.2	Configuration analysis	56
9.3	Thermo-economic evaluation	57
10	Conclusions and recommendations.....	59
	References.....	61
	Appendix A: Location selection process: SMART and AHP criteria.....	67
A.1	SMART	67
A.2	AHP	68
	Appendix B: Comparative data, figures and tables.....	69
B.1	Gas turbine validation data	69
B.2	Steam turbine validation data.....	70
	Appendix C: Simulation flow diagrams.....	71
C.1	Brayton cycle simulation	71
C.2	Rankine cycle simulation	72
C.3	Annual simulation	73
	Appendix D: Solar multiple selection.....	76
	Appendix E: Operating strategy	77
	Appendix F: Thermal efficiency of combined cycle	78
	Appendix G: Typical outputs.....	79
	Appendix H: CAPEX composition of different configurations	83

List of figures

	Page
Figure 1: Stellenbosch University Solar Power Thermodynamic cycle by Kröger (2012).....	3
Figure 2: Sub-components and mass flow of the hybrid solar gas-turbine unit (Spelling, 2013).....	7
Figure 3: Simple gas-turbine combined with storage investigated by Spelling (2013).....	8
Figure 4: Bottoming cycle steam turbine, HRSG and condenser setup investigated by Spelling (2013).....	9
Figure 5: Solarised Rankine cycle configuration proposed by Nel (2014).....	10
Figure 6: Solarised Brayton cycle configuration proposed by Nel (2014).....	10
Figure 7: Solarised combined cycle configuration proposed by Nel (2014).....	10
Figure 8: Non-solar operation of Nel's (2014) combined cycle plant.....	10
Figure 9: Simple Rankine cycle (Cengel and Boles, 2015).....	14
Figure 10: Entropy temperature diagram for an ideal simple Rankine cycle (Cengel and Boles, 2015).....	14
Figure 11: Simple Brayton closed cycle (Cengel and Boles, 2015).....	19
Figure 12: Entropy temperature diagram for an ideal simple Brayton closed cycle (Cengel and Boles, 2015).....	19
Figure 13: Entropy and temperature diagram for stagnation states during a compression process (Cohen et al., 1987).....	25
Figure 14: The cosine effect (adapted from Stine and Geyer, 2001).....	31
Figure 15: Declination, hour and latitude angle representation by Stine and Geyer (2001).....	32
Figure 16: The conservation of etendue by Spelling (2013).....	34
Figure 17: Concentration ratios required for reaching various absorption temperatures (Roldán Serrano, 2017).....	35
Figure 18: South African maps showing (clockwise from the top left) the locations of proposed sites and gas supplies, irradiation, the national electricity gridline and elevation.....	44
Figure 19: Matlab simulation results compared with validation data.....	47
Figure 20: Validation of steam turbine simulation results compared with data from Wagner and Gilmer (2011).	48
Figure 21: Validation of "Black Box" models for gas turbine output	50

Figure 22: Validation of "Black Box" models for steam turbine output	52
Figure 23: Screening curves implemented by the IRP (2016) for various renewable technologies	58
Figure 24: Value tree for site selection process	67
Figure 25: Ushyne (2008) gas turbine simulation results using IpsePro™	69
Figure 26: Wagner and Gilman (2011) SAM simulation's result with which this study's simulation is compared with.....	70
Figure 27: Flow chart of steady state Brayton cycle simulation.....	71
Figure 28: Flow chart of steady state Rankine cycle simulation	72
Figure 29: Flow chart of annual plant simulation.....	73
Figure 30: Flowchart representing the gas turbine only state of operation	74
Figure 31: Flowchart representing the combined cycle state of operation	75
Figure 32: Flowchart representing the steam turbine only state of operation	75
Figure 33: Solar multiple evaluation for SUNSPOT cycle.....	76
Figure 34: Operating strategy of the SUNSPOT cycle.....	77
Figure 35: Thermal efficiency of combined cycle.....	78
Figure 36: A typical three-day summer output for the solar hybrid combined cycle	79
Figure 37: A typical three-day winter output for the solar hybrid combined cycle	80
Figure 38: A typical three-day summer output for the SUNSPOT cycle	81
Figure 39: A typical three-day winter output for the SUNSPOT cycle.....	82
Figure 40: CAPEX breakdown of each plant	83

List of tables

	Page
Table 1: Thermodynamic comparison of gas turbine, steam turbine and combined-cycle processes	12
Table 2: Specific cost estimates for components of the SUNSPOT cycle	41
Table 3: Labour costs transposed to 2017, adjusted from Spelling (2013)	43
Table 4: Site specific parameters	45
Table 5: HRSG design point parameters	46
Table 6: Design point parameters for the Mercury 50 TM	47
Table 7: Design point parameters for SST-060	48
Table 8: Annual simulation results for the SUNSPOT cycle operating at different solar multiples	56
Table 9: Annual simulation results for the different component configurations ...	57
Table 10: Summary of the thermo-economic performance for the SUNSPOT cycle at different solar multiples	57
Table 11: Summary of the thermo-economic performance of the different configurations	58
Table 12: SMART site selection table	67
Table 13: Example for AHP: Altitude comparison	68

Nomenclature

Abbreviations

AM	Air-to-mass ratio
AHP	Analytical hierarchy process
CAPEX	Capital expenditure
CC	Combined cycle
CCPP	Combined cycle power plant
CPC	Compound parabolic concentrator
CR	Concentration ratio
CRS	Central receiver system
crf	Charge rate (fixed)
CSP	Concentrated solar power
DNI	Direct normal irradiance
EOT	Equation of time
EPC	Engineering, procurement and construction
GHI	Global horizontal irradiance
GIS	Geographic information system
HP	High-pressure
HRSG	Heat recovery steam generator
HS	Heliostat
HTF	Heat transfer fluid
IP	Intermediate-pressure
ISCC	Integrated solar combined cycle
IRP	Integrated resource plan
ITD	Initial temperature difference
LC	Longitudinal correction
LCOE	Levelized cost of electricity
LCT	Local clock time
LHV	Lower heating value
MCDA	Multi criteria decision analysis
MS	Marshall and Swift
NTU	Number of transfer units
O&M	Operations and management
OPEX	Operational expenditure
PB	Power block
ppb	Parts per billion
PV	Photovoltaic
SAM	System advisory model
SCF	Solar collector field
SF	Solar field
SMART	Simple attribute rating technique
SUNSPOT	Stellenbosch University solar power thermodynamic
TESS	Thermal energy storage system

TIT	Turbine inlet temperature
USD	United States dollar

Symbols

c	Zhang and Kai constant
d	Diameter
E	Energy
f	Fuel fraction/frequency
h	Enthalpy
I	Irradiance
k	Specific heat ratio
M	Mass flux
m	Zhang and Kai constant
\dot{m}	Mass flow rate
N	Number of days
P	Pressure
Q	Heat
R	Gas constant
r	Fan compression ratio
T	Temperature

Greek Symbols

α	Absorptance
α_r	Rotational speed ratio
γ	Specific heat
Δf	Fractional pressure drop
δ	Declination angle
ε	Emittance
ϵ	Void fraction
η	Efficiency
θ	Angle
Π	Pressure ratio
σ	Stefan-Boltzmann constant
φ	Mass flow coefficient
ω	Hour angle

Superscripts

<i>Inlet</i>	Inlet
--------------	-------

Subscripts

a	Aperture
abs	Absorbed

<i>air</i>	Air
<i>amb</i>	Ambient
<i>available</i>	Available
<i>avg</i>	Average
<i>block</i>	Blocking
<i>carnot</i>	Carnot
<i>civil</i>	Civil
<i>clean</i>	Cleanliness
<i>cond</i>	Condenser
<i>conv</i>	Convection
<i>comb</i>	Combustor
<i>comp</i>	Compressor
<i>cor</i>	Corrected
<i>cos</i>	Cosine
<i>cs</i>	Controlled surface
<i>db</i>	Dry bulb
<i>dp</i>	Design point
<i>ec</i>	Economiser
<i>ev</i>	Evaporator
<i>exh</i>	Exhaust
<i>fuel</i>	Fuel
<i>fan</i>	Fan
<i>fw</i>	Feedwater
<i>gas</i>	Gas
<i>gain</i>	Gained
<i>gen</i>	Generated
<i>gt</i>	Gas turbine
<i>i</i>	Incident
<i>ideal</i>	Ideal
<i>in</i>	Inlet
<i>ise</i>	Isentropic
<i>mech</i>	Mechanical
<i>n</i>	Nominal
<i>opt</i>	Optical
<i>out</i>	Outlet
<i>p</i>	Polytropic
<i>pump</i>	Pump
<i>r</i>	Receiver
<i>rad</i>	Radiative
<i>reaction</i>	Reaction
<i>rec</i>	Received
<i>ref</i>	Reference
<i>refl</i>	Reflected
<i>rej</i>	Rejected
<i>s</i>	Entropy
<i>sc</i>	Solar constant

<i>sh</i>	Super heater
<i>shade</i>	Shading losses
<i>sky</i>	Sky
<i>solTech</i>	Solar technicians
<i>st</i>	Steam turbine
<i>steam</i>	Steam
<i>th</i>	Thermal
<i>th_rankine</i>	Thermal rankine
<i>tower</i>	Tower
<i>wash</i>	Wash
<i>v</i>	Volumetric
<i>z</i>	Zenith

Dimensionless numbers

Bi	Biot number
Nu	Nusselt number
Re	Reynolds number

Chapter 1

Introduction

1.1 Background

On a global scale, countries are focusing their attention on structuring their electricity production fleets to become more sustainable and environmentally friendly. Advocated by the Paris agreement, a collective of countries have determined to keep the global mean temperature rise below 2 °C (United Nations, 2015). At the annual United Nations Climate change conference in 2015, 186 countries presented their action plans to reduce carbon emissions at the Paris agreement (2015). However, 67.2 % of global electricity demand is still only being met by fossil fuels as stated by the International Energy Agency (2015).

South Africa's energy sector is focusing on implementing renewable and sustainable energy projects that are economically viable. Focus is placed on less adverse environmental impact as highlighted in the integrated energy plan by the Department of Energy (2012). Coal-fired power plants have been used to meet the country's base-load energy requirements for the past few decades and shifting to other energy resources pose many challenges regarding cost, despatch ability and supply security. Concentrated solar power (CSP) is currently being researched to be a possible alternative due to thermal energy being stored more efficiently and affordably than electrical energy. South Africa also has a high solar resource availability with direct normal irradiance (DNI) levels reaching values of up to about 3 000 kWh/m² according to the Centre for Renewable and Sustainable Energy Studies (2014). To this date many CSP technologies such as parabolic trough plants and central receiver towers have been successfully implemented to supply heat to a heat transfer fluid (HTF) which in turn heats up steam to drive conventional steam turbines for power production. However, investigating new technologies for generating power remains essential to develop more energy effective, environmental friendly and lower cost methods of using solar radiation.

The solar thermal energy research group (STERG), founded by the Stellenbosch University, forms a hub of affiliated researchers striving towards a cleaner future with the implementation of solar radiation for heating, cooling and power production. As part of a master's degree, this research study will focus on investigating whether the Stellenbosch University Solar Power Thermodynamic (SUNSPOT) cycle as proposed and patented by Kröger (2011) can contribute towards reaching a sustainable future.

1.2 The SUNSPOT cycle

Central receiver systems (CRS) are highly efficient solar collectors. High concentration ratios in the range of typically over 1 000 results in very high temperatures at the receiver outlet. CRS also have considerable lower piping losses and costs on multiple parts compared to line-focused systems. CRS are implemented to heat a typical HTF (such as oil, molten salt or steam) which exchanges heat with the steam driving a steam turbine. Some plants also include thermal storage for longer and more consistent energy production even when DNI levels are inconsistent or zero. The systems described above are summarised by BINE Information service (2013). Kribus et al. (1998) shows that solar combined cycle (CC) power generation is possible at very high thermal to electric efficiencies. This is due to high temperature operation of the Brayton gas turbine such that a high Carnot efficiency is reached. Efficiency is further improved as the exhaust air is used to drive a bottoming Rankine cycle. Study done by Heller and Hoffmann (2013) proposes to use a high-pressure air receiver to drive the Brayton cycle and another low-pressure air receiver that is directly connected to the thermal energy storage system (TESS) for the secondary Rankine cycle.

The SUNSPOT cycle is a CRS driving a combined cycle plant with an addition of auxiliary fuel and storage for excess heat. A field of heliostats concentrates DNI onto a central receiver using air as both the working and heat transfer fluid. The air receiver can be either an open volumetric, pressured or non-pressured air receiver. Depending on the receiver and heliostat field size, the air is generally heated up to around 800 °C and further auxiliary fuel combustion is necessary to reach air temperature of 1 100 °C to drive the gas turbine. Exhaust gas with temperature ranging from 500 °C is either stored in a TESS, with rock bed storage being the proposed system by Allen (2010), or used to heat water and superheat steam directly for driving a steam turbine. The system configuration as defined by Kröger (2011) is seen in Figure 1. The inclusion of auxiliary gas burners results in a hybridized system which benefits the system in making it possible to be used as a peaking plant or for continuous power production, regardless of solar resource availability.

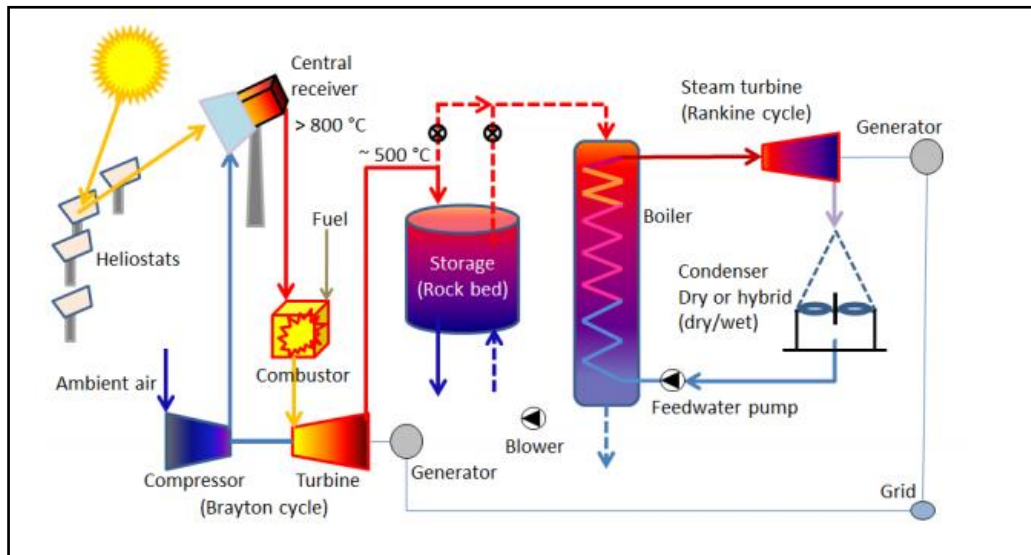


Figure 1: Stellenbosch University Solar Power Thermodynamic cycle by Kröger (2012)

1.3 Objectives

1.3.1 Modelling and simulation of a combined cycle power plant

The first part of the research considers the construction of a simple combined cycle power plant model to validate and understand its operation before moving to combine it with solar power and TESS. Simple models are used to define and simulate the complete Brayton cycle, heat recovery steam generator (HRSG) and Rankine cycle. The scope does not require highly accurate multidimensional models. The models are validated with similar models and existing component data.

1.3.2 Modelling and simulation of the solar components and thermal storage.

The objective of this part is to construct the models required to describe the solar resource, its harnessing and application for the combined cycle. A simple thermal storage model describing the basic thermocline is applied. The models are deduced from work done by other authors who have already validated them to the required accuracy for a high-level analysis.

1.3.3 Analysis of various application approaches to represent the SUNSPOT cycle or its variations

The configurations building up to the SUNSPOT cycle are investigated to find the most optimum integration considering both the total system efficiency and solar fraction. Fuel usage, annual yield and production consistency are then evaluated.

1.4 Methodology

A conventional combined cycle power plant (CCPP) is modelled, simulated and verified. The cycle is then altered by adding solar energy and storage also to show how the initial combined cycle power plant output improves both technically and thermo-economically. The simulations are carried out using Matlab[®] (Mathworks, 2017) and the data analysis is done in Microsoft Excel[®] (Microsoft, 2016).

1.4.1 Literature study

The literature study focusses on developing high level models. Lower level detailed models are not part of the scope of this study. The research focusses on existing models of the various receivers, storage and combined cycle designs. Models, their application and optimal operating conditions are researched for:

- Solar field (heliostat and tower) configuration and optimization models.
- Solarised gas turbines.
- Thermal rock bed storage.
- Heat recovery steam generators.
- Steam turbines and condensers.

1.4.2 Model, simulate and validate the combined cycle, solar and thermal storage components

Theoretical models are constructed pertaining to steam turbine, gas turbine and HRSG operation and performance. The models are individually evaluated to see if high level inaccuracy is acceptable and then combined and re-evaluated. Parametric focus is placed on mass-flow, operational temperatures and pressures, system efficiency and power output. The solar resource availability for annual periods is determined using solar geographic information system (GIS) data and latitude and longitude information. The type of solar collector and absorber system is chosen and the theoretical models for its application defined. The most applicable thermal storage is chosen and modelled using simple thermocline estimates. The simulations are carried out using Matlab[®] (Mathworks, 2017).

1.4.3 Integration from combined cycle to sunspot cycle

With an accurate combined cycle plant model, the solar and storage components are added and evaluated using different integration techniques. This shows how it improves on the initial combined cycle. These configurations are then compared and the most suitable configuration pertaining to system efficiency, physical feasibility, fuel usage, solar share and power output and consistency is chosen.

1.4.4 Final evaluation and documentation of findings

The research concludes by stating the immediate and potential feasibility of implementing the SUNSPOT cycle, what major obstacles there still are to overcome, and propose specific research fields vital to making the SUNSPOT cycle part of South Africa's plan for a more sustainable future.

1.5 Motivation

1.5.1 The case for solar thermal energy and the SUNSPOT cycle

The earth's supply of renewable energy is grouped by three sources and dominated by solar power (Twidell and Weir, 2006). The other two major supplies are found in geothermal sources and the planetary motion of the earth. The amount of solar energy available exceeds the capacity of these two other sources by factors of 4 000 and 40 000 respectively. Twidell and Weir (2006) showed that of the 120 PW solar resource absorbed by the earth, two thirds are available for sensible heating processes and only a fraction (<0.1 %) can be used for photon processes such as photovoltaics (PV). The complexity and costs of harnessing the solar power plays the biggest role in energy generation systems. Even though the PV industry has matured and provides affordable energy, the reason why this study focusses on sensible heat is due to its storage ability. It is required to show that CSP can offer a non-intermittent solution to the energy problem and for that various systems have been developed, tested and commercially implemented. The ongoing research into different technologies is required for CSP to start maturing as an energy solution. The SUNSPOT cycle offers a competitive solution due to its extremely high efficiencies. More research is still required to prove its usefulness and the technology readiness levels of its components need to be developed and matured.

1.5.2 CSP: Peaking and load following solution

This study argues the case for using solar resource not as an intermittent source but in hybrid with conventional fuel as a peaking or load following solution to the South African electricity grid. Silinga and Gausché (2013) argued and showed that CSP can be used competitively as a peaking energy system. They showed that a combined CSP and diesel powered Open Cycle Gas Turbine (OCGT) plant had a much lower levelized cost of electricity (LCOE) and fuel dependency than the standard OCGT plants considered in the current Integrated Resource Plan (IRP, 2016) peaking solutions. Silinga et al. (2014) further showed that with the typical two-tier tariff structure in South Africa it would result in CSP being an optimal solution for peaking and load following profiles.

1.5.3 The motivation for a high-level model of the SUNSPOT cycle

The SUNSPOT cycle might play a significant role in reaching the “2 °C Paris agreement” margin, uninterrupted power supply and sustainable economic growth in a country such as South Africa. Developers need to be convinced that the technology is worth investing in. A high-level model and simulation program is necessary to give this perspective and help evolve the still very crude concept. Research on many of the SUNSPOT components, specifically the air receivers and storage, are vital in proving the concept. Studies done by Allen (2010) and Heller (2013) show that rock bed storage is a likely solution for storage of the SUNSPOT technology. Work was recently done by Lubkoll et al. (2015) on pressurised air receivers and successful modelling and simulation of open volumetric air receivers have been carried through by Ahlbrink et al. (2009). A review done by Avila-Marin (2011) showed that major progress has been made in using air receivers to reach temperatures of over 800 °C. Some aspects of the receivers such as material durability and window design requires further investigation before the necessary technology readiness levels are met. Heller and Gauché (2013) showed significant improved energy output together with decreased auxiliary fuel usage by implementing a dual pressure air receiver. This was due to the ability of the receiver to refocus on the low-pressure part directly charging the storage and thus removing dumping losses. The study however shows that if the technology is to be proved feasible plant components should be optimised, and that a techno-economic study for dispatchable power generation is required.

A major concern regarding the configuration of the SUNSPOT cycle is the trade-off to be made between solar share and conversion efficiencies. With current limitations to the output receiver temperatures keeping the maximum temperature below 1 100 °C, we are caught in a stalemate. The solar share is kept high when the firing turbine inlet temperature is matched with receiver outlet temperature. However, the higher the turbine inlet temperature of a gas turbine the better the thermal energy conversion efficiency. When there is inadequate solar resource available to a system incorporating low solar to heat conversion efficiencies it requires more fuel combustion causing high emissions. Therefore, it is part of this assignment to consider different configuration setups that can resolve these mutually conflicting conditions. The ideal is to retrofit existing combined cycle configurations to allow solar operation. The gas turbines however operate at high turbine inlet temperature's (TIT) and such retrofitting will thus result in very low solar shares and is deemed to be very complicated in practice.

Chapter 2

Solarised combined cycles

The application of solar energy for power production is vast in diversity and has been researched extensively for both PV and thermal applications. This research study focuses specifically on the thermal application of CSP as to compliment a system such as the CCPP. Some of the most compelling research done in this application is by Spelling (2013). He focused on the application of solar to the Brayton cycle before the air enters the combustor. He evaluated this for CCPP and analysed the thermo-economic implications.

Figure 2 shows the hybrid solar gas-turbine unit that Spelling (2013) used to represent the simple cycle. He analysed the application of solar on two specific turbines from Siemens Industrial Turbomachinery namely the SGT-500 and the SGT-750. He found that the turbine operating at a lower firing rate resulted in high annual solar shares reaching 63 % at the expense of a lower cycle efficiency. Both turbines also showed physical limitations to integration of solar. The SGT-750 requires high firing temperatures and the large solar shares required would make it unaffordable. The SGT-500 operating at a lower TIT is fired at such a low temperature that it results in inefficient burning and high CO₂ emissions.

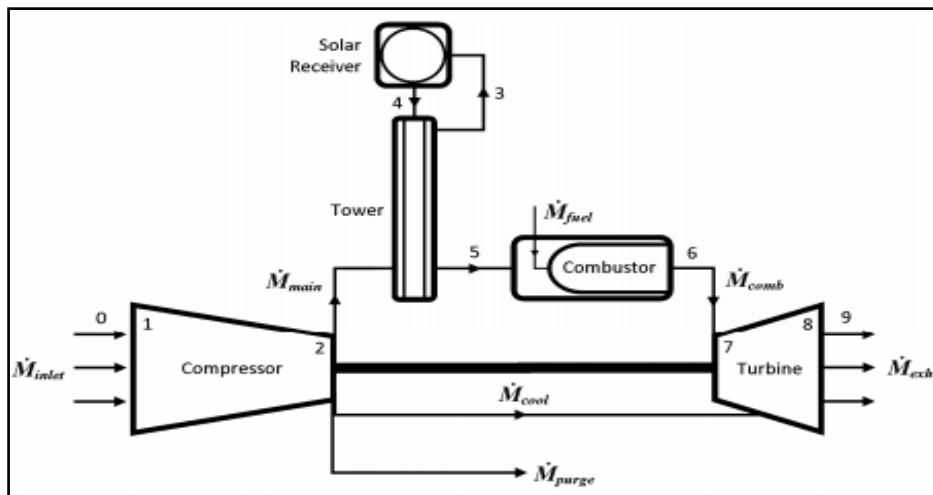


Figure 2: Sub-components and mass flow of the hybrid solar gas-turbine unit (Spelling, 2013)

Spelling (2013) also focused on optimising the gas turbine units. The optimisation showed a reduction in LCOE for turbines operating at moderate solar shares between 14 % and 26 %. Compression pressure ratios greater than 22 were required

to achieve desired conversion ratios. High pressure ratios result complex component design due to limitations on the allowable receiver pressures.

Spelling (2013) further focused resolving the limitations that simple cycle power plants proved to show, especially in terms of the solar share achieved. The first improvement introduced is the addition of thermal storage in parallel between the receiver and combustor as shown in Figure 3. This allows power production from solar generated heat for a more prolonged period independent of immediate radiation. The maximum solar share can now be increased by more than 50 %. The second improvement suggested by Spelling (2013) is to add a bottoming cycle using the exhaust heat from the gas turbine to drive it.

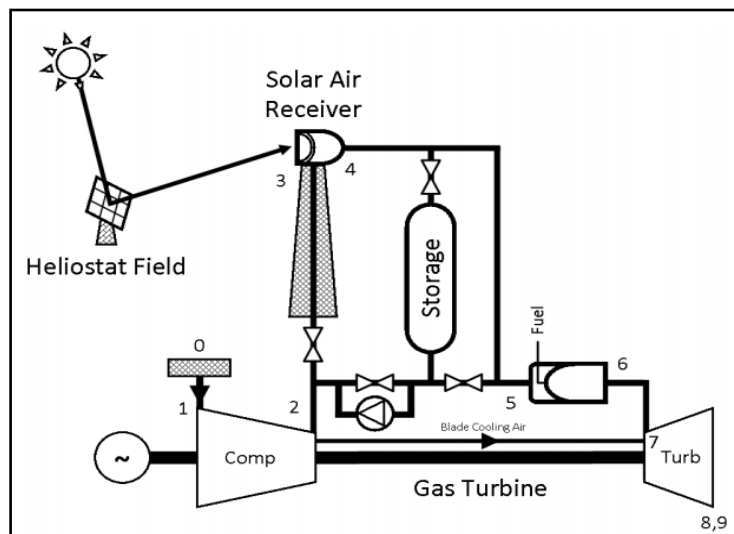


Figure 3: Simple gas-turbine combined with storage investigated by Spelling (2013)

The bottoming cycle, which is presented in Figure 4, consists of a dual pressure steam turbine operating at a high and low temperature. The HRSG is equipped with both high and low-pressure economisers, evaporators and super heaters. It was shown that such a CCPP results in a 15 % decrease in electricity cost compared to simple cycle power generation. However, the configuration did not yield the same annual solar share compared to the SC because of the higher firing temperatures required for CC's. When the CC was combined with the storage component solar shares rose to over 90 %. Spelling (2013) argues that such a configuration results in a lower LCOE along with much lower carbon emissions when compared to any modern conventional power plant design.

efficient for gas turbine operation but limited by the maximum solar field temperature that can be reached. The exhaust gas from the gas turbine is then either used for the boiler operation or stored by means of thermal storage to be used later. The storage charges at a rate that is dependent on the relationship between the mass flow from the exhaust and of that required by the steam turbine. As seen in Figure 8 the plant operation during night time and cloudy days is much different. The whole Brayton cycle section is removed from the operation and the heat stored in the thermal storage is used by the boiler to generate steam. The combined cycle configuration is beneficial because it allows a more diverse range of temperatures and increases the overall efficiency.

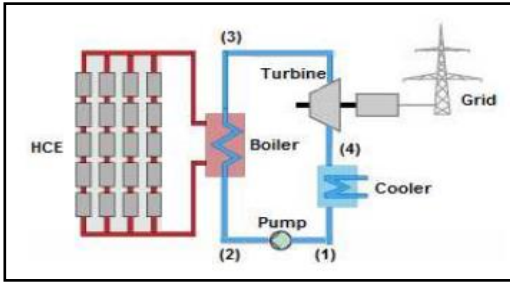


Figure 5: Solarised Rankine cycle configuration proposed by Nel (2014)

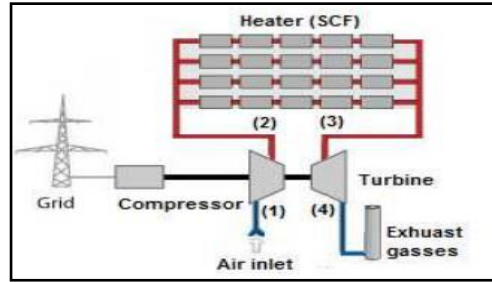


Figure 6: Solarised Brayton cycle configuration proposed by Nel (2014)

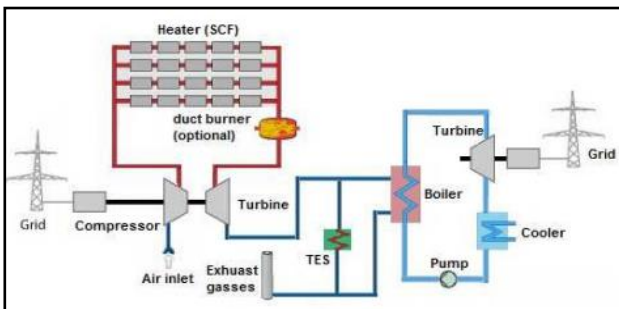


Figure 7: Solarised combined cycle configuration proposed by Nel (2014)

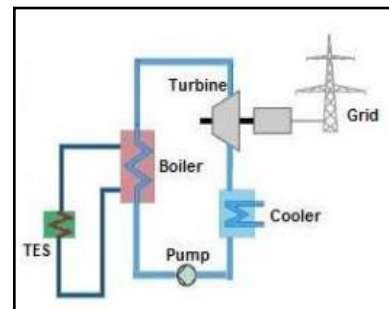


Figure 8: Non-solar operation of Nel's (2014) combined cycle plant.

Chapter 3

Conventional combined cycle plant

The CCPP is a combination of two well-known thermodynamic cycles, namely the Rankine and Brayton cycle. Combining these cycles results in higher system efficiencies and the combination of cycles implementing different HTF's results in utilising complimenting advantages such as temperature ranges. The cycle operating at the higher temperature range, in this case the Brayton cycle, is referred to as the topping cycle. The cycle operating at the lower temperature range is referred to as the bottoming cycle. The gas turbine contributes approximately two thirds of the total combined cycle power output.

The use of air and steam for the Brayton and Rankine cycle respectively is typical. Air is readily available and can be used in modern gas turbines at temperature ranges from 1 000 °C to as high as 1 600 °C for the turbine inlet temperature. Water is used for the bottoming cycle because it is widely available, inexpensive, suitable for low and medium temperature ranges and is non-hazardous. Kehlhofer et al. (1999) argues that even though organic fluids such as ammonia could be more effectively implemented in the low exhaust temperature range, technological development in higher gas turbine outlet temperature will make these advantages less significant. With these technology improvements solar powered and hybrid CCPP are considered to reduce the construction of baseload power plants such as coal fired and nuclear power plants. This is due to higher thermal efficiencies, less fuel dependency and improved environmental impacts.

The biggest benefit of the CC is the higher efficiency yield. This improvement can be explained in terms of the Carnot efficiency. It describes the ratio of the difference between the temperatures of the energy supplied and dissipation heat over the temperature of the energy supplied for a theoretical ideal cycle. Equation 3.1 is given by Cengel and Boles (2015) as:

$$\eta_{carnot} = 1 - \frac{T_{out}}{T_{in}} \quad [3.1]$$

On a thermodynamic basis there are many energetic (such as heat) and exergetic (such as irreversibilities with regard to the second law of thermodynamics) losses that the Carnot efficiency does not take into consideration. Considering only the Carnot efficiency it is better to have a larger difference in temperatures at which the working fluid receives and rejects heat. Combining the Brayton cycle and the steam Rankine cycle can yield such an improved Carnot efficiency as calculated in Table 1. Actual efficiencies are however around 75 % and 80 % of the Carnot efficiency for the combined cycle and conventional steam power respectively making the

difference between the two less extreme. Kehlhofer et al. (1999) demonstrated that the optimum gas turbine varies for simple cycle and combined cycle application due to the optimum point for turbine efficiency and exhaust temperature and the role that the exhaust temperature has on the efficient operation of the steam cycle.

Table 1: Thermodynamic comparison of gas turbine, steam turbine and combined-cycle processes

Cycle	Brayton Cycle	Rankine Cycle	Combine Cycle
Typical temperature of heat supplied [K]	1 200-1 600	650-850	1 200-1 600
Typical temperature of heat rejected [K]	800-900	300-350	300-350
Carnot Efficiency [%]	25-50	46-65	71-81
Typical actual thermal efficiencies [%]	30-40	25-40	55-60

3.1 Concepts and selection criteria

Kehlhofer et al. (1999) gives the basic descriptions for typical CC concepts, their operation and benefits. These concepts are still applicable today with most CC plants. Depending on the output they typically vary between single, dual and triple pressure steam cycles with either reheat or non-reheat turbines. As with any other plant, there are certain design procedures that can be used to simplify the selection process. Kehlhofer et al. (1999) highlights the initial plant's operating and performance requirements that should be analysed. The following are some general requirements to establish:

- The power demand, including minimum and maximum limits and grid limitations (and frequency connection), to set the gas turbine's base load point.
- Auxiliary process demands will result in specific temperature, pressure and mass flow requirements.
- Type of load application along with expected operating hours and number of stop/starts annually.
- The competing levelized cost for operating power plants.

The ambient conditions also play a role in the design of the plant. Most gas turbine performance characteristics are quoted at ISO standard conditions (15 °C, 101.3 kPa, 60 % relative humidity), and developing a new turbine for specific ambient conditions is not justified economically. However, the gas turbine will perform differently at varying conditions and therefore will affect the steam generation process. The steam turbine is designed for a specific application with steam pressure playing a significant role.

The two ambient conditions that affects the combined cycle operation the most is the air temperature and pressure. As air temperature rises, it reduces the air density and therefore the mass flow rate, which lowers the gas turbine output. When the density of air decreases more power is required by the compressor. The ambient air

pressure also decreases at higher elevations resulting in lower air densities. When the mass flow decreases along with the rising of air temperature the pressure ratio in the turbine decreases. The increase of ambient temperature does result in a higher exhaust gas from the gas turbine and therefore improves on the steam turbine performance. However, changes in mass flow are more dominant than changes in exhaust temperature of the gas turbine. Higher relative humidity also effects the output of the plant to some degree. There is a higher moisture content in the air, which results in a loss of thermal energy at combustion due to vaporisation.

The resources available is another important aspect to consider when designing a CCPP. These resources include the fuel source and cooling media. Generally, where it is inexpensive and readily available, water is used to remove the waste heat from the condenser due to its excellent heat-transfer properties and high specific thermal capacity. The temperature of the cooling medium influences the efficiency of the thermal process. A lower cooling medium temperature results in a lower condenser pressure, and the steam turbine output increases due to a greater enthalpy drop. Above a condenser pressure of 100 mbar there is minimal change in enthalpy drop in the turbine. However, at higher pressures a lower volume flow rate is required resulting in a smaller turbine and lower costs (Kehlhofer et al., 1999). In the condenser the best vacuums are created with direct water cooling. Water cooling with a wet-cooling tower with direct air cooling is less efficient in creating such vacuums.

Considering the fuel source, the focus varies between sulphur content and the lower heating value (LHV) of the fuel. The sulphur content has an impact on the design of the HRSG. This is because the HRSG should be operated at levels above the sulphur content dew point. The LHV of the fuel is the determining factor. When using a fuel with a low LHV a higher combustion rate is required to ensure the required chemical heat supply, resulting in higher turbine output and efficiency. The enthalpy drop in the turbine is determined by the chemical composition of the fuel, therefore the LHV cannot be used as the only measure by which the type of fuel is determined. A way of improving the efficiency by which the fuel burns, is to account for the sensible heat by preheating the fuel using an economizer in the HRSG. Kehlhofer et al. (1999) argued that by increasing the temperature of natural gas from 15 °C to 150 °C has an efficiency improvement of 0.7 % on the total cycle. Fuels commonly used are liquid petroleum gas, diesel oil and natural gas.

3.2 Rankine cycle

Cengel and Boles (2015) describes the ideal simple Rankine cycle (Figure 9) as the isentropic compression in a pump (1-2), isobaric heat addition in a boiler (2-3), isentropic expansion in a turbine (3-4) and isobaric heat rejection in a condenser (4-1). A typical temperature/entropy diagram can be seen in Figure 10. The typical working fluid used is steam due to its high thermal capacity and density. For an ideal system the thermal efficiency for the Rankine cycle is given as:

$$\eta_{th-rankine} = 1 - \frac{q_{out}}{q_{in}} \quad [3.2]$$

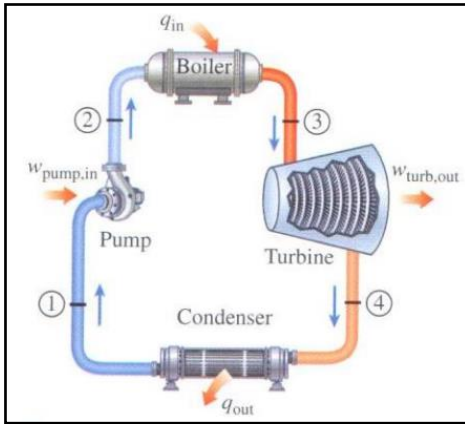


Figure 9: Simple Rankine cycle (Cengel and Boles, 2015)

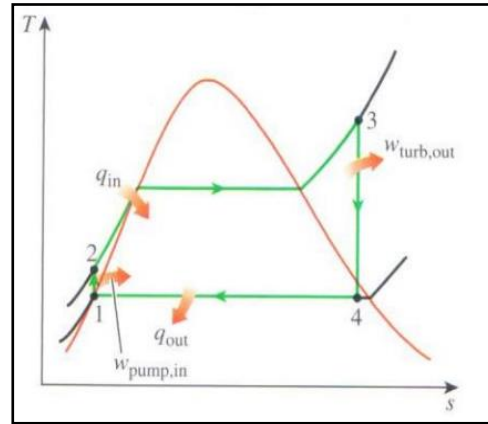


Figure 10: Entropy temperature diagram for an ideal simple Rankine cycle (Cengel and Boles, 2015)

3.2.1 Steam turbine

As stated in the previous chapter, the Carnot efficiency is solely for the ideal case and there are numerous factors that causes deviation from this efficiency. The two most prominent factors are fluid frictional losses and thermal losses. The fluid friction in the piping, turbine, condenser and boiler causes significant pressure drops which are accounted for by increasing the pump specifications. The thermal losses are due to heat losses in the elements with large temperature differentials and more heat is required by the boiler to maintain the same output. For both the pump and turbine there are losses due to irreversibilities. Isentropic efficiencies are used to account for these losses. Rankine cycles can be improved by utilising a lower condenser pressure; superheating the steam and/or increasing boiler pressure.

If the expansion of steam is not fully isotropic, as shown in Figure 10, there is zero heat exchanged between the turbine and the environment and the internal entropy dissipation can be characterised by an isentropic efficiency (η_{s-st}), the change in entropy over an actual steam turbine expansion is given by:

$$h_{stout} = h_{stin} - \eta_{sst}(h_{stin} - h_{sst}) \quad [3.3]$$

The isentropic expansion enthalpy is represented by h_s . The electricity generated is then a function between this actual change in entropy, mass flux through the turbine and the represented loss efficiencies for the turbine and generator. The total efficiency is represented by η_{mec} as seen in Equation 3.4.

$$\dot{E}_{st} = \eta_{mecst} \dot{M}(h_{stin} - h_{stout}) \quad [3.4]$$

The thermodynamic model can be implemented by making use of Stodola's steam expansion model (Cooke, 1983) which was also implemented by Spelling (2011). He showed that the turbine needs to be divided into segments for the application of Stodola's ellipse theorem, with each section having a nominal isentropic efficiency as specified by the manufacturers. Cooke (1983) showed that Equation 3.5 is used to calculate each outlet section with a calculated ellipse constant (Y). Therefore, using an iterative process the steam properties can be calculated for each section starting from the inlet conditions of pressure (P), temperature (T) and mass flow coefficient (Φ).

$$P_{stout} = \sqrt{P_{stin}^2 - \dot{M}_{stin}^2 T_{stin} Y} \quad [3.5]$$

With

$$Y = \frac{P_{in,nom}^2 - P_{out,nom}^2}{P_{in,nom}^2 \times \Phi_{in,nom}^2}$$

$$\Phi = \frac{\dot{M}\sqrt{T}}{P}$$

Kehlhofer et al. (1999) lists the most important requirements for the steam turbine in a CCPP as being highly efficient; with short start-up and installation times and floor mounted installation. A CCPP steam turbine's power output is usually less than conventional plant turbines and higher than industrial turbines with typical live steam temperatures and pressures lying between these two applications. With modern gas turbine exhaust temperatures reaching higher values the CCPP steam turbine live steam temperature is much similar to conventional plants. Typically for CC implementation, steam is generated and enters the turbine at different pressure levels resulting in an increase in mass flow rate from the entrance of the turbine up to the exhaust.

3.2.2 Deaerator and condenser

There are different ways of deaerating steam to remove the incondensable gases. Deaeration is necessary due to keeping oxygen levels below 10 ppb for corrosion prevention. Gasses are released when water is sprayed and heated. The deaerator is normally placed on top of the feedwater tank, where heating steam is inserted into the lower part and as it rises through, heating the water droplets to saturation temperature causing the incondensable gasses to be released. A steam cushion between the water and air ensures that reabsorption is avoided. The process either takes place under vacuum condition or above atmospheric pressure. The advantage of applying vacuum deaeration is that additional heat exchangers aren't required due to all the heating being done in the feedwater tank. Lower quality steam is required for deaeration therefore more steam can be expanded yielding higher turbine output. With overpressure deaeration the incondensable gasses can be

exhausted directly into the atmosphere without effecting the condenser evacuation system. The condenser is also used to deaerate the steam. If the condenser is effective in deaerating the steam the feedwater tank and deaerator can be removed completely from the system and condensate is pumped directly from the condenser to the HRSG (Kehlhofer et al, 1999). A water buffer is then required because of the lack of a feedwater tank therefore the condenser hot water capacity should be increased. The water temperature should be raised to above the sulphur condensation temperature before entering the HRSG. The type of cooling technology, ambient temperature and cooling load plays a significant part in the resulting condenser pressure that is attained. A lower condenser pressure results in a higher turbine output. The following three typical cooling systems are applied to CC plants:

- In very arid areas, with limited water supply, dry air cooling is recommended even though it results in reduced output and efficiency due to limited vacuum generation at the turbine exit.
- If water supply is partially limited, water can be used to replace evaporation and blow down losses in an indirect cooling system. For CC plants the required amount of water ranges at 0.3 kg/s/MW installed capacity.
- Direct water cooling requires 12-18 kg/s/MW of water and serves as the full heat sink.

Wagner and Gilman (2011) argued that the significant improvement in performance comes with a high cost in water consumption. They claimed that 94 % of a typical 100 MW plant's water consumption is due to evaporation. This study will focus on using an air-cooled condenser due to CSP plants being situated mostly in arid regions with low water supply. The difference between the condensate temperature and the inlet air temperature is called the initial temperature difference (ITD). The difference between the ITD and the outlet difference in temperature along with the mass flow rate of the air determines the amount of heat that's rejected (Equations 3.6 and 3.7).

$$\dot{q}_{rej} = \dot{m}_{air} c_p (T_{ITD} - \Delta T_{out}) \quad [3.6]$$

$$\dot{q}_{rej} = \dot{m}_{st} (h_{ST_{out}} - h_{cond}) \quad [3.7]$$

The air temperature at the inlet of the condenser is heated slightly by the work applied on it by the fan. Wagner and Gilman (2011) gave Equation 3.8 to represent this. The parasitic power consumption of the fan is calculated by the isentropic compression of the air. Wagner and Gilman (2011) showed that the pressure increase (r_p) can be estimated at 1.0028 with the isentropic and mechanical efficiency of the fan being 80 % and 94 % respectively. These values have also been used by Spelling (2013) in his work.

$$T_{fan_{out}} = T_{db} \times r_p^{\frac{R}{C_p}} \quad [3.8]$$

$$h_{fan_{out}} = h_{fan_{in}} + \frac{1}{\eta_{fan_{ise}}} (h_{fan_{out_{ise}}} - h_{fan_{in}}) \quad [3.9]$$

$$\dot{W}_{fan} = \frac{\dot{m}_{air}}{\eta_{fan_{mech}}} (h_{fan_{out}} - h_{fan_{in}}) \quad [3.10]$$

3.2.3 Pump

The pump pressurises the condensate from the condenser to the operating pressure required by the steam turbine. This process is ideally isentropic but due to frictional and thermal losses an isentropic efficiency is applied to account for these. Equations 3.11 and 3.12 represent the real compression and parasitic power consumption in the pump respectively. Hirsch et al. (2017) recommended the use of isentropic efficiency of 90 %. A conservative mechanical efficiency of 95 % is further assumed for the pump.

$$\eta_{pump_{ise}} (h_{pump_{out}} - h_{pump_{in}}) = h_{pump_{out_{ise}}} - h_{pump_{in}} \quad [3.11]$$

$$E_{pump} = \frac{M_{pump} (h_{pump_{out}} - h_{pump_{in}})}{\eta_{pump_{mech}}} \quad [3.12]$$

3.2.4 Heat recovery steam generator

The HRSG has a significant impact on the performance on a CCP and should therefore be carefully considered. For this application a relatively simple one-dimensional model for the HRSG will be implemented due to the possible complexity of such a system. This section considers the parametric design of the HRSG and will conclude with a simple performance model of a HRSG.

The purpose of a HRSG is to transfer heat from one fluid to another. The HRSG is characterised by two different flow arrangements. Parallel flow is where both the hot and cold fluid moves in the same direction from entrance to exit. Counter flow is where the fluids enter at opposite sides and opposite flow direction occurs. Cross flow occurs when fluid flows are perpendicular to one another. Counter and cross flow is mostly implemented for CCP use due to the larger temperature differential associated with such a flow.

The pinch point temperature is a key parameter in the optimisation of the steam cycle according to Kehlhofer et al. (1999). This parameter describes the difference in temperature between the exhaust gas side and evaporator outlet on the water/steam side. Another important parameter is the approach temperature, which is the difference in temperatures between the water at the economizer outlet and the saturation temperature in the drum. There are two typical HRSG setups namely, the

HRSG without supplementary firing and those that incorporate supplementary firing. HRSG without supplementary firing are typically once through HRSG either in the vertical or horizontal position. They are highly efficient in heat recovery where the pressure losses at the exhaust-gas side are low. They have low-temperature corrosion prevention and allow a large permissible pressure gradient for start-up procedure. Modern technology is reducing the need for supplementary firing, with exhaust temperatures of modern gas turbines very close to the allowed TIT. It is also less efficient in the CC setup. It is often rather used in cogeneration power plants where the amount of process steam required varies.

The heat exchanger utilised in a HRSG plays an important role in achieving high thermal efficiencies in the steam turbine. HRSG are specifically tailored for certain CC applications. Changes in the HRSG design affects the combined cycle total efficiency and power production. Increasing the HRSG performance does however have severe cost implications. Da Rocha (2010) mentioned a 3-4 % increase in plant cost for a total efficiency increase of one percent by alteration of the HRSG. Ravi Kumar et al. (2007) observed that for a given dual pressure cycle high thermal efficiencies results from raising the pressure at the high-pressure section and lowering the pressure at the low-pressure section.

As with all fluid systems a pressure drop is associated with the HRSG. The pressure loss in the HRSG occurs mostly in the evaporator during the boiling process. The pressure drop in the boiler substantially outweighs those associated with the economiser and super heater. The process of calculating this pressure loss is highly technical and will result in unwanted numerical detail. A simple pressure drop of 3 % is estimated for the evaporator section. If a counter flow heat exchanger is implemented, the heat transfer is correlated for the economiser, evaporator and super heater by the following steady state equations:

$$\dot{Q}_{sh} = \frac{U_{sh}A_{sh}F_{sh}\left(T_{gt_{out}}-T_{stHP_{in}}-\left(T_{shgas_{out}}-T_{shsteam_{in}}\right)\right)}{\left(\ln\frac{T_{gt_{out}}-T_{stHP_{in}}}{T_{shgas_{out}}-T_{shsteam_{in}}}\right)} + \frac{U_{sh}A_{sh}F_{sh}\left(T_{gt_{out}}-T_{stIP_{in}}-\left(T_{shgas_{out}}-T_{stHP_{out}}\right)\right)}{\left(\ln\frac{T_{gt_{out}}-T_{stIP_{in}}}{T_{shgas_{out}}-T_{stHP_{out}}}\right)} \quad [3.13]$$

$$\dot{Q}_{ev} = \frac{U_{ev}A_{ev}F_{ev}\left(T_{evg_{in}}-T_{evsteam_{out}}-\left(T_{evg_{out}}-T_{evfw_{in}}\right)\right)}{\left(\ln\frac{T_{evg_{in}}-T_{evsteam_{out}}}{T_{evg_{out}}-T_{evfw_{in}}}\right)} \quad [3.14]$$

$$\dot{Q}_{ec} = \frac{U_{ec}A_{ec}F_{ec}\left(T_{ecgas_{in}}-T_{ecfw_{out}}-\left(T_{hrsggas_{out}}-T_{ecfw_{in}}\right)\right)}{\left(\ln\frac{T_{ecgas_{in}}-T_{ecfw_{out}}}{T_{hrsggas_{out}}-T_{ecfw_{in}}}\right)} \quad [3.15]$$

The heat transfer is then correlated with change in enthalpy by:

$$\dot{Q}_{sh} = \dot{m}_{gas} (h_{gt_{out}} - h_{sh_{gas_{out}}}) = \dot{m}_{steam} (h_{stHP_{in}} - h_{sh_{steam_{in}}} + h_{stIP_{in}} - h_{stHP_{out}}) \quad [3.16]$$

$$\dot{Q}_{ev} = \dot{m}_{gas} (h_{sh_{gas_{out}}} - h_{ev_{gas_{out}}}) = \dot{m}_{steam} h_{fg@sat} \quad [3.17]$$

$$\dot{Q}_{ec} = \dot{m}_{gas} (h_{ec_{gas_{in}}} - h_{ec_{gas_{out}}}) = \dot{m}_{steam} (h_{ec_{fw_{out}}} - h_{fw_{in}}) \quad [3.18]$$

3.3 Brayton cycle

In a typical gas turbine setup air enters at ambient conditions and is compressed to 1 400 - 3 000 kPa, after which it is used to burn the fuel with typical temperatures higher than 1 000 °C. It is then expanded in the turbine generating power and leaves the turbine at ambient pressure around 450 - 650 °C. The performance of the turbine is dependent on the turbine efficiency, TIT and pressure ratio.

The Brayton cycle (Figure 11) is described by Cengel and Boles (2015) as the isentropic compression (1-2), isobaric heat addition (2-3), isentropic expansion (3-4) and isobaric heat rejection (4-1) in a power generating system using air as the working fluid. The simple cycle process flow in terms of temperature and entropy can be seen in Figure 12.

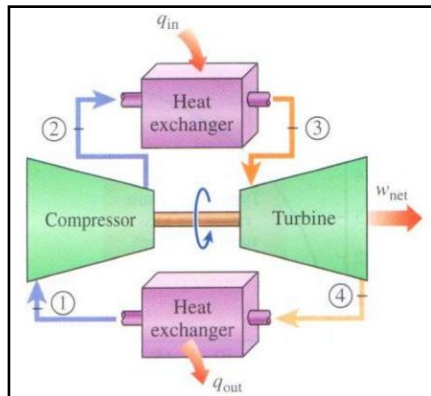


Figure 11: Simple Brayton closed cycle (Cengel and Boles, 2015)

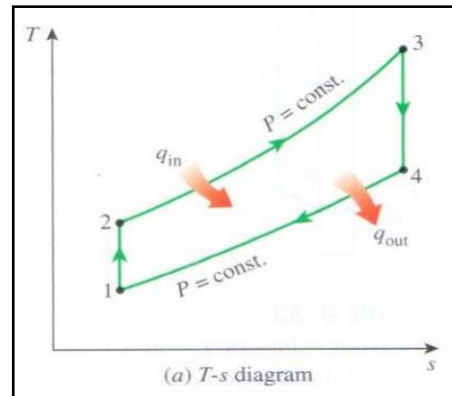


Figure 12: Entropy temperature diagram for an ideal simple Brayton closed cycle (Cengel and Boles, 2015)

Usually the section 4-1 is removed and what is known as an open cycle configuration exists. Some other implications result from ideal conditions as given by Cohen et al. (1987). Kinetic energy of the working fluid remains constant between the outlet and inlet between components. Pressure losses are ignored in the ducting as well as the heat exchangers, combustion chambers and intercoolers. Constant properties for the working fluid are assumed and its composition and mass

flow rate remain unchanged throughout the components of the cycle. Heat transfer is achieved in the heat exchanger at a specified efficiency. The thermal efficiency of the Brayton cycle with regards to the pressure ratio (Π_{gt}) and specific heat ratio (k) is given by Cengel and Boles (2015) as:

$$\eta_{th-brayton} = 1 - \frac{1}{\Pi_{gt}^{\frac{k-1}{k}}} \quad [3.19]$$

The efficiency of the Brayton cycle increases with both parameters. The TIT is limited by the maximum temperature that the turbines can withstand, constraining the fuel/air ratio to be used. This have been improved on in recent technological advances in metallurgical engineering where the use of computer aided design and numeric solutions has made the design of more efficient blade turbomachinery components possible. The simple cycle can be improved on by adding reheating, regeneration of intercooling stages where economically viable. Similar to the Rankine cycle discussed earlier, the Brayton cycle also suffers from some irreversibilities. The heating and cooling processes are not completely isobaric and some pressure loss occurs. The actual work input and output for the compressor and turbine are more or less the same. The following sub-sections highlight the models implemented by Spelling (2013) and other authors.

3.3.1 Compressor

The compressor is used to compress air from ambient conditions over a specified pressure ratio (Π_{comp}). The ambient air pressure can be assumed to be adjusted with Equation 3.20 for different heights above sea-level (Kurz, 2005). The results of this formulation have been validated by the property tables found in Cengel and Boles (2015).

$$P_{amb} = P_{sealevel} \times e^{\frac{elevation(ft)}{27\,200}} \quad [3.20]$$

The model is required to determine the power necessary for this compression and determine the specific thermodynamic condition at each state. For a simplified model it is required to assume zero heat transfer from the compressor to the environment and that internal potential and kinetic energy variations are negligible. A pressure loss factor (f_{dP}^{inlet}) is used to account for air-filter dissipation and the internal entropy dissipation is accounted for by an isentropic efficiency (η_{s-comp}). The compressor exit pressure and enthalpy are then calculated by the respective equations given by Spelling (2013).

$$P_{comp_{in}} = P_{amb} (1 - \Delta f_{dP}^{inlet}) \quad [3.21]$$

$$P_{comp_{out}} = P_{comp_{in}} \Pi_{comp} \quad [3.22]$$

$$h_{comp_{out}} = h_{comp_{in}} + \frac{(h_{s-comp_{out}} - h_{comp_{in}})}{\eta_{s_{comp}}} \quad [3.23]$$

The total electric power required by the compressor to achieve this pressure ratio is calculated as a function of the enthalpy difference, mechanoelectric efficiency ($\eta_{mech-comp}$) and mass flux ($\dot{M}_{comp-in}$).

$$\dot{E}_{comp} = \frac{\dot{M}_{comp_{in}}(h_{comp_{out}} - h_{comp_{in}})}{\eta_{mech_{comp}}} \quad [3.24]$$

Spelling (2013) defined the isentropic efficiency as a function of the polytropic efficiency (η_{p-comp}), pressure ratio, specific heat (c_p) and gas constant (r). This is a robust relation with the polytropic efficiency being constant for specific technology levels. This relation shows that the isentropic efficiency of a compressor decreases with an increase in pressure ratio.

$$\eta_{s_{comp}} = \frac{\frac{r}{c_p} \Pi_{comp} - 1}{\frac{c_p \eta_{p_{comp}}}{r} \Pi_{comp} - 1} \quad [3.25]$$

Cohen et al. (1987) showed that the outlet temperature can now be given as a function of the isentropic efficiency and pressure rise over the compressor.

$$T_{comp_{out}} = T_{comp_{in}} \left(1 + \frac{\frac{\gamma-1}{\gamma} \Pi_{comp}^{\frac{\gamma}{\gamma-1}} - 1}{\eta_{s_{comp}}} \right) \quad [3.26]$$

Losses due to windage and bearing friction should be accounted for regarding the compressor. These are very small and are estimated as 1 % of such a cycle (Cohen et al., 1987), other power requirements by auxiliary components are simply subtracted as they are specified. The work required by the compressor can then be calculated as:

$$W = \frac{1}{\eta_{mech}} \dot{M}_{comp} (h_{comp_{out}} - h_{comp_{in}}) \quad [3.27]$$

3.3.2 Combustor

In the combustion chamber a secondary mass flow of fuel (\dot{M}_f) is introduced and ignited with the presence of oxygen in the already heated air. Combustion energy is absorbed by the air and fuel to reach the minimum required TIT. Therefore, the lower heating value of the fuel (LHV_f) is required to increase the enthalpy of both the air (Δh_a) and the fuel gas (Δh_f). The fuel ratio required is then the simple relation between the LHV_f and the enthalpy changes. The total mass flow ($\dot{M}_{comb-out}$) at the

end of the combustor is then the sum between the gas and fuel mass flows. The sub chapters describe certain variations on ideal combustion.

$$m_f = \frac{\dot{M}_f}{\dot{M}_{sol,out}} = \frac{\Delta h_a}{LHV_f - \Delta h_f} \quad [3.28]$$

3.3.2.1 Pressure losses

The pressure losses in the combustion chamber are caused by the exothermic nature of the reaction causing momentum fluxes but more significant losses occur due to the flame stabilising devices and mixers causing aerodynamic resistance. Cohen et al. (1987) describes these losses as the loss in stagnation pressure (Δp_b). Heat exchangers also exhibit losses in both the gas-side (Δp_{hg}) and air-side (Δp_{ha}) passages. These losses reduce the pressure ratio of the turbine relative to the compressor resulting in a reduced work output. Cohen et al. (1987) then computes the pressure levels as:

$$p_{comb,out} = p_{comb,in} \left(1 - \frac{\Delta p_b}{p_{comb,in}} - \frac{\Delta p_{ha}}{p_{comb,in}} \right) \quad [3.29]$$

$$p_{comb,in} = p_a + \Delta p_{hg} \quad [3.30]$$

Cohen et al. (1987) further developed an expression to account for these losses using empirical data from experiments with hot and cold runs. For this study this correlation is excluded from the simulation and a constant pressure drop of 5 % is assumed due to inaccessible hot and cold run correlation data for the Mercury 50™. The author however considers it important to include them for future designs when such data is available.

3.3.2.2 Variation of specific heat

Cycle performance estimation is highly influenced by the variation of properties such as the specific heat and its ratio. These two values for a real gas are mostly a function of temperature alone for operation in its normal working ranges. The specific heat ratio is presented by Cohen et al. (1987) as a function of the universal gas constant, specific heat and molecular mass:

$$\frac{\gamma-1}{\gamma} = \frac{R_0}{M c_p} \quad [3.31]$$

Pressure can have a very small effect on the specific heat ratio but this effect will only be significant above temperatures of 1 500 K, which is beyond the ranges required for the combined cycle plant being simulated. It is noticed that Equation 3.31 is used to calculate the temperatures of Equations 3.26 and then substituted back in equation 3.31, therefore some approximations and iterations are required to find the correct values. Cohen et al. (1987) has given the following values as reasonably accurate fixed values to implement, saving computational time.

$$C_{pa} = 1.005 \frac{kJ}{kgK} \quad \gamma_a = 1.4$$

$$C_{pg} = 1.148 \frac{kJ}{kgK} \quad \gamma_g = 1.333$$

3.3.2.3 Fuel ratio

The amount of fuel required to reach the required TIT is a function of that temperature, the compressed gas temperature and the LHV specific to the fuel. The combustion process is fully adiabatic, with no work transfer. Cohen et al. (1987) gave the energy balance as a function of the fuel ratio (f):

$$\Sigma(m_{comb_{out}} h_{comb_{out}}) - (h_{comb_{in}} + f h_{fuel}) = 0 \quad [3.32]$$

Assuming a reference temperature of 298 K the energy balance is expanded to:

$$(1 + f)c_{p-comb_{out}}(T_{comb_{out}} - 298) + fLHV + c_{p-comb_{in}}(298 - T_{comb_{in}}) + f c_{p-fuel}(298 - T_{fuel}) = 0$$

The last term reduces to zero due to small fuel ratio's (<0.05 %) and fuel temperature at room temperature.

3.3.2.4 Combustion efficiency

Cohen et al. (1987) defines the combustion efficiency as a function of the theoretical and actual fuel/air ratio.

$$\eta_b = \frac{\text{theoretical } f @ \Delta T}{\text{actual } f @ \Delta T} \quad [3.33]$$

3.3.3 Turbine

For typical combined cycle setups, the multistage axial gas turbines are mostly used. The same assumptions from the compressor stages applies to the turbine. The pressure loss at the exhaust is represented by a pressure loss factor (f_{dP}^{exh}) and an isentropic efficiency (η_{st}) accounts for internal dissipation. A standard adiabatic expansion represents the true expansion through the turbine. The assumption was made that there is only marginal difference between the air and gas composition. In the work done by Spelling (2013), cooling air was accounted for. This cooling air is the medium that ensures that the temperature of the combusted gas does not exceed that allowed by the material of the turbine. However, for this study we assume that the flow rate of the air used for cooling is equal to the air that is bled and purged throughout the turbine.

The thermodynamic states are correlated by the pressure drops from the turbine entrance towards the exhaust taking into account the pressure loss factor and pressure ratio over the turbine (Π).

$$P_{gt_{in}} = P_{gt_{out}} \times \Pi_{gt} \quad [3.34]$$

$$P_{gt_{exh}} = P_{gt_{out}} (1 - \Delta f_{dP}^{exh}) \quad [3.35]$$

Assuming that the gas expands isentropically under the ideal gas law assumption, the isentropic temperature to which it expands can be given by Equation 3.36 where the entropy change is characteristically zero (Cengel, 2015):

$$T_{gt_{out_{ise}}} = T_{gt_{in}} \Pi_{gt}^{\frac{R}{c_{p_{avg}}}} \quad [3.36]$$

The enthalpy balance, considering the isentropic efficiency together with the isentropic expansion enthalpy ($h_{s-turb-out}$), is:

$$h_{gt_{out}} = h_{gt_{in}} - \eta_{sgt} (h_{gt_{in}} - h_{s_{gt_{out}}}) \quad [3.37]$$

The same correlation (Equation 3.25) used for the compressor applying the polytropic efficiency and turbine pressure ratio is used. Finally, the total shaft power generated (E) is calculated using a specific mechanical efficiency (η), the mass flow through the turbine (\dot{M}) and the entropy difference between the turbine inlet and outlet.

$$\dot{E}_{gt_{out}} = \eta_{gt_{mech}} \dot{M}_{gt_{in}} (h_{gt_{in}} - h_{gt_{out}}) \quad [3.38]$$

Assuming that the air/fuel mixture still operates in the ideal gas range then the outlet temperature can be approximated by:

$$T_{gt_{out}} = T_{gt_{in}} + \frac{h_{gt_{out}} - h_{gt_{in}}}{c_{p_{avg}}} \quad [3.39]$$

According to Boyce (2006) for off-design conditions with the load above 50 % of design load the turbine efficiency can be assumed constant. For this turbine, we will use an efficiency of 88 %.

3.3.3.1 Ideal shaft power cycle

In order to establish the governing equations for the Brayton cycle, ideal conditions are assumed initially and then later the various component losses are attributed. For ideal conditions the efficiency of the Brayton cycle is calculated as given in Equation 3.19. Cohen et al. (1987) has given the specific work output as:

$$\frac{W_{gt_{ideal}}}{c_{p_{comp_{in}}} T_{comp_{in}}} = \left(\frac{T_{gt_{in}}}{T_{comp_{in}}} \right) (\eta_{th_{brayton}}) - \left(\Pi_{gt}^{\frac{k-1}{k}} - 1 \right) \quad [3.40]$$

T_{gt-in} , which is the TIT, is sometimes also referred to as the metallurgical temperature limit. After the differentiation of Equation 3.40 it is found by Cohen et al. (1987) that when the outlet temperatures of the compressor and turbine are the same it results in a maximum work output.

3.3.3.2 Kinetic energy losses

Due to the high fluid velocities associated with turbomachinery, changes in velocity do in fact occur at the inlets and outlets of components and will cause kinetic energy losses. Figure 13 visualises these concepts on a temperature and entropy diagram for a compression process between two static processes 1 and 2.

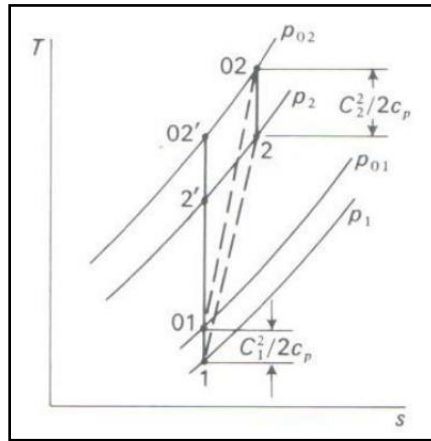


Figure 13: Entropy and temperature diagram for stagnation states during a compression process (Cohen et al., 1987)

The concept of a stagnation temperature (T_0) is introduced as a function of the static temperature (T) and kinetic energy (C). The function is given by Cohen et al. (1987) as:

$$T_0 = T + \frac{C^2}{2c_p} \quad [3.41]$$

This results in the energy equations being expressed as a function of only specific heat and stagnation temperature for both compression and heating processes. The stagnation pressure, for the assumption of isentropic conditions, is then also equated in like manner.

$$\frac{p_0}{p} = \left(\frac{T_0}{T} \right)^{\frac{\gamma}{\gamma-1}} \quad [3.42]$$

Bearing these concepts in mind the compressor and turbine efficiencies, which reflects the isentropic efficiency for an essentially adiabatic process, is given by Cohen et al. (1987) as Equations 3.43 and 3.44 respectively. These relations are based on the assumption of using a mean specific heat over the relevant range.

$$\eta_c = \frac{T'_{compout} - T_{compin}}{T_{compout} - T_{compin}} \quad [3.43]$$

$$\eta_t = \frac{T_{gtin} - T_{gtout}}{T_{gtin} - T'_{gtout}} \quad [3.44]$$

When these efficiencies are given and the pressure ratios are known the temperature relations are then given by Cohen et al. (1987) for the compressor and turbine respectively as:

$$T_{compout} - T_{compin} = \frac{T_{compin}}{\eta_{comp}} \left((\Pi_{comp})^{\frac{\gamma-1}{\gamma}} - 1 \right) \quad [3.45]$$

$$T_{gtin} - T_{gtout} = \eta_{gt} T_{gtin} \left(1 - \left(\frac{1}{\Pi_{gt}} \right)^{\frac{\gamma-1}{\gamma}} \right) \quad [3.46]$$

3.3.4 Generator

The generator is used to generate electrical power ($E_{gt-elec}$) from the supplied shaft power from the turbine. The conversion efficiency includes both mechanical and electrical inefficiencies. The mechanical inefficiency arises from bearing friction and other parasitic losses. Electrical losses are due to the stator and rotor reaction causing resistive heating. Spelling (2013) used the following correlation.

$$\dot{E}_{gt-elec} = \eta_{mech_{gasgen}} \eta_{elec_{gasgen}} (\dot{E}_{gtout} - \dot{E}_{comp}) \quad [3.47]$$

3.3.5 Recuperator

The recuperator is modelled to use in the validation process of the Mercury 50™. The recuperator uses the exhaust heat to preheat the combustion air, thereby lowering the exhaust heat and increasing the Carnot efficiency of the system. A simple shell and tube heat exchanger is assumed and modelled using the logarithmic temperature difference method as explained under Chapter 3.2.4 for the heat exchangers used in the HRSG. A counter flow setup is assumed and a nominal pressure loss of 3 %. The surface area and overall heat transfer coefficient is estimated using design point temperatures and mass flows through the system. The recuperator is then removed for combined cycle application and replaced with the pressurised air receiver for the SUNSPOT cycle application.

3.3.6 Characteristic curves for the compressor/turbine combination

Every turbine and compressor unit have a specific operational curve that characterises the distinct properties and behaviour at various pressure drops, shaft speeds and mass flows. The accessibility of this data is very restricted due to commercial reasons. Using a specific turbine or compressor for this study requires such data and will also make it difficult to build a model that is robust and adaptable to different components. The compromise on experimental data for the curves can possible lead to less accurate results but the accuracy for certain turbines and compressors can be validated beforehand to give the user a sense of whether it has a significant effect on the results. The analytical expressions considered in this study stems from the work done by Zhang and Cai (2002) who derived these equations. They assumed that the analytical performance can be determined with quite high accuracy given that the individual component analytical performance resembles the real experimental performances reasonably.

The characteristic curves plotted for gas turbines and compressors uses corrected and non-dimensional characteristic speed, pressure ratio and mass-flow lines to represent the performance. These are calculated as follow.

$$N_{cor} = \frac{N}{\sqrt{T_{in}}} \quad N_n = \frac{N_{cor}}{N_{cor_{dp}}} \quad [3.48]$$

$$\Pi = \frac{p_{out}}{p_{in}} \quad \Pi = \frac{\Pi}{\Pi_{dp}} \quad [3.49]$$

$$\dot{M}_{cor} = \frac{\dot{M}_{in}\sqrt{T_{in}}}{p_{in}} \quad \dot{M}_n = \frac{\dot{M}_{cor}}{\dot{M}_{cor_{dp}}} \quad [3.50]$$

It is important to know that the above equations will be upheld for both the compressor and turbine even though for the rest of this document Equation 3.51 will be used for turbine pressure ratio.

$$\Pi_{gt} = \frac{P_{gt_{in}}}{P_{gt_{out}}} \quad [3.51]$$

After computation of the characteristic performance to ensure steady gas turbine running the following conditions are required. In an ideal system, ϕ and μ will be unity.

$$N_{gt} = N_{comp}; \quad \frac{G_{gt}}{G_{gt_{dp}}} = \frac{\mu G_{comp}}{G_{comp_{dp}}}; \quad \Pi_{gt} = \phi \Pi_{comp}$$

3.3.6.1 Expressions for compressor

$$\Pi_n = c_1 \dot{M}_{comp_n}^2 + c_2 \dot{M}_{comp_n} + c_3 \quad [3.52]$$

$$\eta_{comp_p} = \left(1 - c_4(1 - N_{comp_n})^2\right) \left(\frac{N_{comp_n}}{\dot{M}_{comp_n}}\right) \left(2 - \frac{N_{comp_n}}{\dot{M}_{comp_n}}\right) \quad [3.53]$$

With:

$$c_1 = \frac{N_{comp_n}}{p\left(1 - \frac{m}{N_{comp_n}}\right) + N_{comp_n}(N_{comp_n} - m)^2}$$

$$c_2 = \frac{p - 2mN_{comp_n}^2}{p\left(1 - \frac{m}{N_{comp_n}}\right) + N_{comp_n}(N_{comp_n} - m)^2}$$

$$c_3 = -\frac{pmN_{comp_n} - m^2N_{comp_n}^3}{p\left(1 - \frac{m}{N_{comp_n}}\right) + N_{comp_n}(N_{comp_n} - m)^2}$$

The values of these constants are therefore determined using the compressor specific values m , p and c_4 which must be found by trial and error. Zhang and Cai (2002) found these values to be 1.06, 0.36 and 0.3 respectively and for this study they will be used as the initial guesses and altered until they represent the design point conditions of the compressor. It is also important to ensure that $\sqrt[3]{p} \geq \frac{2m}{3}$ and that the flowrate results in an efficiency given on the negative slope of the curve. If it occurs before the curve turning point stalling occurs and the speed of rotation should be decreased.

3.3.6.2 Expressions for turbine

Assuming the design point values are known, the mass-flow and efficiency characteristics can be described by:

$$\dot{M}_{gt} = \dot{M}_{gt_{dp}} \alpha_r \sqrt{\frac{T_{gt_{in dp}}}{T_{gt_{in}}}} \times \sqrt{\frac{\Pi_{gt_n}^2 - 1}{\Pi_{gt_{dp}}^2 - 1}} \quad [3.54]$$

$$\eta_{gt_p} = \left(1 - t(1 - N_{gt_n})^2\right) \left(\frac{N_{gt_n}}{\dot{M}_{gt_n}}\right) \left(2 - \frac{N_{gt_n}}{\dot{M}_{gt_n}}\right) \quad [3.55]$$

With

$$\alpha_r = \sqrt{1.4 - 0.4 \times \frac{N_{gt}}{N_{gt_{dp}}}}$$

The parameter t is defined by Zhang and Cai (2002) to be 0.3 and will also be considered for this study.

3.3.6.3 Limitations to application

It is important to note that during normal operation the compressor can stall or surge when the mass-flow is reduced to such an extent that the airflow starts pulsating causing mechanical vibration and an increase in noise. It can be conservatively assumed that this phenomenon will only start occurring when the pressure ratio curves gradient tends to zero. Thus, the pressure ratio reaches a maximum for a certain speed (Dixon, 2010). Choking occurs as a result in resistance drop along the discharge line. This is due to an increase in mass-flow rate and therefore the tendency of some part of the compressor to reach sonic flow, in other words the Mach number tends to one. This point occurs at the same mass flow rate for any rotational speed. These two restrictions above will be mitigated by the following limits. The first is that the mass flow should be larger than that where the derivative of Equation 3.52 tend to zero and secondly there will be a basic upper limit applied to the mass-flow rate.

$$-\frac{c_2}{2c_1} < \dot{M}_{comp_n}$$

Equation 3.54 places the following restriction on the mass flow rate through the turbine:

$$\frac{M_{gt_n}^2}{\alpha_r} \times \frac{T_{gt_{in}}}{T_{0gt_{in}}} \times (\Pi_{0gt}^2 - 1) > -1$$

Chapter 4

Model description of solar components and thermal storage

4.1 General solar resource, optics and collection principles

4.1.1 Energy available from the sun

The sun radiates heat from its surface at an effective surface temperature, of which the value depends on the application of interest. The sun's heat is a result of thermonuclear fusion reactions in its core. For photovoltaic systems the measured peak wavelength is approximated for a temperature of 6 050 K to account for the spectral distribution of black-body emitters (Spelling, 2013). This study is interested in the solar thermal application of the sun's energy and therefore uses the temperature of 5 778 K approximated due to the radiation of black-bodies. Stine and Geyer (2001) estimated that the energy released at the core of the sun is 3.83×10^{17} GW. It is approximated that the energy originates from a single point and is equal to its resulting radiation intensity times the emittance area. Therefore, the intensity decreases as the distance from the sun increases. This is due to the inverse square relation for a spherical surface area ($A = 4\pi r^2$). The distance between the earth and the sun results in a radiation intensity of 1 367 W/m² (Stine and Geyer, 2001). This value is commonly referred to as the solar constant (I_{sc}). Due to the elliptical orbit of the earth the distance between the earth and the sun changes slightly. The solar irradiance (I_0) just outside the earth's atmosphere can then accurately be estimated by Equation 4.1 (Stine and Geyer, 2001). Variations of this equation do exist but for this research Equation 4.1 is deemed accurate enough.

$$I_0 = I_{sc} \left(1 + 0.034 \cos \left(\frac{360N}{365.25} \right) \right) \quad [4.1]$$

The amount of irradiation reaching the earth's surface is affected by the weather conditions and the angle of incidence. The atmospheric effects are due to a combination of ozone, dust, air molecules, dirt and vapour particles. Some irradiance is reflected or scattered back to the top of the atmosphere and some is diffused towards the earth. Diffuse radiation can still be used for thermal applications but for concentrated solar power DNI is a requirement. Of the initial solar irradiance, around 30-90 % is captured or reflected by atmospheric effects,

depending on the cloud cover (Stine and Geyer, 2001). The design point DNI is dependent on the site and usually it's 95th percentile value for that site is used. Typical meteorological year (TMY) data sets for some locations across the world are available. TMY is the typical weather set for each month, comprised and developed from historical data. This project implements data complimentary from SoDa-Pro[®] (CAMS radiation services, 2016).

4.1.2 Solar angles

For the collection of irradiation, it is important to know the exact angle between the surface of the collector and the sun ray. This angle is commonly referred to as the angle of incidence (θ_i) and Stine and Geyer (2001) gives its correlation as can be seen in Equation 4.2. The angle of incidence is therefore a function of the zenith angle (θ_z), the declination angle (δ) and the hour angle (ω).

$$\theta_i = \cos^{-1}(\sqrt{\cos^2(\theta_z) + \cos^2(\delta) \sin^2(\omega)}) \quad [4.2]$$

The reason the angle is of such importance, especially for heliostat field arrays, is due to the cosine effect. The cosine effect is the reduction of irradiance by the cosine of the angle of incidence. Figure 14 shows how this practically applies for objects outside the atmosphere where the angle of incidence is equal to the zenith angle. The incident angle at any location on the earth's surface can be determined using the location and temporal data available. Temporal data is used to determine both the hour angle and the declination angle as seen in Figure 15.

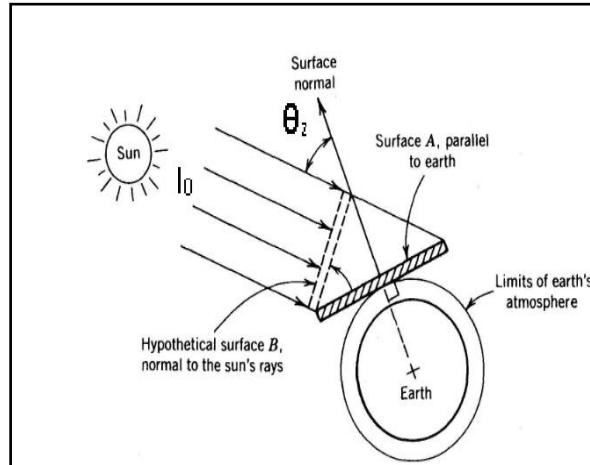


Figure 14: The cosine effect (adapted from Stine and Geyer, 2001)

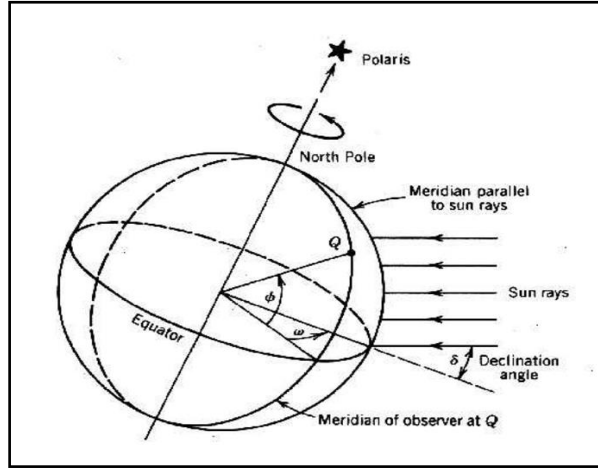


Figure 15: Declination, hour and latitude angle representation by Stine and Geyer (2001)

The hour angle represents the earth's periodical rotation around its polar axis and is 15° per hour (Equation 4.3). For the hour angle calculation, the solar time is required and not the conventional time. The equation of time (EOT) is used to calculate the respective time for the specific day of the year. Stine and Geyer (2001) represents an approximate version of the EOT by Equation 4.5 and this is deemed accurate for system performance analysis but not for control tracking implementation due to its variance of up to 30 seconds. The value for N starts at one for the first day of January and considers leap years. The solar time is accurately estimated by Equation 4.4 as a function of the local clock time (LCT), longitudinal correction (LC) and the EOT. The LCT is corrected for active daylight savings, thus the subtraction of an hour. The longitudinal correction is the difference between the local longitude and the longitude of standard time zone meridian normalised to 15° .

$$\omega = 15 \times (t_s - 12) \quad [4.3]$$

$$t_s = LCT + \frac{EOT}{60} - LC \quad [4.4]$$

$$EOT = 0.258 \cos(x) - 7.416 \sin(x) - 3.648 \cos(2x) - 9.228 \sin(2x) \quad [4.5]$$

$$x = \frac{360}{365.242} \times (N - 1) \quad [4.6]$$

The declination angle is defined as the angle between a sunray and the equatorial plane as seen in Figure 14. This angle depends on the day of the year as seen by Equation 4.7. At the summer and winter solstices this angle reaches a maximum and minimum of 23.45° and -23.45° respectively. Twice a year the declination angle would be zero and observed on the equator as the sun shining from precisely above during noon. These conditions are referred to as equinox.

$$\delta = \sin^{-1}(0.3979 \cos(0.98563(N - 173))) \quad [4.7]$$

The last angle necessary to calculate the angle of incidence is the zenith angle. This is mostly referred to as the complement of the altitude angle (α) which is the angle between the central ray from the sun and the horizontal plane from which this ray is observed. Stine and Geyer (2001) gave the correlation for the zenith angle by Equation 4.8 as a function of the declination, hour and latitude angle(φ). The latitude angle represents the angle between the equatorial plane and the line drawn from the observing point to the centre of the earth.

$$\theta_z = 90^\circ - \alpha = 90^\circ - \sin^{-1}(\sin(\delta) \sin(\varphi) + \cos(\delta) \cos(\omega) \cos(\varphi)) \quad [4.8]$$

4.1.3 Other collection principles and challenges

The amount of irradiance measured is a combination of the DNI and the global horizontal irradiance (GHI). For concentrating principles, the DNI is of interest, with the GHI only playing a role in the thermal heating of piping. For this project such detail will not be necessary to consider. The DNI is the amount of irradiance coming directly from the sun that has not been reflected or absorbed. The DNI levels are dependent on the amount of atmosphere it must travel through. This is determined by the zenith angle and the height above sea-level and a common metric used to quantify this phenomenon is called the air-to-mass (AM) ratio. Twidell and Weir (2006) gave the correlation for AM in Equation 4.9.

$$AM = \sec(\theta_z) \quad [4.9]$$

CSP is concerned with focusing the sun's rays to increase the heat flux on a certain area. Not only the DNI and its general optics are important but also the method of concentrating the sun rays. Sun rays can be focused in two or three dimensions, or in other words, along a line or to a point respectively. Spelling (2013) showed in detail how line focussing systems can only reach concentration ratios (CR) of 208 where a CR of 43 400 can be reached for point focussing systems. The CR is the ratio between the aperture area and the receiver area. This value is found using the law of etendue conservation, which is another way of saying radiation is conserved. Etendue is defined as the product of the area through which the radiation passes and the square of the solid angle accompanied with it as shown in Equation 4.10 and seen in Figure 16. The aperture solid angle is a function of the distance between the sun and earth and the sun's circumference and is estimated at 4.8 mrad (Spelling, 2013). Maximising the CR, it is thus necessary to assume that the receiver solid angle is 90° resulting in the CR value of 43 400. For a two-dimensional concentration the areas are replaced with aperture widths and only the solid angle thus giving the maximum as the square root of the three-dimensional CR.

$$A_a \sin^2 \theta_a = A_r \sin^2 \theta_r \quad [4.10]$$

Also written as

$$\frac{A_a}{A_r} = \frac{\sin^2 \theta_r}{\sin^2 \theta_a} = CR_g \quad [4.11]$$

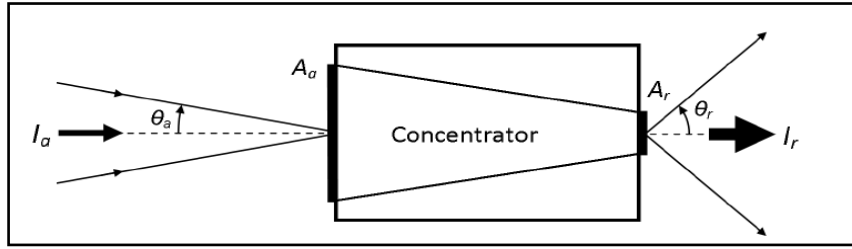


Figure 16: The conservation of etendue by Spelling (2013)

A final concern on optics concentration is focussed on the receiver's ability to retain the heat absorbed. Heat in the form of concentrated irradiance is absorbed by the receiver and would then typically be transferred to a HTF. The amount of irradiance that reaches the receiver depends on the CR of the concentrator, optical efficiencies and the solar field efficiencies that will be described in Chapter 4.2. However, a component of the heat absorbed is lost due to convection and radiation of the receiver. Convection is driven by the temperature difference between the receiver and ambient air around the receiver area. The thermal coefficient is assumed constant over the receiver and manufacturer specific. The receiver also radiates temperatures back to the sky at a rate consistent with the difference between the square of squares of the receiver temperature and the outer sky temperature. Due to the transparency of air, when a body on earth radiates energy towards the atmosphere the temperature difference between the body and the sky should refer to a sky temperature higher up in the air. The common estimate for the sky temperature is given as being 6 °C less than the ambient temperature (Twidell and Weir, 2006). The other constant involved with the radiative heat loss is the Stefan Boltzman constant (σ), the receiver emittance (ε) and the surface area of the receiver. It can be concluded that the loss function is dominated by radiation at very high temperatures and the total heat absorbed is given by:

$$\dot{Q}_{abs} = \alpha_{abs} \eta_{opt} \dot{Q}_{rec} - \dot{Q}_{conv} - \dot{Q}_{rad} \quad [4.12]$$

With

$$Q_{rec} = (\eta_{SF} CR) I_{DNI} A_r \quad [4.13]$$

$$Q_{conv} = A_r U_{conv} (T_r - T_a) \quad [4.14]$$

$$Q_{rad} = A_r \varepsilon_r \sigma (T_r^4 - T_{sky}^4) \quad [4.15]$$

The solar thermal efficiency of the concentrator and receiver is expressed (Equation 4.16) as the ratio between the heat absorbed and the irradiance available over the aperture area. In Figure 17, the optical limit can be seen for the maximum CR value.

It can be seen clearly that for the application to gas turbines that a very high concentration ratio is required to achieve the desired temperature at an acceptable efficiency.

$$\begin{aligned}\eta_{solar_{thermal}} &= \frac{\dot{Q}_{abs}}{A_a I_{DNI}} & [4.16] \\ &= \frac{\alpha_{abs} A_r (\eta_{SF} \eta_{opt} CR) I_{DNI} - (A_r U_{conv} (T_r - T_a) + A_r \epsilon_r \sigma (T_r^4 - T_{sky}^4))}{A_a I_{DNI}} \times \left(1 - \frac{T_a}{T_r}\right) \\ &= \alpha_{abs} \eta_{SF} \eta_{opt} - \frac{U_{conv} (T_r - T_a) + \epsilon_r \sigma (T_r^4 - T_{sky}^4)}{CR \times I_{DNI}} \times \left(1 - \frac{T_a}{T_r}\right)\end{aligned}$$

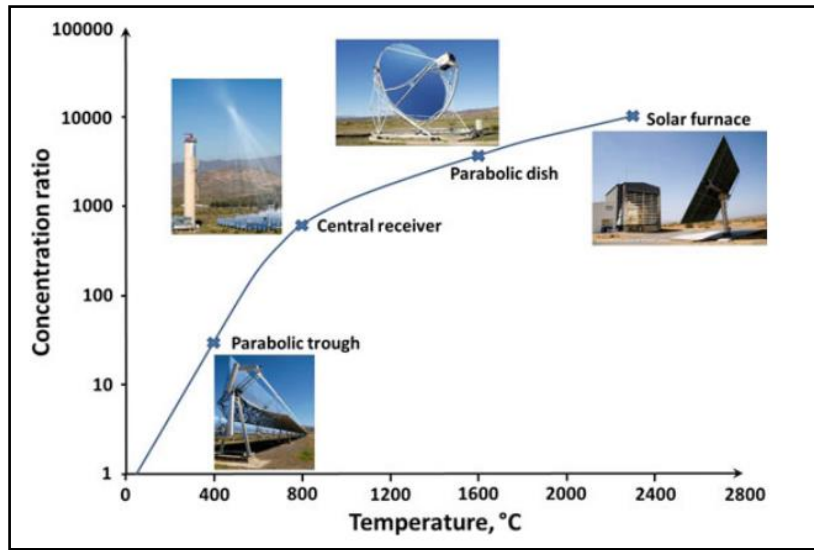


Figure 17: Concentration ratios required for reaching various absorption temperatures (Roldán Serrano, 2017)

4.2 Collector: Heliostat field and tower

The heliostat field is used to focus the DNI onto a single point or area. The efficiency by which these rays are focussed is defined as the ratio of the total thermal irradiation concentrated on the receiver over the total available DNI. It is common practice to approximate this efficiency as a product of multiple efficiencies that includes losses due to blocking, shading, the cosine effect, reflectance, cleanliness and availability.

$$\eta_{SF} = \eta_{block} \eta_{shade} \eta_{cos} \eta_{refl} \eta_{clean} \eta_{available} = \frac{\dot{Q}_{rec}}{I_{DNI} A_{SF}} \quad [4.17]$$

Some of these losses are purely a function of the solar incidence angle and heliostat field orientation. Assuming that the heliostat field is in a circular form and evenly distributed, Gauche et al. (2012) showed that the optical efficiency of the field can be given by the polynomial in Equation 4.18. This efficiency accounts for blocking, shading and cosine losses. It is based on the GemaSolar plant and assumes that the heliostat field and tower remain unchanged during optimisation.

$$\eta_{optical} = 0.4254\theta_z^6 - 1.148\theta_z^5 + 0.3507\theta_z^4 + 0.755\theta_z^3 + 0.5918\theta_z^2 + 0.0816\theta_z^1 + 0.832 \quad [4.18]$$

The reflectance efficiency is dependent on the design and material of the heliostat and is therefore a constant value, as with the cleanliness that can be controlled due to diligent maintenance. Kolb (2011, pg. 20) gave these values as 0.94 and 0.95 for reflectance and cleanliness respectively. Assuming a surround field as for Gemasolar, except for the power ratio of 2 between north and south, he gave the heliostat availability as 0.99, which is sufficiently accurate for this research.

The size of the heliostat to be used in this project is estimated using a correlation given by Dersch et al. (2011). Approximating that a 640 MW plant will use heliostats with a reflective area of 200 m² the generic size of the heliostat is given by Equation 4.19. This is based on the Sanlucar 120 heliostats used by PS10 and PS20 which are larger than the Gemasolar plant whose heliostats have a reflective area of 120 m² (Gauche et al., 2012). This results in a conservative application of Gauche's polynomial. The accompanying tower height is then also given by Equation 4.20.

$$A_{heliostat} = 200 \sqrt{\frac{Q_{rec}}{640MW}} m^2 \quad [4.19]$$

$$h_{tower} = 36.7 \dot{Q}_{rec}^{0.288} m \quad [4.20]$$

4.3 Central receiver system: Pressurised air receiver

The CRS consists of the tower and a receiver. For the SUNSPOT cycle this receiver needs to be pressurised and currently two major types of receivers are currently being investigated. These are typically tubular receivers and volumetric cavity receivers. This project focusses on volumetric receivers due to the high temperature ranges they function in. As a standard, the receiver used in the SOLGATE program is used. Tests done by Dr Rainer Buck in 2005 showed that the receiver reached an outlet temperature of 1 030 °C (Heller, 2016). Heller (2016) argued that this was due to a very conservative window cooling mechanism that was fitted and that temperatures around 1 100 °C can be reached. The DLR deems that current

pressurized receivers can withstand pressures up to 15 bar (Ushyne, 2008). The pressurized air receivers are a likely solution but a lot of R&D is still required for such high temperature and pressure applications. This project assumes that the necessary R&D will allow the use of such a receiver for power generation in the near future, with the application of conservative parameter selection. The report on SOLGATE (2005) confirmed the previous assumption due to the current research being done on window cooling. The blower used for this purpose consumes parasitic energy equal to 0.2 % of the total electricity generated by the gas turbine.

The receiver's ability to absorb heat is a function of the optical efficiency of the glass covering and the absorptivity of the porous material. Thermal losses by the receivers can be accounted for by convection and radiation. At high temperatures this loss function is dominated by the radiation component and therefore, to remove the requirement to establish a complicated heat transfer coefficient, it is assumed that only the radiative losses are significant (Spelling, 2013). The heat gained by the compressed air is given by Equation 4.21. The average temperature of the air inside the receiver is a sufficient approximation as is also used in the TRNSYS® (Thermal Energy System Specialists, 2017) library developed by Schwarzbözl et al. (2002). They validated the assumption of approximating the porous material as a black body absorber with a certain absorptivity (α_{abs}). According to Heller et al. (2016) the porous material used for the SOLGATE receiver system is a ceramic foam called silicon carbide (SiC) that has been coated with another silica layer and tempered to achieve an absorption efficiency of 96 %. Ceballos-Mendivil et al. (2013) argued that SiC is an advantageous material to use for receivers due to its high melting point, absorption, porosity and its thermomechanical properties at high temperatures. For a temperature range between 600 and 1 500 K, according to Cengel and Ghajar (2015), the emissivity of SiC ranges between 0.87 and 0.85. Even though the receiver is to operate at higher range, for this investigation the more conservative value of 0.87 will be used. Developed receivers require secondary concentration in the form of a compound parabolic concentrator (CPC). This reflector has its own optical efficiency which can be assumed to be 86 % if no detailed solar field data is provided (Heller, 2016).

$$\dot{Q}_{abs} = \eta_{opt} \alpha_{abs} \eta_{CPC} \dot{Q}_{rec} - A_{rec} \epsilon_{rec} \sigma (T_{air_{avg}}^4 - T_{sky}^4) \quad [4.21]$$

Heller (2016) used the experimental data that was derived from the work done by Buck in 2005 to establish a correlation for the total thermal efficiency of the receiver. To be very conservative in its approximation, only efficiencies below 90 % were curve fitted along with an extra 5 % deduction in efficiency. This resulted in Equation 4.22. This correlation is used to verify assumptions highlighted in the previous paragraph.

$$\eta_{rec_{thermal}} = 0.956 - 1.7 \times 10^{-4} T_{rec_{out}} [K] \quad [4.22]$$

Spelling (2013) gave a correlation (Equation 4.23) for the optical efficiency as a function of the operating pressure. At higher pressures, thicker glass is required to

withstand it, therefore decreasing the optical efficiency. Experimental data from the SOLGATE receiver is given as 6.5 bar and 87 % for the nominal operating pressure and efficiency respectively.

$$\log(\eta_{optical}) = \frac{P_{rec}}{P_{nom}} \log(\eta_{optical_{nom}}) \quad [4.23]$$

4.4 Thermal storage: Packed rock-bed storage

Kröger (2011), Heller and Gauché (2013) and Allen (2015) proposed that the thermal energy storage (TES) system for the SUNSPOT cycle be a non-pressurised rock bed storage. Using dolerite rock from the surrounding area in South Africa, this offers a great reduction in costs for the thermal storage. Allen (2010) also showed that the dolerite proved very resilient to thermal cycling as would be typical in this application. Course dolerite has an average particle diameter (d_p) of 39 mm, volumetric diameter (d_v) of 49 mm, specific heat of 815 J/kg K (between 50-60 °C) and conductivity (k_p) of 2-2.5 W/m K. The thermal heat capacity implemented by Allen et al. (2015) is a function of temperature in degrees Celsius given by:

$$c_{p,r} = -0.00129T_p^2 + 1.518T_p + 748 \quad [4.24]$$

The most important aspects of the storage that is required to be modelled for this research study is the heat transfer capability and the associated pressure drop through the system. Heller (2016) described the thermal model of the TES in Equation 4.25 by referring to a corrected effectiveness-number of transfer units (E-NTU) method. The correction in this equation accounts for the temperature gradients inside of larger particles.

$$NTU^* = \frac{h_v L}{\dot{m} c_{p,f}} \times \frac{20}{\frac{3h_v d_p^2}{4k_f(1-\epsilon)} + 20} \quad [4.25]$$

With

$$h_v = h \left(\frac{6(1-\epsilon)}{d_p} \right) \quad [4.26]$$

$$G = \frac{\dot{m}_f}{A_{cs}} \quad [4.27]$$

The E-NTU is given as a function of the area specific heat transfer coefficient (h), air mass flow rate (\dot{m}), bed length (L), specific heat capacity of the HTF ($c_{p,f}$), particle diameter (d_p), thermal conductivity of the HTF (k_f) and the void fraction of the bed (ϵ). Allen et al. (2015) showed that using a simple estimate for the Nusselt number using Equation 4.28 where the area surface heat transfer is thus expressed in terms of the volume-equivalent sphere diameter. This estimate was proven

satisfactory at high temperatures and mass fluxes greater than 0.2 kg/m²s. The conditions required to implement this Nusselt number correlation is a Biot number smaller than 0.2 and it was validated against other familiar and recognised correlations at $0.35 < \epsilon < 0.45$, $0.009 < d_v < 0.049$ and $80 < Re_{pv} < 600$.

$$Nu = \frac{hk_f}{d_p} = Re_{pv}^{0.6} \quad [4.28]$$

Where

$$Re_{pv} = Re_v(1 - \epsilon) = \frac{\rho v_s d_v}{\mu} = \frac{G d_v}{\mu} \quad [4.29]$$

$$v_s = \frac{\dot{m}}{\rho A_{cs}} \quad [4.30]$$

$$Bi = \frac{h d_v}{2k_p} \quad [4.31]$$

$$d_v = \left(\frac{6}{\pi} \left[\frac{1}{n} \sum_{i=1}^n V_{pi} \right] \right)^{\frac{1}{3}} \quad [4.32]$$

The pressure drop formulation is the second important aspect of the model. This is because of the adverse effects that backpressure has on gas turbine operation. Allen et al. (2015) gave the correlation for the friction factor over the bed due to co/counter current flow as Equation 4.33. The constant in this equation has been determined empirically and validated with experimental data. Values for the void fraction, volumetric diameter and Reynold's number ranged between 0.38-0.46, 9-30 mm and 100-1 000, respectively.

$$f_v = \frac{620}{Re_v} + \frac{13.7}{Re_v^{0.08}} \quad [4.33]$$

Heller (2016) then gave the pressure drop as Equation 4.34 by adding a correctional friction factor, stating that this accounts for the degradation of the rock due to thermal cycling. The pressure drop is thus a function of these friction factors, the bed length, void fraction, fluid properties and dimensions and a superficial approach flow velocity (U_{sf}).

$$\Delta p = f_{cor} f_v \left(\frac{L \rho_f U_{sf}^2}{2 d_v} \right) \left(\frac{1-\epsilon}{\epsilon^3} \right) \quad [4.34]$$

For this study rock bed properties similar to Heller (2016) is used. The void fraction in the bed is assumed to be 0.45, with a thermal conductivity and density of 2.5 W/mK and 2 657 kg/m³, respectively. These values are required to calculate the require storage volume for a certain capacity.

$$Q_h = V_{required} ((1 - \epsilon) \rho_r c_{p,r} + (\epsilon) \rho_f c_{p,f}) \quad [4.34]$$

Chapter 5

Thermo-economic considerations

Thermo-economic indicators are used to compare different types of power plants with one another objectively. They are likely to include the initial capital expenditure (CAPEX), operation and management expenditure (OPEX) and annual plant yield. There are various performance indicators, especially on a financial basis such as the net present value, debt-service coverage ratio and internal rate of return. These are pure financial indicators and this study will only focus on one indicator that combines both the economic and thermodynamic side of the plant.

The principle cost measure to be used to evaluate the systems with is the levelized cost of electricity (LCOE). This measure is used extensively across the world to evaluate power generating systems. Equation 5.1 shows that this measure takes into consideration the capital (CAPEX) and operating (OPEX) cost as well as the annual yield (E_{annual}) and a fixed charged rate (crf) as given by Heller (2016). This rate is a function of both the annual interest rate (k_d) and lifetime (n) of project. Pitz-Paal et al. (2003) gave the typical interest rate to be 8 % with a plant lifetime of 30 years. The following chapter contains a summary of the specific CAPEX and OPEX costs as used by Spelling (2013), Pitz-Paal et al. (2003), Solgate (2005) and Heller (2016).

$$LCOE = \frac{crf \times CAPEX + OPEX}{E_{annual}} \quad [5.1]$$

$$crf = k_d \times \frac{(1+k_d)^n}{(1+k_d)^n - 1} \quad [5.2]$$

5.1 CAPEX

The CAPEX component is further expressed as the sum of the engineering, procurement and construction (EPC) cost for the power block, thermal storage, solar field and air receiver. The procurement costs towards these areas are specific costs relating to the sizing or specifications of the components as can be found in Table 2. The costs used by Spelling (2013) were scaled by a factor (Equation 5.3) using the Marshall and Swift index to evaluate the relevant 2010 dollar value from the original published date from his sources. This project's data is presented for 2017 and no Marshall and Swift Index data is available after 2012. The alternative is to use the Nelson-Farrer index by the Oil&Gas Journal (Nelson-Farrer Cost Index, 2017). This index has historically correlated well with the Marshall and Swift index.

$$f_{MS_{2010}} = \frac{I_{MS_{2010}}}{I_{MS_{ref}}} \quad [5.3]$$

The sizing for the Brayton and Rankine cycle are of the same scale that was described in the Solgate (2005) project, so for the power block components these values are rather used. They also implemented the Mercury 50™ gas turbine making these costing estimates very accurate. The bottoming cycle used in this study is of similar size to the one used for the 16.1 MW plant studied in the Solgate (2005) project. These costs need to be scaled from 2005 to 2017 using the Nelson-Farrer index. Spelling (2013) gave the values as 1 942 for 2005 and 2 338 for 2010. The index value for December 2016 will be used as the 2017 value which was given as 2 649.9 on the Oil&Gas Journal website (Nelson-Farrer Cost Index, 2017). Values in euro are also scaled to dollar using the average exchange rates of those years as given by the OFX Group Ltd online. Results are given in both euro and rand for international and national comparisons. The specific cost for the thermal storage and high-pressure air receiver is given by Heller (2016) whose studies were based on work done by Buck in 2005, the Solgate (2005) project for the receiver and for the thermal storage research by Allen et al. (2016). The other specific costs related to the solar field, control and receiver tower are also deduced from the Solgate (2005) project. The cost assumptions are extremely conservative in the fact that they do not take any technology maturation into account.

Table 2: Specific cost estimates for components of the SUNSPOT cycle

Component	2017 Cost Value	Unit	Reference value	Original Source
Mercury 50 Gas Turbine (Conventional)	394.210	€/kW _e	Gas Turbine electric output	Solgate (2005)
Mercury 50 Gas Turbine (Solar retrofitted)	1 062.962	€/kW _e	Gas Turbine electric output	Solgate (2005)
Bottoming cycle (Steam turbine and HRSG)	818.713	€/kW _e	Steam Turbine electric output	Solgate (2005)
Solar heliostat field	180.153	€/m ²	Aperture area	Solgate (2005)
Pressurised air receiver	235.082	€/kW _{th}	Thermal heat absorbed by HPRS	Heller (2016)
Thermal rock bed storage	11.693	€/kWh _{th}	TES Capacity	Heller (2016)
Central receiver tower	16 565.286	€/m	Tower height	Solgate (2005)
Control and automation	614.035	k€	-	Solgate (2005)

The construction and engineering costs is given as a fraction of the procurement costs. The cost of installation is estimated by Spelling (2013) to be 20 % of the cost of procurement, which is the same as used in the Ecostar (2005) report. Spelling (2013) further used a reference value to scale for the civil costs associated with the power block setup (Equation 5.4). The reason is that the power block for this system is more expensive due to technology innovations and the civil cost is not affected by this. The reference cost (C_{civil_ref}) value is 7.6 million USD for a reference plant of 52.8 MW_e power output.

$$C_{PBcivil} = c_{civil_{ref}} \left(\frac{E_{gen}}{E_{ref}} \right) \quad [5.4]$$

The total civil construction and installation costs is thus given by Equation 5.5. It is assumed that the civil costs in this case will include engineering and contingency costs (Ecostar, 2005) therefor the total EPC costs is given by Equation 5.6. The purchase cost for land in this area ranges from 5 000 to 10 000 R/hectare for poor agricultural areas which results in a very low addition to the total CAPEX (0.02 % of solar field cost) and is excluded from this study.

$$C_{civil} = C_{PBcivil} + 0.2(C_{procurement} - C_{PB}) \quad [5.5]$$

$$C_{EPC} = C_{procurement} + C_{civil} \quad [5.6]$$

5.2 OPEX

5.2.1 Power block and equipment repair costs

The operations and management (O&M) cost are derived from the Ecostar (2005) report. These values are transposed from 2005 to 2017 using the Nelson-Farrer index given above. The report assumes a fixed O&M for the power block at 36.84 €/kW and variable cost of 3.41 €/MWh generated. A general assumption of 1 % of the total plant procurement cost is assumed for the O&M of all the other equipment of the plant (Ecostar, 2005).

5.2.2 Labour costs

The labour costs are deduced from the work done by Spelling (2013) and Table 3 outlines the resulting values used for this study. Labour cost per specific employee is described which is more accurate than the average value assumed in the Ecostar (2005) report for the assumed number of 30 employees. Spelling (2013) uses data from Ecostar (2005) and NREL to calculate the amount of solar field technicians and control room operators using Equations 5.7 and 5.8 respectively. The constants recommended are three technicians per 100 000 m² of aperture area ($\eta_{solTech}$) and two control room operators per 100 000 m² of aperture area ($\eta_{control}$). The salary values are given for the year 2010. The labour cost is transposed to 2017 using the South African labour index values of 100 (2010) and 142 (2017) found on Trading Economics (2017). For the conventional CCPP the solar specific employees are acquitted such as the field technicians and control room operators.

$$N_{solTech} = 1 + \eta_{solTech} A_{HS} N_{HS} \quad [5.7]$$

$$N_{control} = 1 + \eta_{control} A_{HS} N_{HS} \quad [5.8]$$

Table 3: Labour costs transposed to 2017, adjusted from Spelling (2013)

Employee type	Number of employee	Salary USD/yr
Plant Manager	0.25	134 900
Plant Engineer	1	130 640
Maintenance Supervisor	1	68 160
Power Block Technician	1	56 800
Solar Field Technician	$N_{solTech}$	56 800
Operations Manager	1	119 280
Control Room Operator	$N_{control}$	56 800

5.2.3 Fuel costs

The fuel cost used are the same as that applied by the updated IRP (2016) for both the open cycle gas turbine and combined cycle gas turbine plants. This value is expressed 115.5 R/GJ combusted fuel. The fuel price in South Africa has remained relatively stable at the same value from 2015 to 2017 and this report thus assumes that the value from the IRP (2016) is still valid for 2017. Due to the transport of the fuel a 20 % levy is added to the fuel cost.

5.2.4 Water usage

The water usage of the SUNSPOT cycle is due to two factors namely the washing of the heliostats and of the compressor. Spelling (2013) gave Equations 5.9 and 5.10 to account for these two respectively. The volume of water required to wash the heliostats is a function of the total aperture area and a specific water consumption (v_{HS}) which is given as 50 litre/m²/yr. The compressor is assumed to be washed online and Equation 5.10 gives the annual water requirement at a certain washing frequency per year (f_{wash}) with an absolute (v_{c0}) and specific (v_{c1}) water consumption of 90 litre and 0.5 litre/kg/s (Spelling, 2013). The cost of municipal water in Cape Town, South Africa at the beginning of 2017 is given by City of Cape Town (2017) for level 1 industrial water consumption to be 22.38 R/m³.

$$V_{waterHS} = v_{HS}N_{HS}A_{HS} \quad [5.9]$$

$$V_{waterComp} = f_{wash}(v_{c0} + v_{c1}\dot{M}_{comp}) \quad [5.10]$$

Chapter 6

Design criteria and validation of components

6.1 Site selection

The selection of the right site has a significant impact on the power plant performance. Two parameters that have a high degree of impact on a solar power plant's performance is the average ambient temperature and 95th percentile value of typical DNI. Gas turbines operate more efficiently and at a higher output at lower altitudes due to the higher density of the air. Regarding the cost of the plant the general distance to the fuel source and electricity grid plays a significant role. The values for these parameters of each site is given in Table 4. The distance to an electricity gridline is given qualitatively as such estimates is hard to make accurately. Figure 18 shows the typical distribution of these parameters over South Africa.

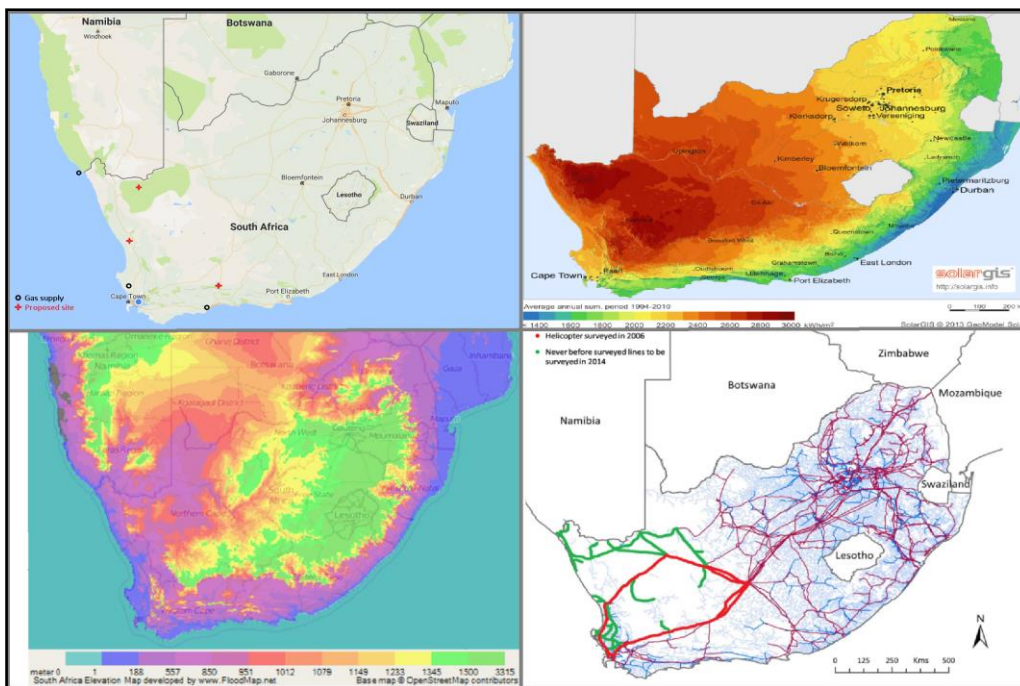


Figure 18: South African maps showing (clockwise from the top left) the locations of proposed sites and gas supplies, irradiation, the national electricity gridline and elevation

Site specific simulations will take long to construct and evaluate with regards to one another. The decision had to be made beforehand using multi criteria decision analysis (MCDA). Two different decision-making tools are used, one that has objective scales and another that is more comparative in nature. The simple attribute rating technique (SMART) was designed by Ward Edwards (Von Winterfeldt & Edwards, 1986) to give an objective method of making decisions. The process and results of using this method is given in Appendix A.1. The SMART method showed that Vredendal is by far the most beneficial with Prince Albert, Aus and Arandis grouped together second with similar results. To validate this another decision making theory is utilised called the Analytical Hierarchy Process (AHP). This method is different in that the site parameters are regarded in preference with one another individually and then the sites are compared with respect to the best option of that site parameter. This method is preferred to SMART due to its qualitative versatility and pairwise considerations. It however lacks the numerical consistency inherent to SMART. Appendix A.2 shows how this method is used and the result it produced. Fortunately, it produced the same decision outcome for the best option being Vredendal with a different priority in 3rd to 5th best options. Vredendal is thus the site selected for this study.

Table 4: Site specific parameters

Location	DNI95 [W/m ²]	Altitude [m]	Average ambient temperature [T]	Distance to grid	Distance to gas reserve [km]
Prince Albert	1 006.5	869	290.3	Moderate	190
Aggeney's	1 028.8	694	291.7	Moderate	650
Vredendal	988.3	315	291.1	Close	260
Aus	954.4	534	291.6	Moderate	125
Arandis	924.0	530	293.0	Close	92
Kokerboom	989.3	1 017	293.7	Moderate	555

6.2 Power block selection and integration

The Mercury 50TM gas turbine was selected for this study. It has already been tested experimentally in a solar retrofit setup for the SOLGATE project (Solgate, 2005). Here, the recuperator was exchanged with a pressurised air receiver and heliostat collector field by which it is charged. It has also been verified by Teraji (2005) to outperform a majority of commercially available gas turbines in the 4 to 8 MW range. In another report he also commented that the Mercury 50TM is well equipped for CSP tower integration and has been designed to be compatible with high inlet temperatures to the combustor (Teraji, 2015). Reports from Kurz (2005) and Teraji (2005) are used to characterise the turbine for this study's purposes. The gas turbine is rated at 4.6 MW_{el}. Steam turbines become less efficient the smaller their capacities are therefore two gas turbines are implemented. Assuming a 40 % contribution by the steam turbine to the total power output at design point, the steam turbine should be rated at approximately 6 MW_{el}. An ideal steam turbine for this is the Siemens Steam Turbine SST-060 or SST-110. It can operate up and to a

maximum of 131 bar and 530 °C live steam conditions. Both the gas and steam turbine steady state models are validated and confirmed to be an accurate representation of off-design performance. This validation is found in Sections 6.2.1 and 6.2.2. Appendices C.1 and C.2 contain the simulation protocols of the Brayton and Rankine cycles respectively.

The design point of the HRSG is found by trial and error, using the specifications for the steam turbine as described in Table 7, Section 6.2.2. It is ensured that with the resulting HRSG specifications that an evaporator approach temperature at the lowest possible ambient temperature is still greater than 0 °C. The resulting HRSG parameters are displayed in Table 5 for Vredendal at an altitude of 315 m and an average temperature of 18 °C.

Table 5: HRSG design point parameters

Parameter	Value	Unit
Overall heat transfer coefficient (HRSG)	159.501	W/K
Overall heat transfer coefficient (Super heater)	23.597	W/K
Overall heat transfer coefficient (Evaporator)	77.548	W/K
Overall heat transfer coefficient (Economiser)	101.528	W/K
Overall heat transfer coefficient (Condenser)	1 213.830	W/K

6.2.1 Validation of gas turbine model

The Mercury 50™ have been used by numerous authors for application in solar hybrid cycles and is therefore chosen for this study as well. Table 6 shows the design point parameters of the Mercury 50™ as used to validate the model. The data in the table represents values used for the Solugas project by Teraji (2005), Kurz (2005) and Ushyne (2005). With performance data of the Mercury 50™ not commercially available, the author relied on assumptions and data from other authors to build the model. At a turbine inlet temperature close to 1 100 °C the polytropic efficiencies are assumed to be that for a mid-range technology level with single stage cooling (Spelling, 2013). Spelling (2013) also used a constant pressure drop through the combustion chamber of 4 %. For this project a value of 5 % is assumed to incorporate a more conservative approach for the fact that such high inlet temperature combustors have not been developed this well yet. Other data such as the turbo machinery's mechanic efficiencies are estimated to be 99 %. The data used to validate the Mercury 50™ performance is provided by Ushyne (2008) and they sourced it directly from TurboMach, the manufacturers. With most of the design point parameters for the turbine section in place the recuperator's pressure drop is calculated thermodynamically to result in the required pressure drop over the turbine. As can be seen in Figure 19 the simulation represents the operational data well with some small deviation in the low and high temperature ranges. The simulation results are compared to the results from Ushyne (2008) in Appendix B.1 where they used a simulation tool called IpePro. It is seen that they had similar problems but also described their results as accurate enough to employ for transient simulations. The thermal efficiency of a cycle is dependent on the LHV of the fuel

used. To make a fair comparison the LHV is calculated from representative data of the Ushyne project (2008). A value of 48.36 MJ/kg is calculated and is used throughout this study.

Table 6: Design point parameters for the Mercury 50™

Parameter	Value	Unit	Reference
Power rating	4 600	kW	Teraji (2005)
Turbine inlet temperature	1 435	K	Ushyne (2008)
Exhaust flow rate	17.7	kg/s	Ushyne (2008)
Pressure ratio – Compressor	9.9	-	Teraji (2005)
Rotational speed	15 000	rpm	2014 Performance Specs
Turbine polytropic efficiency	87	%	Spelling (2013)
Compressor polytropic efficiency	88	%	Spelling (2013)
Ambient temperature	288	K	Ushyne (2008)
Combustion chamber pressure drop	5	%	Assumed
Recuperator pressure drop	3	%	Calculated

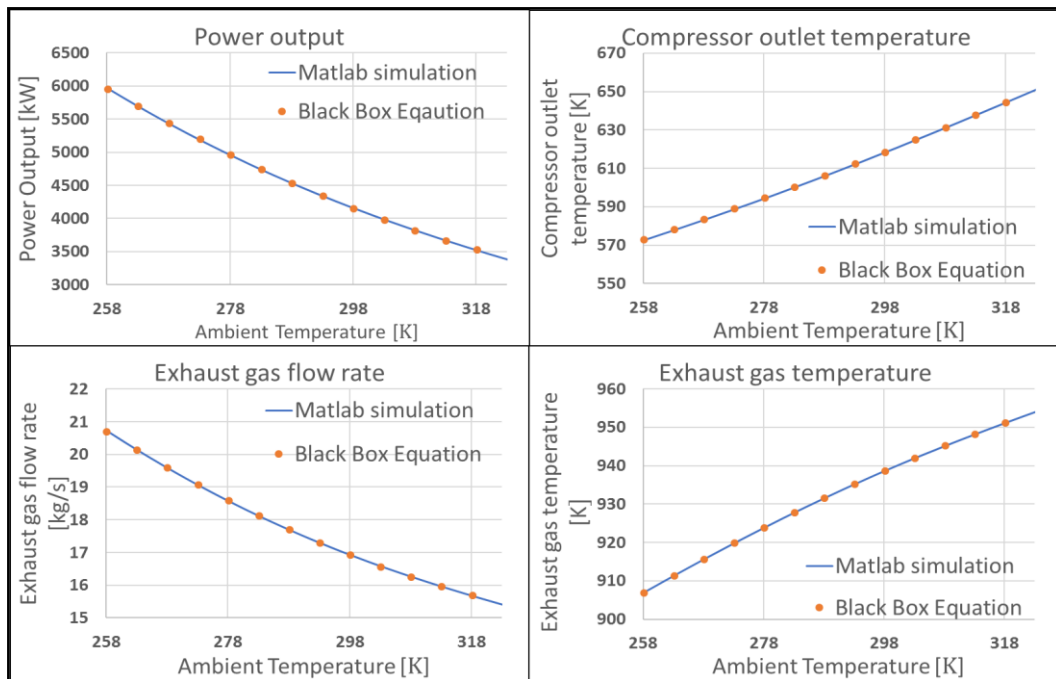


Figure 19: Matlab simulation results compared with validation data

6.2.2 Validation of steam turbine and HRSG models

The SST-060 design point parameters are given in Table 7 as deduced from the technical brochure (Siemens, 2017). The multiple efficiencies are again compiled from numerous authors that has done work on small scale steam turbines. In the technical manual for SAM, Wagner and Gilman (2011) stated that for steam turbines implemented for CSP at the output level of a typical 10 MW turbine can be assumed around 70 %. This efficiency was also validated as a typical small-scale turbine efficiency by Ushyne (2008). The turbine mechanical efficiency is given as

99.5 % by Hirsch et al. (2017) in their CSP Bankability report. They also recommended a generator efficiency of 98.5 %.

Table 7: Design point parameters for SST-060

Parameter	Value	Unit
Turbine inlet pressure (live steam pressure)	13 100	kPa
Turbine outlet pressure (condensing pressure)	10	kPa
Turbine inlet temperature (live steam temperature)	530	°C
Steam flow rate	6.8	kg/s

While finding the appropriate HRSG design parameters the highest possible operating pressure that the turbine can operate at is 11 200 kPa. This shows that the cycle is not optimised but given the restriction on available data for components this less optimal configuration is accepted noting that this will have an adverse effect on the thermal efficiency on the subsystem and whole system. This is confirmed by the very high HRSG approach temperature of almost 100 °C, resulting in low Carnot efficiency estimates. The results from the SAM technical manual (Wagner and Gilmer, 2011) is used as shown in Figure 20. The power output is normalised to the design point power output and plotted along the change in condensing pressure. This study's steady state simulation produced results much similar to that of SAM (Wagner and Gilmer, 2011) found in Appendix B.2.

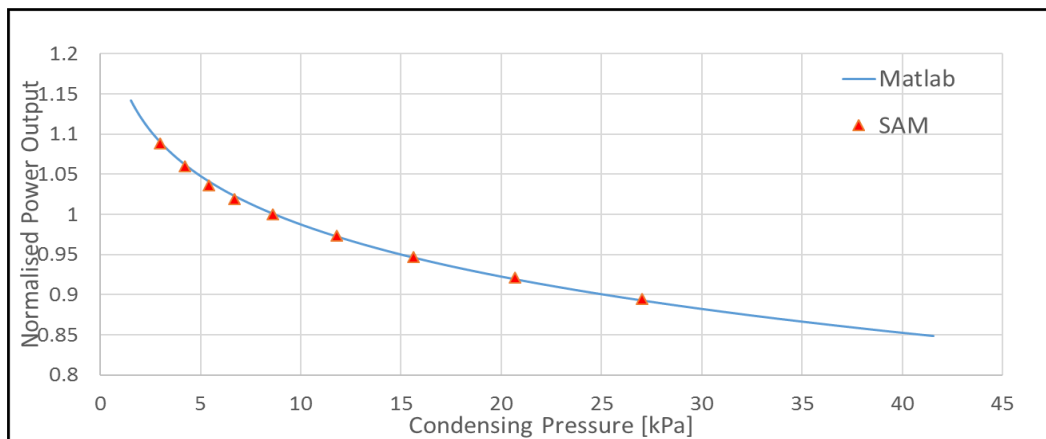


Figure 20: Validation of steam turbine simulation results compared with data from Wagner and Gilmer (2011).

6.3 Central receiver

The site-specific data such as the longitude, latitude, 95th percentile DNI and average ambient day temperature is incorporated for solar noon during the winter solstice, which is December 21st, to calculate all the respective solar angles and design point conditions. Efficiencies given in Section 4.3 for the solar field and receiver are assumed and with the calculated zenith angle of 13.323° the solar

field's optical efficiency is calculated as 82.9 % and the total field's efficiency is 73.3 %. The operating pressure of the central air receiver at design point is 10.03 bar resulting in an optical efficiency of 80.7 %. A comparative study is done to validate the assumptions made with a correlation derived from Heller (2016). For receiver outlet temperatures ranging from 800 °C to 1 100 °C the maximum deviation recorded is only 1.5 % and at the design point at 1 100 °C only a 0.25 % deviation resulted. Assuming the central receiver should ideally heat the compressed gas up to 1 100 °C the total required thermal power absorbed is 27 226 MW_{th}. A short analysis on the effect of the solar multiple as seen in Appendix D showed that a SM larger than two will not have any significant improvement on the system therefore a SM of 2 is selected. For this SM and rated thermal power the receiver area is specified as 65.28 m² and the concentration ratio is calculated to be 961.18. This results in a receiver thermal efficiency of 62.3 %, which includes the CPC efficiency. The total solar field area required is 125 510 m², fitted with 73.902 m² heliostats resulting in a total of 1 698 heliostats. The accompanying tower height is 132.98 m and the resulting solar to thermal efficiency is 43.8 %. The Solgate (2005) report showed that the solar field requires around 4.5 Wh/m²/day to operate.

6.4 Rock bed thermal storage

Considering the average Biot number constraint imposed by Allen et al. (2015) the nominal heat transfer coefficient is calculate using Equation 4.25. Using this heat transfer coefficient, the mass flux is determined and well above 0.2 kg/m²s therefor ensuring a developed thermocline and coherence between analytical design and experimental data (Allen et al., 2015). The total cross-sectional area required to ensure this mass flux for design point gas turbine exhaust flow rate is 124 m². Ensuring a charging effectiveness of 99 % (Allen et al, 2016) the effectiveness-NTU method (Equation 4.28) was used to determine the minimum length to be 2.6 m. This length is thus required for a developed thermocline. The length required for the total capacity is calculated using Equation 4.34. If this is smaller than the required effective length, then the effective length is assumed as the functional storage length. The effective length is also added to ensure minimal heat loss when fully charged. The total length calculate was 9.5 m. Von Backstrom et al. (2016) used a square flow region estimated at 4.2x4.2 m² for a bed length of 11 m. For a bed length of 9.5 m, this study will use a scaled area of 3.627x3.627 m² resulting in a cross-sectional area of 13.157 m². On a modular level, at least ten units is to be implemented for the cross-sectional flow area to be realised. The plant considered by Zangenah et al. (2012) had a thermal loss of 14 % for a 3 MWh_{th} storage unit. An internal report by Von Backstrom et al. (2016) showed that with the increase in capacity there is a considerable decrease in thermal loss with 16 MWh_{th} and 100 MWh_{th} having losses of 10 % and 1 % per day respectively due to improved insulation and more favourable containment surface area to volume flow. Assuming an eleven-hour capacity for the unit considered thermal losses are estimated thus at 1 % for a 240.8 MWh_{th} industrial scale unit. This is claimed due to improved containment surfaces that can be insulated (Von Backstrom et al., 2016).

Chapter 7

Off-design considerations

Implementing CSP for power production the annual yield per year is highly influenced by the off-design characterisation of the components (Wagner & Gilman, 2011). The off-design performance for the gas and steam turbines are evaluated for a range of ambient conditions using iterative steady state simulations as outlined in Appendix C.1 and C.2. Assuming full load power production for the gas turbine their performance can be reasonably evaluated by polynomials using only ambient temperature as the variable. These models are also referred to as “Black Box” models. The fuel usage is then later recalculated using the amount of heat absorbed by the receiver. An aspect that was considered to have a marginal effect on operation is the slight change in flow rate through the turbine due to less fuel being combusted. Figure 21 shows how the “Black Box” models represented the simulation data for four distinct parameters which are used in the annual simulation.

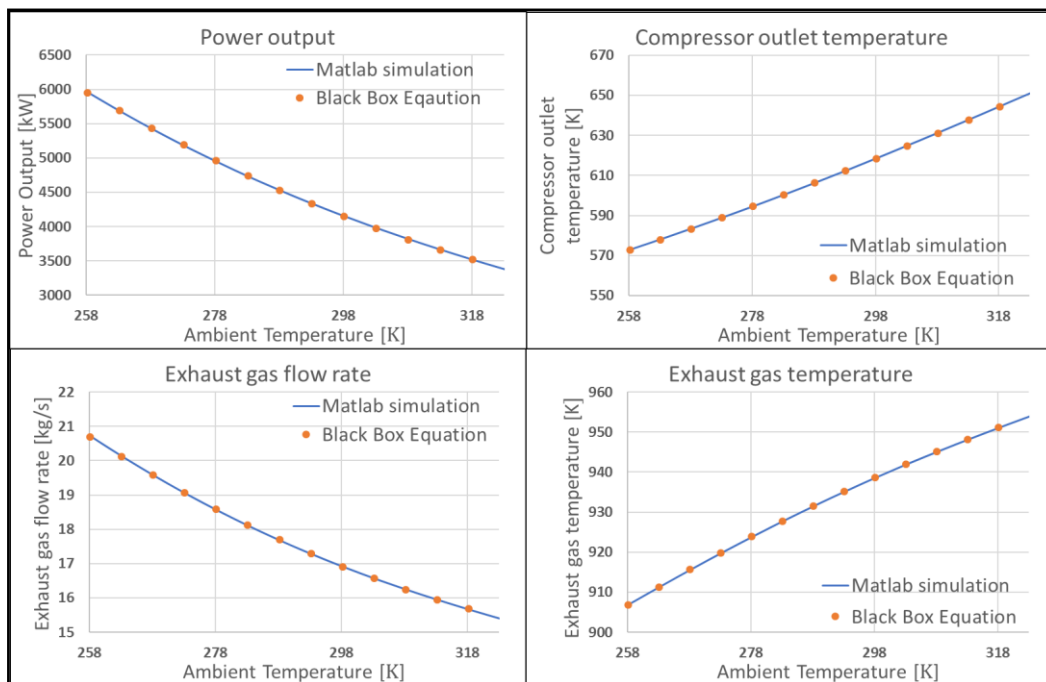


Figure 21: Validation of "Black Box" models for gas turbine output

The “Black Box” equations required to represent the steam turbine output are a bit more involved and requires the consideration of multiple parameters. To calculate the performance parameters of the steam turbine the variable that will change is

condenser pressure, HTF flow rate and temperature. If the properties of the heat transfer fluid, which is the exhaust gas, are kept constant the condenser pressure at full load application is in effect only a function of ambient temperature. These parameters not only have an individual effect on the performance of the turbine but how they interact also plays a role (Wagner & Gilman, 2011). To account for these interactions this study used a much similar, slightly less complex approach as Wagner and Gilman (2011). The design point parameters are determined for these parameters and the steam turbine power output. The percentage of change (Δ) in design point power output can then be represented by polynomials of the absolute change (δ) in one parameter with the other two being kept constant. It is found that for both variation in exhaust gas and ambient temperatures the polynomial is first order and for the variation in exhaust gas flow rate it was second order (Equations 7.1, 7.2 and 7.3).

$$\Delta P(T_{htf}) = A(\delta T_{htf}) + B \quad \text{with } T_{amb} \text{ \& } \dot{M}_{htf} \text{ constant} \quad [7.1]$$

$$\Delta P(T_{amb}) = A(\delta T_{amb}) + B \quad \text{with } T_{htf} \text{ \& } \dot{M}_{htf} \text{ constant} \quad [7.2]$$

$$\Delta P(\dot{M}_{htf}) = A(\delta \dot{M}_{htf})^2 + B(\delta \dot{M}_{htf}) + C \quad \text{with } T_{amb} \text{ \& } T_{htf} \text{ constant} \quad [7.3]$$

The total change in power output is then represented by a cumulative function that can be written in sequence as in Equations 7.4 to 7.6 and is also similar to work done by Hirsch et al. (2017) in their CSP Bankability report, Appendix D: Power Block. In order to validate these models, it is required to have the power output with the random change in all three variables. Such a representation is very tedious to construct and it would be difficult to visualise this on a graph. The gas turbines outlet conditions (exhaust gas temperature and flowrate) however, vary with the change in ambient temperature.

$$P(\dot{M}_{htf}) = P_{dp} + P_{dp} \times \Delta P(\dot{M}_{htf}) \quad [7.4]$$

$$P(\dot{M}_{htf}, T_{htf}) = P(\dot{M}_{htf}) + P(\dot{M}_{htf}) \times \Delta P(T_{htf}) \quad [7.5]$$

$$P(\dot{M}_{htf}, T_{htf}, T_{amb}) = P(\dot{M}_{htf}, T_{htf}) + P(\dot{M}_{htf}, T_{htf}) \times \Delta P(T_{amb}) \quad [7.6]$$

In the two top graphs and bottom left graph of Figure 22 the results of these polynomials are validated. The bottom right graph in Figure 22 shows the result of the ‘‘Black Box’’ equation for the steam turbine power output as a function of ambient temperature. Important to note is that each temperature represents the changes in both the exhaust gas temperature and flowrate. The ‘‘Black Box’’ represents the actual simulation data quite well with an average deviance of 0.25 %.

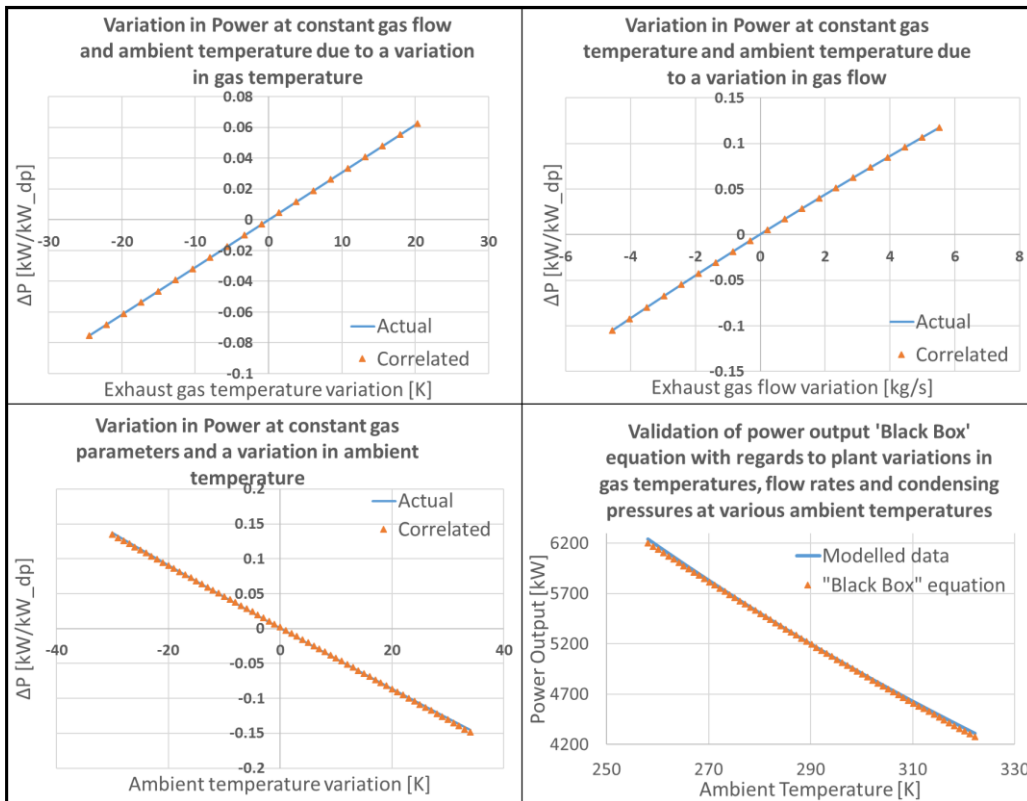


Figure 22: Validation of "Black Box" models for steam turbine output

Chapter 8

Configuration and dynamic simulation criteria for SUNSPOT cycle

8.1 Configuration details

Four different cycles are evaluated over a five-year period. Initially, only the conventional CC is simulated to find a base from which the alternative options can be evaluated from. The CC is then altered in three separate ways. First to evaluate the major improvement of adding the solar resource only a solar retrofitted combined cycle is simulated. It is then further developed into the SUNSPOT cycle by adding the storage in parallel with the HRSG. To make a fair evaluation of the SUNSPOT cycle a CC with only the addition of storage is also simulated, operating with the same strategy as the SUNSPOT cycle.

8.2 Transient simulation details

8.2.1 Thermal inertia of steam turbine

Hirsch et al. (2017) researched the standardization of CSP system modelling. They gave some direction into what the effects and temporal implications of cold, warm and hot start sequences are for the steam cycle as used in a solar configuration. They implemented a 100 MW plant requiring a 250 MW_{th} load and it is deduced that for smaller or larger system the estimations they made can be scaled linearly with sufficient accuracy. Hirsch et al. (2017) showed that for a warm start per day, typical of CSP, the required downtime should not be more than eight hours. For this research, it is assumed that a twelve-hour period will still be sufficient. Their estimates reflected a start-up period of 30 minutes and a thermal load requirement of 10 % of the nominal thermal load required by the system. The HRSG's inertia is included in this.

8.2.2 Thermal inertia of gas turbine

It is generally expected that the Solugas plant (a solar hybrid gas turbine using the Mercury 50™) can reach maximum load from start up within 30 minutes (Quero et

al., 2013). These authors concluded that a reasonable assumed start up period for the gas turbine can be taken as short as 10 minutes.

8.2.3 Thermal inertia of receiver and piping system

It is assumed that the piping system as well as the receiver has the same thermal inertia as the gas turbine and that the power lost during heat up is recovered by the off-load performance of the gas turbine during start up resulting in a zero-net sum.

8.2.4 Operating strategy

The operating strategy is chosen to replicate the current demand curve in South Africa. The current demand in South Africa has a small peak in the morning with a large peak during the late afternoon and early evening. The typical constant day demand is also higher than the average night time demand. From 06:00 to 15:00 only the two gas turbines are running, using a combination of fuel and solar resource to heat up the air. During this period the thermal storage is being charged, which will thus total in a nine-hour charging period. To capitalise on the tariff hike in late afternoon, the steam turbine is started at 15:00 resulting in maximum output for the plant during this period, running on only the exhaust heat of the gas turbines. At 21:00 the gas turbines switch off and the steam turbine continues running at 100 % capacity. Running the steam turbine during the night also favours higher thermal efficiency due to lower condensing temperatures. A schematic on the operating strategy is found in Appendix E.

To make a fair comparison the other cycles operating strategies are chosen to result in the same net power production as the SUNSPOT cycle. Therefore, the CC as well as its solar retrofit derivative runs for fifteen hours a day from 06:00 to 21:00. This then results in a load factor of 62.5 %, which is slightly higher than typical CC load factors as given by the IRP (2016). The CC with storage follows the same operating strategy as the SUNSPOT cycle.

8.2.5 Balance over solar receiver

The “Black Box” models are used during the transient simulation for the operation of the steam and gas turbines. The only heat balance in the dynamic simulation occurs within the solar receiver iteration. Equation 4.21 (from section 4.3) is used to calculate the heat absorption and this is used to calculate the receiver outlet temperature. Depending on the allowed combustor inlet temperature the heliostats are focussed or defocused to reach that temperature and the balance is reiterated. The annual simulation procedure is given in Appendix C.3 for all four different configurations.

Chapter 9

Results and discussion

9.1 Steady state models

The steady state models were validated with relevant data as seen in Chapter 6.2.1 and 6.2.2 for the gas and steam turbine respectively. Chapter 7 showed that the off-design performance can essentially be captured well enough by “Black Box” models. The turbines selected in Chapter 6.2 are well equipped for combined cycle operation but it was found that they are not optimised for one another which made finding the design points for the HRSG more involved. For typical combined cycles of this size (<20 MW) the thermal efficiency should be in the range of around 50 %. Due to utilising a non-reheat steam turbine at single pressure the Rankine efficiency to start with is only 27 %. The HRSG is then specified to ensure a positive approach temperature at the evaporator for the multiple conditions associated with the gas turbine exhaust with ambient temperatures varying from -15 to 50 °C. This results in the HRSG exhaust gas temperature being almost 100 °C higher than the economiser feed water inlet temperature, resulting in significant waste heat. Using these temperatures and design point cycle efficiencies the total system efficiency of the cycle is estimated at 41.3 %. The equation used to calculate this is derived in Appendix F.

The program is written to simulate a given power plant and not as an optimisation program. The studies done during the Solgate project (2005) showed that for the PGT 10 (16.1 MW combined cycle system) the gas turbine efficiency was 31.1 % and the total combined cycle efficiency 44.6 %. Which shows that for this scale of plants the thermal efficiencies remain quite low and given the lower gas turbine thermal efficiency of the Mercury 50TM compared to the PGT 10, the calculated efficiency compares well with the Solgate project (2005).

9.2 Dynamic simulations

The irradiation and weather data has been used to evaluate the combined cycle, the combined cycle with thermal storage, the solar retrofitted combined cycle and the SUNSPOT cycle. Both the SUNSPOT cycle and the solar retrofitted cycle were also evaluated at various solar multiples. A SM is chosen by which these plants are evaluated against the traditional combined cycle plant. In Appendix G, Figure 36 and Figure 37 show the typical summer and winter’s day operation of the solar retrofitted combine cycle. Figure 38 and Figure 39 show these results for the

SUNSPOT cycle. These figures show how the availability of DNI during the day reduces the fuel usage significantly. It is important to notice how the combined cycle output reproduces the typical demand curve of South Africa, with the higher demand during the day, the peak over the evening and the lower demand during late evening and early morning.

9.2.1 Solar multiple of SUNSPOT cycle system evaluation

Table 8 gives the results for the SUNSPOT cycle operating at the various SM's. The annual power production stays the same due to the hybrid nature of the power plant. The increase in SM therefor only reduces the fuel requirement of the plant and therefor it's thermal efficiency. Figure 33 in Appendix D showed that by increasing the SM further than 2 shows minimal improvement in the thermal design of the power plant. For this reason, a SM of two is chosen for the comparison between configurations. The major setback of using a SM of 2 is that solar resource is wasted because of spillage and the results show that the SUNSPOT with a SM of two is more than 12 % less solar efficient than when the SM is one. This can be improved by using a multiple pressure receiver design as proposed by Heller (2016). At a systems perspective the solar fraction of the thermal requirement is increased by almost 10 % by doubling the SM. The concept of hybrid operation is the focus of this study and requiring the larger solar field to improve the solar fraction of the hybrid system is justified even though Spelling (2013) argued that the most optimal LCOE is found with solar shares between 14 % and 26 %. Increasing the solar share would also improve the power plant's vulnerability to fluctuating fuel prices.

Table 8: Annual simulation results for the SUNSPOT cycle operating at different solar multiples

Parameter	SM 1	SM 1.5	SM 2	SM 2.5
Annual power production [TWh]	72.145	72.145	72.145	72.145
Annul fuel consumption [Ton]	9 350.00	8 368.75	7 999.47	7 793.38
Thermal Efficiency	57.44 %	64.17 %	67.14 %	68.91 %
Solar Efficiency	34.49 %	27.67 %	22.07 %	18.24 %
Solar Fraction	31.27 %	37.96 %	40.50 %	41.92 %
Load Factor	58.23 %	58.23 %	58.23 %	58.23 %
Load Factor at 30% utility (baseload)	100 %	100 %	100 %	100 %

9.2.2 Configuration analysis

Comparing the results between the different configurations in Table 9, it is interesting to find that the addition of storage along with the change in the operating strategy of the plant increases the plant thermal efficiency and annual power production. This is because the steam turbines are now generating power in the evening when there is lower ambient temperature, thus a lower condensing pressure is reached. This increase in output outweighs the loss of thermal energy inside the thermal storage. Adding the storage also resulted in the capability of the plant to theoretically produce electricity as a base load plant throughout the year. The

changes to plant design also shows minimal negative impact on the typical output of a combined cycle plant as seen by the very small changes in load factor. Adding the solar resource at a SM of two reduces the fuel consumption with more than 40 % and therefor the thermal efficiency by which the fuel is burned is increased by 30 % from conventional CC technology towards the SUNSPOT cycle technology. The low solar efficiencies are due to defocusing the heliostats at high irradiation and current limitation to central receiver systems and high-pressure air receivers.

Table 9: Annual simulation results for the different component configurations

Parameter	Combined Cycle	Combined Cycle with Storage	Solar Retrofitted Combined Cycle	SUNSPOT
Annual power production [TWh]	72.946	73.629	71.408	72.145
Annul fuel consumption [Ton]	14 381.24	14 400.4	7 997.2	7 999.5
Thermal Efficiency	37.76 %	38.06 %	66.47 %	67.14 %
Solar Efficiency	-	-	22.18 %	22.07 %
Solar Fraction	-	-	40.51 %	40.50 %
Load Factor	58.88 %	59.43 %	57.64 %	58.23 %
Load Factor at 30% utility (baseload)	63 %	100 %	63 %	100 %

9.3 Thermo-economic evaluation

The specific costs as defined in Chapter 5 is used to calculate the total CAPEX and OPEX for each plant. Figure 40 in Appendix H shows the typical breakdown of CAPEX cost associated with each plant. Equation 5.1 is used to calculate the LCOE and this is then converted to R/kWh using the exchange rate averaged in January 2017 (14.5 R/€). From Table 10 it is seen that with the increase in SM the CAPEX increases to a proportion that outweighs that of the amount of fuel that is saved, thus the increase in LCOE. The OPEX of the SUNSPOT cycle compared to that of the combined cycle does not seem as low as expected. The reason is that for the combined cycle 83.7 % of the OPEX consist of fuel costs. For the SUNSPOT cycle the fuel costs accounts only for 62.3 %. The labour cost for the SUNSPOT cycle is significantly higher than for a conventional plant due to the number of technicians required in the solar field and control room as implied by Table 3. This also caused an increase in OPEX as the SM is increased.

Table 10: Summary of the thermo-economic performance for the SUNSPOT cycle at different solar multiples

Economic Parameter	Combined Cycle	SUNSPOT SM 1	SUNSPOT SM 1.5	SUNSPOT SM 2	SUNSPOT SM 2.5
CAPEX	€ 9 896 807	€ 43 576 791	€ 50 628 550	€ 57 621 833	€ 64 580 994
OPEX	€ 7 273 611	€ 5 658 634	€ 5 417 917	€ 5 435 842	€ 5 465 784
LCOE (€/kWh)	€ 0.112	€ 0.132	€ 0.137	€ 0.146	€ 0.155
LCOE (R/kWh)	R 1.623	R 1.915	R 1.993	R 2.121	R 2.251

The revised IRP (2016) assumed that CC gas turbine plants operating at a high load factor (>60 %) can reach a LCOE of 1.00 R/kWh. These are plants of rated capacity 732 MW_e. To make a fair comparison with these plants this study's results are scaled to a similar range output and cost. The output should also be modified using the typical thermal efficiency of such plants (55 %) and the calculated thermal efficiency (41.3 %) of the modelled plant as in Appendix F. Even though this is a rough estimate, the LCOE scaled is of similar value which is used in the revised IRP (2016) and therefore acceptable to make realistic comparisons. It is seen in Table 11 that even though the CC with storage can be used as a base-load or load following power producer it has a slightly higher cost due to the storage costs. This is similar with regards to the two hybrid models. With the current technology available the SUNSPOT cycle does not yet compete with the CC technologies even though it's OPEX is 25 % less than that for the CC. Using the IRP (2016) as a guideline, the SUNSPOT cycle does however compare well with other CSP plants and renewable technologies as seen in Figure 23 at the same load factor, except for wind, solar photovoltaic, biogas and biomass forestry residue.

Table 11: Summary of the thermo-economic performance of the different configurations

Economic Parameter	Combined Cycle	Combined Cycle with Storage	Solar Retrofitted Combined Cycle	SUNSPOT Cycle
CAPEX	€ 9 896 807	€ 13 347 983	€ 54 288 983	€ 57 621 833
OPEX	€ 7 273 611	€ 7 312 775	€ 5 404 598	€ 5 435 842
LCOE (€/kWh)	€ 0.112	€ 0.115	€ 0.143	€ 0.146
LCOE (R/kWh)	R 1.623	R 1.674	R 2.077	R 2.121

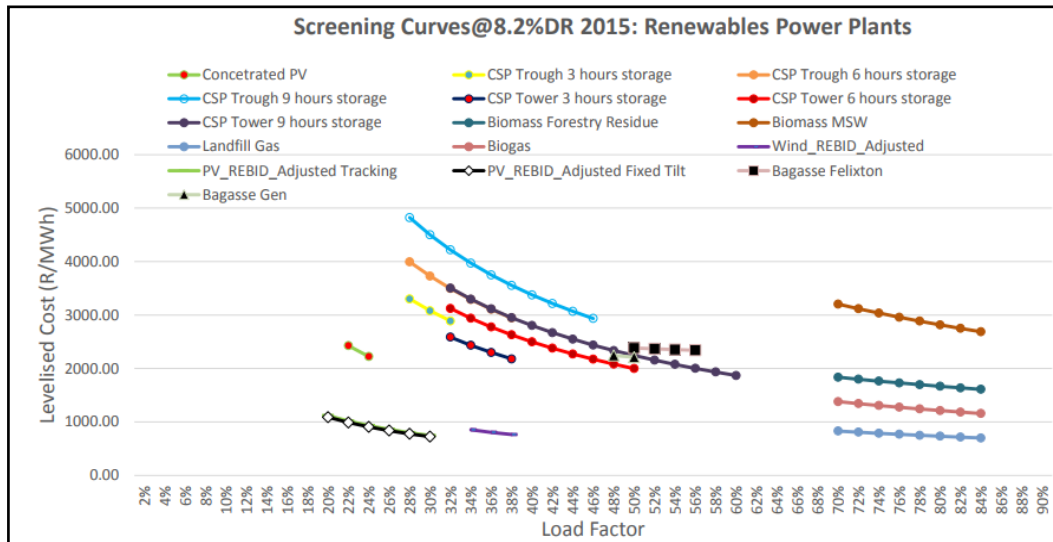


Figure 23: Screening curves implemented by the IRP (2016) for various renewable technologies

Chapter 10

Conclusions and recommendations

This study set out to make a case for the further research in using the SUNSPOT cycle as a solution to the current electricity problem in South Africa. Extensive research on solarised combined cycles in Chapter 2 shows that the SUNSPOT cycle is novel in its design. It shows that the concept of storage in parallel with the HRSG is the major derivative from the typical approaches to the solarised combined cycle. As a prerequisite to simulating the SUNSPOT cycle an important objective was set to capture the essence of typical combined cycle operation. The thermodynamics and the operation of the independent systems such as the Brayton and Rankine cycle are studied in Chapter 3. These theoretical models are used to simulate the off-design performance of the power cycles. They are validated by existing simulation and experimental data. Chapters 6.2.1 and 6.2.2 show that the program gives an accurate description of the off-design performance of the Brayton and Rankine cycles respectively. High level models for the solar and thermal storage components of the SUNSPOT cycle are studied in Chapter 4 and they are integrated with the combined cycle in an annual dynamic simulation tool using Matlab[®] (Mathworks, 2017). “Black Box” models are derived in Chapter 7 to capture the essence of the off-design operation of this plant and these models are validated using the iterative simulation results and found to be very accurate representations. To evaluate the cycle on a thermo-economic basis various economic models are used to estimate the typical CAPEX and OPEX cost of these cycles in Chapter 5. Vredendal is selected using both the SMART and AHP decision making criteria as a good location to evaluate the SUNSPOT cycle (Chapter 6.1). The major contributions of this site are the low elevation and very high annual DNI levels. Location specific data is used to determine the design point parameters of the combine cycle, central receiver system and thermal storage in the rest of Chapter 6. Chapter 8 describes the different configurations to be evaluated along with some general transient simulation criteria that is followed such as the operating strategies and thermal inertia of the plants.

The results in Chapter 9 show that the design point thermal efficiency, even though it is quite low, is a good representation of combined cycle efficiencies of such small plants that are not optimised. For both the solar hybrid systems a SM of two is found to give the best desired plant performance. Using a SM of two these plants are compared to the results of a combined cycle. It is shown that the addition of storage increases plant output due to lower ambient temperature by which the steam turbine operates. This performance enhancement of less than 1 % thermal efficiency is not justified by the increase in LCOE unless it is desired to operate the plant as a baseload or typical load following plant. The addition of solar proved to enhance the fuel efficiency of the plant significantly but the CAPEX of these plants is still

too high to justify it. Solarised gas turbines are currently only in the development phase and therefore unjustifiably expensive. As shown in Table 2 solar retrofitting the gas turbine increased the gas turbine cost by almost 2.7 times, which results in a 79 % increase in the power block cost of the plants. Considering this, the SUNSPOT cycle still compares favourably with regards to other CSP options at a LCOE of 2.12 R/kWh at a load factor of 57.64 %.

The SUNSPOT cycle is a competent design and with the continuation of research in both the high-pressure air receiver and thermal storage, along with the maturation of the central receiver system it could perhaps someday compete on an economical scale. The main argument for the SUNSPOT cycle lies in the dispatch ability of its power and with a variation in operating strategies it is more useful than its solar retrofitted CC counterpart. It is important to note that this comparison is made between plants of different sizes. With the increase in capacity the thermal performance of the combined cycle also improves. It is recommended that further study investigates how a SUNSPOT cycle of the same capacity compares with current CSP. Studies in the thermo-economic optimisation of the SUNSPOT cycle similar to those done by Spelling (2013) on the solarised Brayton cycle is highly motivated to show what an optimal SUNSPOT cycle could be capable of. Finally, the areas of greatest concern in research regarding the SUNSPOT cycle would be to increase solar efficiency while maintaining a high solar fraction and lowering the LCOE. The first can only be done by improving the current solar thermal efficiency of central receiver systems and the high-pressure air receiver. The high LCOE is largely affected by components that are either still in the development phase or very young in their roll-out maturity. This study thus advocates the continued research in solarised gas turbines, CRS, pressurised air receivers and rock bed (or other innovative) TESS. To conclude the SUNSPOT cycle can in theory compete with current power generation processes but research in the areas mentioned will be pivotal in realising this.

References

Ahlbrink, N., Belhomme, B. and Pitz-Paal, R. 2009. *Modelling and Simulation of a Solar Tower Power Plant with Open Volumetric Air Receiver*. 7th Modelica Conference, Como, Italy.

Allen, K.G. 2010. *Performance characteristics of packed bed thermal energy storage for solar thermal power plants*. M.Sc. Eng. University of Stellenbosch. [Online]. Available: <http://scholar.sun.ac.za/handle/10019.1/4329> [Accessed 17 June 2017].

Allen, K.G., Von Backström T.W. and Kröger, D.G. 2015. *Rock bed pressure drop and heat transfer: Simple design correlations*. Solar Energy, Volume 115, pg. 525-536. [Online]. Available: <http://www.sciencedirect.com/science/article/pii/S0038092X15000997> [Accessed 18 June 17]

Allen, K.G., Von Backström, T.W., Joubert, E. and Gauché, P. 2016. *Rock bed thermal storage: Concepts and costs*. AIP: Conference Proceedings. [Online]. Available: <http://dx.doi.org/10.1063/1.4949101> [Accessed 21 June 17]

Avila-Marin, A.L. 2011. *Volumetric receivers in Solar Thermal Power Plants with Central Receiver System technology: A review*. Solar Energy, Volume 85 (1), pg. 891-910.

BINE. 2013. *Solar thermal power plants*. [Online]. Available: <http://www.bine.info/en/publications/themeninfos/publikation/solarthermische-kraftwerke-2/>. [Accessed 17 July 2016].

Boyce, M.P. 2012. *Gas Turbine Engineering Handbook*. 4th Edition. Elsevier. [Online]. Available: <http://www.sciencedirect.com.ez.sun.ac.za/science/article/pii/B978012383842100024X>. [Accessed 14 February 2017]

CAMS radiation services (SoDa-Pro[®]). 2016. [Online]. Available: <http://www.soda-pro.com/web-services/radiation/cams-radiation-service> [Accessed 4 October 2017]

Ceballos-Mendivil, L., Cabanillas-López, R., Tánori-Córdova, Murrieta-Yescas, R., Zavala-Rivera, P., Estrada-Gasca, C. and Castorena-González, J. 2013. *Materials used in receptors in central tower thermo-solar plants: a review*. In: SolarPACES. [Online]. Available: http://www.sistemanodalsinaloa.gob.mx/archivoscomprobatorios/15_memoriaextenso/10339.pdf. [Accessed 31 May 2017]

- Cengel, Y.A. and Ghajar, A.J. 2015. *Heat and mass transfer: Fundamental and application*. 5th Edition. New York: McGraw-Hill Education.
- Cengel, Y.A. and Boles, M.A. 2015. *Thermodynamics: An engineering approach*. 8th Edition. New York: McGraw-Hill Education.
- City of Cape Town. 2017. [Online]. Available: <http://www.capetown.gov.za> [Accessed 22 September 2017]
- Cohen, H., Rogers, G.F.C. and Saravanamuttoo, H.I.H. 1987. *Gas turbine theory*. 3rd Edition. Longman Group UK Limited.
- Cooke, D. 1983. *Modelling of Off-Design Multistage Turbine Pressures by Stodola's Ellipse*. Energy Incorporated. Richmond.
- COP21. 2015. *November 30 to December 12 - PARIS agreement*. [Online]. Available: <http://www.cop21.gouv.fr/en/more-details-about-the-agreement/>. [Accessed 17 July 2016].
- Crossway (Kindle version). 2001. *The Holy Bible: English Standard Version*[®]. Illinois: Good News Publishers.
- CRSES. 2014. *SolarGIS DNI South Africa*. [Online]. Available: http://www.crses.sun.ac.za/files/research/publications/SolarGIS_DNI_South_Africa_width15cm_300dpi.png. [Accessed 17 July 2016].
- Dixon, S.L. and Hall, C.A. 2010. *Fluid mechanics and thermodynamics of turbomachinery*. 6th Edition. Oxford: Elsevier Inc.
- Da Rocha, A.M. 2010. *Analysis on solar retrofit in combined cycle power plants*. Master's thesis. Institut fur Energietechnik und Thermodynamik. Wien.
- Department of Energy. 2012. *Integrated Energy Plan*. [Online]. Available: http://www.energy.gov.za/files/IEP/IEP_Publications/Draft-2012-Integrated-Energy-Plan.pdf. [Accessed 17 July 2016].
- Dersch, J., Schwarzbözl, P. and Richert, T. 2011. *Annual Yield Analysis of Solar Tower Power Plants With GREENIUS*. Journal of Solar engineering, Volume 133, pg. 2-3.
- Fend, T., Hoffschmidt, B., Pitz-Paal, R., Reutter, O. and Rietbrock, P. 2004. *Porous materials as open volumetric solar receivers: Experimental determination of thermo-physical and heat transfer properties*. Energy, Volume 29 (1), pg. 823-833.

- Gauché, P., Pfenninger, S., Meyer, A.J., von Backström, T.W. and Brent, A.C. 2012. *Modelling dispatchability potential of CSP in South Africa*. In: Southern African Solar Energy Conference [Online]. Available: <http://sterg.sun.ac.za/wp-content/uploads/2012/07/PL-031.pdf> [Accessed 29 May 2017]
- Heller, L. and Gauché, P. 2013. *Dual-pressure air receiver cycle for direct storage charging*. In: Proceedings of SolarPACES, Volume 0, pg. 1-10. Las Vegas, USA.
- Heller, L., Gauché, P. and Heide, S. 2013. *Investigation of the Thermal Storage System for a 5MWe Concentrated Solar Power Pilot Plant*. Master's thesis, Technische Universität Dresden, Germany.
- Heller, L. and Hoffmann, J. 2013. *Comparison of different configurations of a combined cycle CSP plant*.
- Heller, L. and Hoffmann, J. 2016. *Development of a dual-pressure air receiver system for the SUNDISC cycle*. Doctorate dissertation, Stellenbosch University, South Africa.
- Heller, P., Pfänder, M., Denk, T., Tellez, F., Valverde, A., Fernandez, J. and Ring, A. 2006. *Test and evaluation of a solar powered gas turbine system*. Solar Energy, Volume 80, pg1225-1230. [Online]. Available: <http://www.sciencedirect.com/science/article/pii/S0038092X05002161> [Accessed 31 May 2017]
- Hirsch, T., Yildiz, E., Haller, U., Dersch, J., Rau, C., Schmidt, N. and Heide, S. 2017. *CSP Bankability project report. Appendix D – Power Block*. [Online]. Available: http://www.dlr.de/sf/de/desktopdefault.aspx/tabid-11126/19467_read-48251/. [Accessed 28 June 2017]
- IEA. 2013. *Key World Energy Statistics*. Technical report, International Energy Agency, Paris.
- Jonsson, M., Bolland, O. and Bücker, D. 2005. *Gas turbine cooling model for evaluation of novel cycles*. Proceedings of the International ECOS Conference. Trondheim.
- Kehlhofer, R.H., Warner, J., Nielsen, H., and Bachman, R. 1999. *Combined cycle gas and steam turbine power plants*. Tulsa, Oklahoma: PennWell Publishing Company.
- Kolb, G.J. 2011. *An evaluation of possible next-generation high-temperature molten-salt power towers*. Sandia National Laboratories. [Online]. Available: <http://large.stanford.edu/courses/2014/ph241/dunham1/docs/119320.pdf>. [Accessed 30 May 2017]

- Kröger, D.G. 2011. *SUNSPOT - The Stellenbosch University Solar Power Thermodynamic Cycle*. [Online]. Available: <http://sterg.sun.ac.za/wp-content/uploads/2011/05/SUNSPOT-2.pdf>. [Accessed 16 October 2017]
- Kribus, A., Zaibel, R., Carey, D., Segal, A., and Karni, J. 1998. *A solar driven combined cycle power plant*. *Solar Energy*, Volume 62 (2), pg. 121-129.
- Kurz, R. 2005. *Gas turbine performance*. The thirty-fourth turbomachinery symposium: Conference Proceedings.
- Lubkoll, M., von Backström, T.W, Harms, T.M. and Kröger, D.G. 2015. *Initial analysis on the novel Spiky Central Receiver Air Pre-heater (SCRAP) pressurized air receiver*. *Energy Procedia*, Volume 69 (1), pg. 461-470.
- Mathworks (MATLAB®). 2017. [Online]. Available: <https://uk.mathworks.com/products/matlab.html> [Accessed 4 October 2017]
- Microsoft (Excel®). 2016. [Online]. Available: <https://products.office.com/en-gb/excel> [Accessed 4 October 2017]
- Nel, C.J. 2014. *Simulation and characterisation of a concentrated solar power plant*. Master's thesis. Potchefstroom. North-West University.
- Nelson-Farrar Cost Indexes. 2017, March 4. *Oil&Gas Journal*. [Online]. Available: <http://www.ogj.com/articles/print/volume-115/issue-4/processing/nelson-farrar-cost-indexes.html>. [Accessed 21 September 2017]
- NREL. 2017. *Concentrating Solar Power Projects: ISCC Kuraymat*. [Online]. Available: https://www.nrel.gov/csp/solarpaces/project_detail.cfm/projectID=65 [Accessed 4 October 2017]
- Pitz-Paal, R., Dersch, J. and Milow, B. 2003. *ECOSTAR Roadmap Document*. Technical Report, DLR. [Online]. Available: <http://www.promes.cnrs.fr/uploads/pdfs/ecostar/ECOSTAR.Roadmap.pdf> [Accessed 20 September 2017]
- Quero, M., Korzynietz, R., Ebert, M., Jiménez, A.A., del Río, A. and Brioso, J.A. 2013. *Solugas: Operation experience of the first solar hybrid gas turbine system at MW scale*. *SolarPaces 2013*. [Online]. Available: <http://www.sciencedirect.com/science/article/pii/S187661021400647X>. [Accessed 8 August 2017]
- Ravi Kumar, N., Rama Krishna, K. and Sita Rama Raju, A.V. 2007. *Thermodynamic analysis of heat recovery steam generator in combined cycle power plant*. *Thermal Science*, Volume 11(4), pg. 143-156.

- Ray, A. 1980. *Dynamic modelling of power plant turbines for controller design*. Applied mathematical modelling, Volume 4(2), pg. 109-102.
- Roldán Serrano, M.I. 2017. *Green Energy and Technology. Chapter 2: Concentrating Solar Thermal Technologies*. [Online]. Available: <http://www.springer.com/in/book/9783319458823> [Accessed 22 May 2017]
- Schwarzbözl, P., Eiden, U. and Pitz-Paal, R. 2006. *STEC: A TRNSYS Model Library for Solar Thermal Electric Components*. Reference Manual, Version 3.0, Deutsches Zentrum für Luft- und Raumfahrt, Köln. [Online]. Available: <http://citeseerx.ist.psu.edu/viewdoc/download?doi=10.1.1.551.4821&rep=rep1&type=pdf> [Accessed 31 May 2017]
- Siemens. 2017. *Siemens Steam Turbines*. [Online]. Available: <https://www.energy.siemens.com> [Accessed 30 April 2017]
- Silinga, C. and Gausche, P. 2013. *Scenarios for a South African CSP peaking system in the short term*. SolarPaces 2013: Conference Proceedings.
- Silinga, C., Gauché, P., Rudman, J. and Cebecauer, T. 2014. *The South African REIPPP two-tier CSP tariff: Implications for a proposed hybrid CSP peaking system*. SolarPaces 2014: Conference Proceedings.
- SoDa. 2017. *Solar Radiation Data*. CAMS Radiation Service. Sophia Antipolis Cedex, France.
- SOLGATE: Project Report. 2005. *Solar hybrid gas turbine electric power system*. Technical Report, European Commission, Brussels, Belgium. [Online]. Available: https://ec.europa.eu/research/energy/pdf/solgate_en.pdf. [Accessed 31 May 2017]
- South African Labour Costs. 2017. *Trading Economics*. [Online]. Available: <https://tradingeconomics.com/south-africa/labour-costs>. [Accessed 21 September 2017]
- Spelling, J.D. 2011. *Steam turbine optimisation for solar thermal power plant operation*. KTH Royal Institute of Technology, Stockholm.
- Spelling, J.D. 2013 *Hybrid solar gas-turbine power plants – a thermo-economic analysis*. Doctoral thesis. KTH Royal Institute for technology, Stockholm.
- Stine, W.B. and Geyer, M. 2001. *Power from the Sun*. 1st Edition, Chapters 2 & 3. [Online]. Available: <http://www.powerfromthesun.net/book.html>. [Accessed 25 May 2017]
- Teraji, D.G. 2005. *Mercury™ 50 field evaluation and product introduction*. Industrial applications of gas turbines committee. Paper No: 05-IAGT-1.1

- Teraji, D.G. 2015. *Concentrated solar power hybrid gas turbine demonstration test results*. Proceedings of the ASME 2015 Power and Energy Conversion Conference.
- Thermal Energy System Specialists (TRNSYS®). 2017. [Online]. Available: <http://www.trnsys.com> [Accessed 18 October 2017]
- Twidell, J.W. and Weir, A.D. 2006. *Renewable energy sources*. Abingdon: Taylor & Francis Ltd, pg. 7-12.
- United Nations. 2015. *Adoption of the Paris agreement*. [Online]. Available: <https://unfccc.int/resource/docs/2015/cop21/eng/l09r01.pdf>. [Accessed 22 July 2016]
- USHYNE: Final Report. 2008. *Upscaling of solar-hybrid gas turbine cogeneration units*. German Aerospace Centre (DLR).
- Von Backström, T.W., Allen, K.G. and Joubert, E.C. 2016. *Report 3: Initial design of a pilot scale thermal storage system*. Internal report. Stellenbosch University.
- Von Winterfeldt & Edwards. 1986. *Decision Analysis and Behavioral Research*. Cambridge University Press.
- Wagner J.W. and Gilman P. 2011. *Technical manual for the SAM physical trough model*.
- Zhang, N. and Cai, R. 2002. *Analytical solutions and typical characteristics of part-load performance of single shaft gas turbine and its cogeneration*. Energy Conversion and Management, Volume 43, pg. 1323-1337.
- Zanganeh, G., Pedretti, A., Zavattoni, S., Barbato, M., Steinfeld, A. 2012. *Packed bed thermal storage for concentrated solar power: Pilot-scale demonstration and industrial-scale design*. Solar Energy, Volume 86, pg. 3084-3098
- 2014 Performance Specs. 2014. *Gas Turbine World*. 30th Edition, Volume 44 (1)

Appendix A: Location selection process: SMART and AHP criteria

A.1 SMART

The first step in a SMART analysis is to setup a value tree. For selecting a site it is determined that there are two areas in which the system is validated, namely, cost and performance. The distances to the grid and fuel supply is the parameters relating to cost. The performance is influenced by the DNI, ambient temperature and altitude. The value tree seen in Figure 24 is typical to this system. The data from Table 4 is used and scaled linear between maximum and minimum values as seen in Table 12. The different parameters are also evaluated as to relative importance towards the most important one and this swing weight leads to a percentage value of parameter compliment to decision as seen in the second column of Table 12. A swing weight is also determined between cost (25 %) and performance (75 %). The results of the scaling are then multiplied through the swing weights and added to deliver a final result. It is clear that Vredendal would be the best decision according to the SMART method.

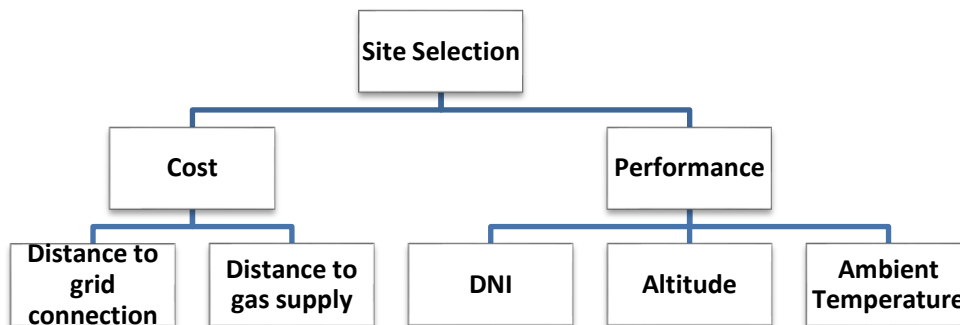


Figure 24: Value tree for site selection process

Table 12: SMART site selection table

Parameter	Swing Weight	Min	Max	Prince Albert	Vredendal	Aggeneys	Aus	Arandis	Kokerboom
DNI	29.4%	900	1029	0.83	0.69	1	0.42	0.19	0.69
Altitude	26.5%	315	1200	0.37	1	0.57	0.74	0.76	0.21
Ambient T	14.7%	290.3	298	1	0.9	0.82	0.83	0.65	0.56
Grid distance	11.8%	0.6	1	0.6	1	0.6	0.6	1	0.6
Gas distance	17.6%	92	650	0.82	0.7	0	0.94	1	0.17
Results				70.40%	84.10%	53.40%	67.80%	64.70%	44.20%

A.2 AHP

For this study the AHP method will assume the same value tree as defined by the SMART in Appendix A.1. The AHP is a tedious process of evaluating each division, parameter and option within that parameter with one another on a qualitative basis. The following assertions with their accompanying numerical value can be made. A division, parameter or option can be equally important (1), weakly more important (2), moderately more important (3), strongly more important (4) or highly more important (5) than another with regards to that parameter (in the case of an option) or division (in the case of a parameter). Tables for each parameter (with options), division (with parameters) or choice (with divisions) is then constructed with the relative numerical values as per evaluation. An example is given in Table 13 for the different options with regards to Altitude. How one would read would be something like: “*Vredendal is moderately more preferred to Prince Albert with regards to altitude*”. These tables are then normalised to unity and the value tree is updated with these values. A multiplication function is used to multiply from the bottom of the value tree up to the top and adding the results for each option to give totals on which the selection will be based. The AHP also resulted in delivering Vredendal as the best selection.

Table 13: Example for AHP: Altitude comparison

							Comparative value		Normalised			
Altitude	Prince Albert		Vredendal		Aggeneyns		Aus		Arandis		Kokerboom	
Prince Albert	1	0.11	0.33	0.11	1	0.11	0.5	0.09	0.5	0.09	2	0.13
Vredendal	3	0.32	1	0.34	3	0.32	2	0.38	2	0.38	4	0.27
Aggeneyns	1	0.11	0.33	0.11	1	0.11	0.5	0.09	0.5	0.09	2	0.13
Aus	2	0.21	0.5	0.17	2	0.21	1	0.19	1	0.19	3	0.2
Arandis	2	0.21	0.5	0.17	2	0.21	1	0.19	1	0.19	3	0.2
Kokerboom	0.5	0.05	0.25	0.09	0.5	0.05	0.33	0.06	0.33	0.06	1	0.07
Totals	9.5	1	2.91	1	9.5	1	5.33	1	5.33	1	15	1

Appendix B: Comparative data, figures and tables

B.1 Gas turbine validation data

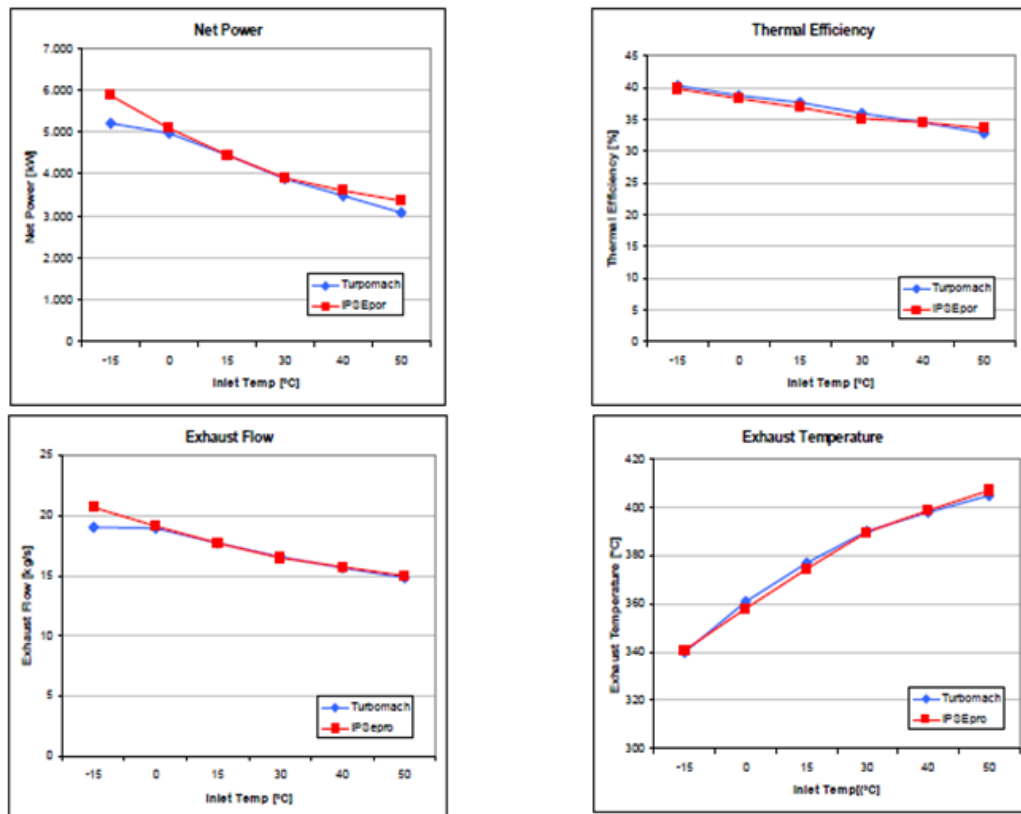


Figure 25: Ushyne (2008) gas turbine simulation results using IpsePro™.

B.2 Steam turbine validation data

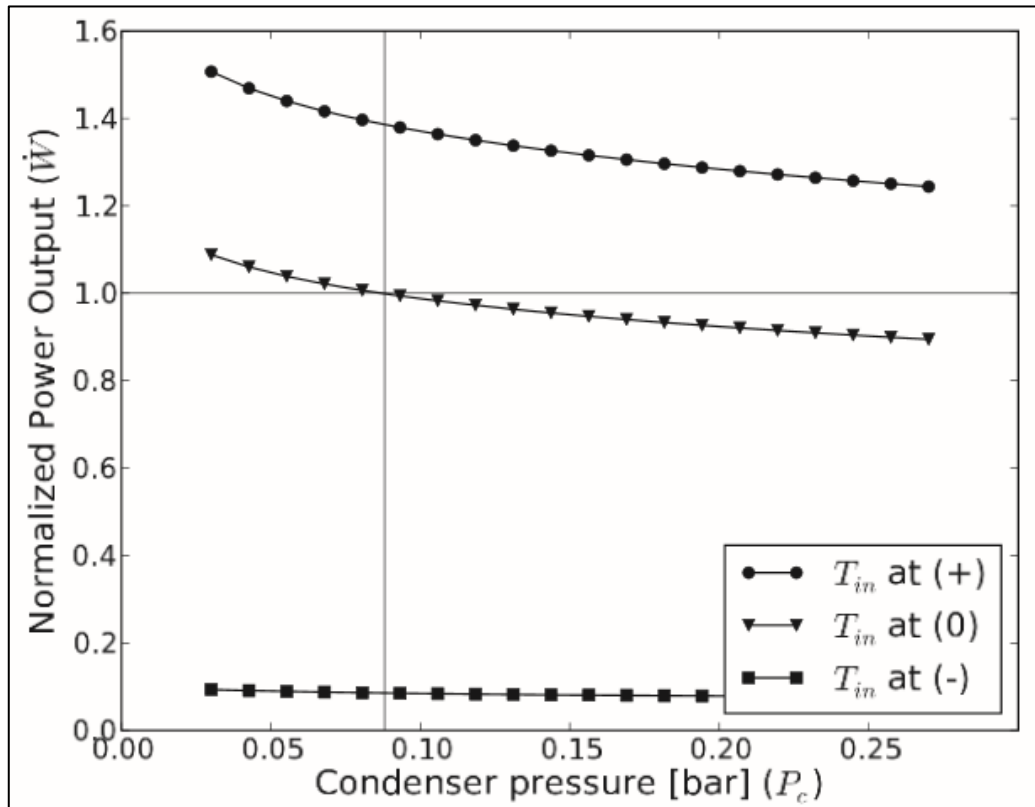


Figure 26: Wagner and Gilman (2011) SAM simulation's result with which this study's simulation is compared with.

Appendix C: Simulation flow diagrams

C.1 Brayton cycle simulation

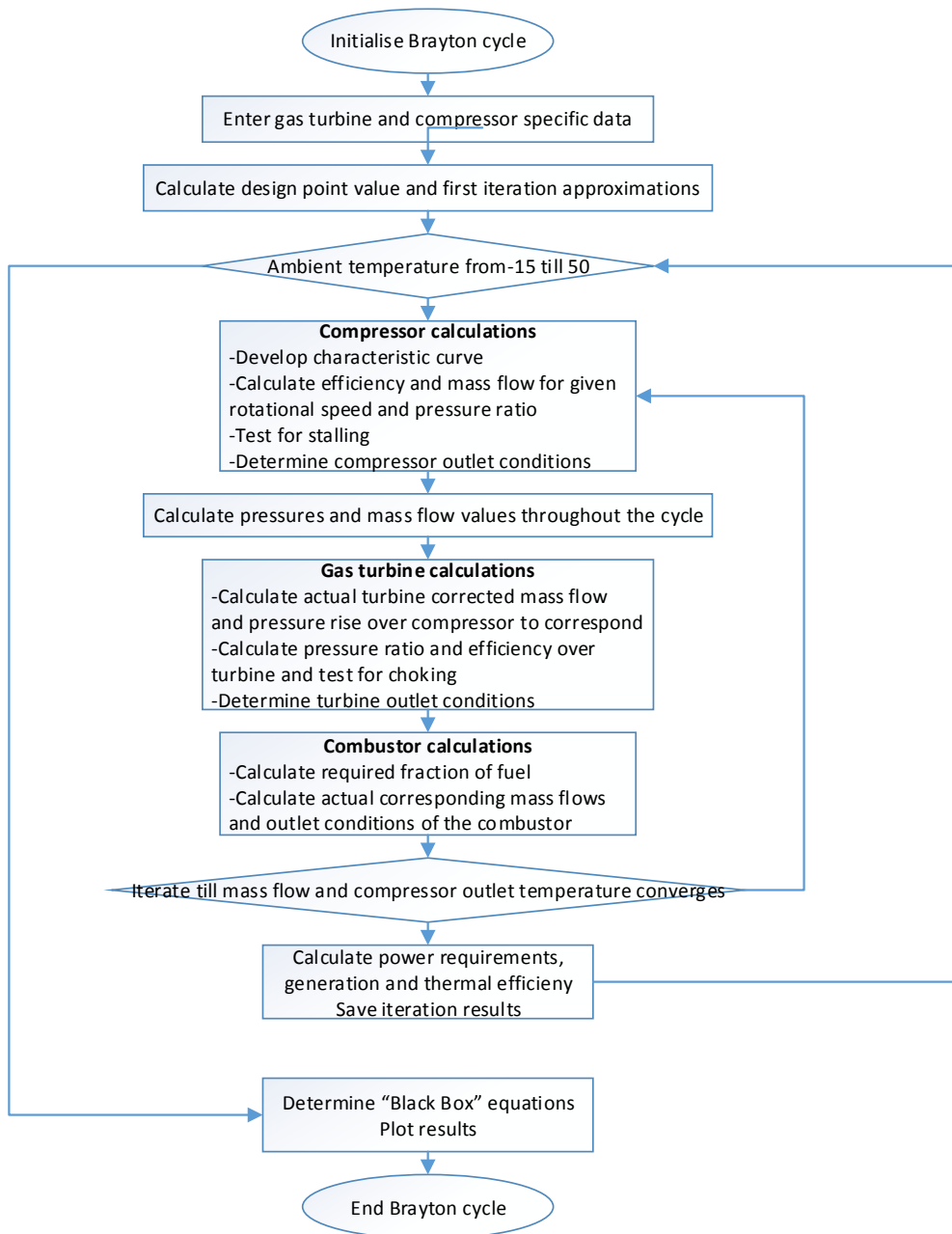


Figure 27: Flow chart of steady state Brayton cycle simulation

C.2 Rankine cycle simulation

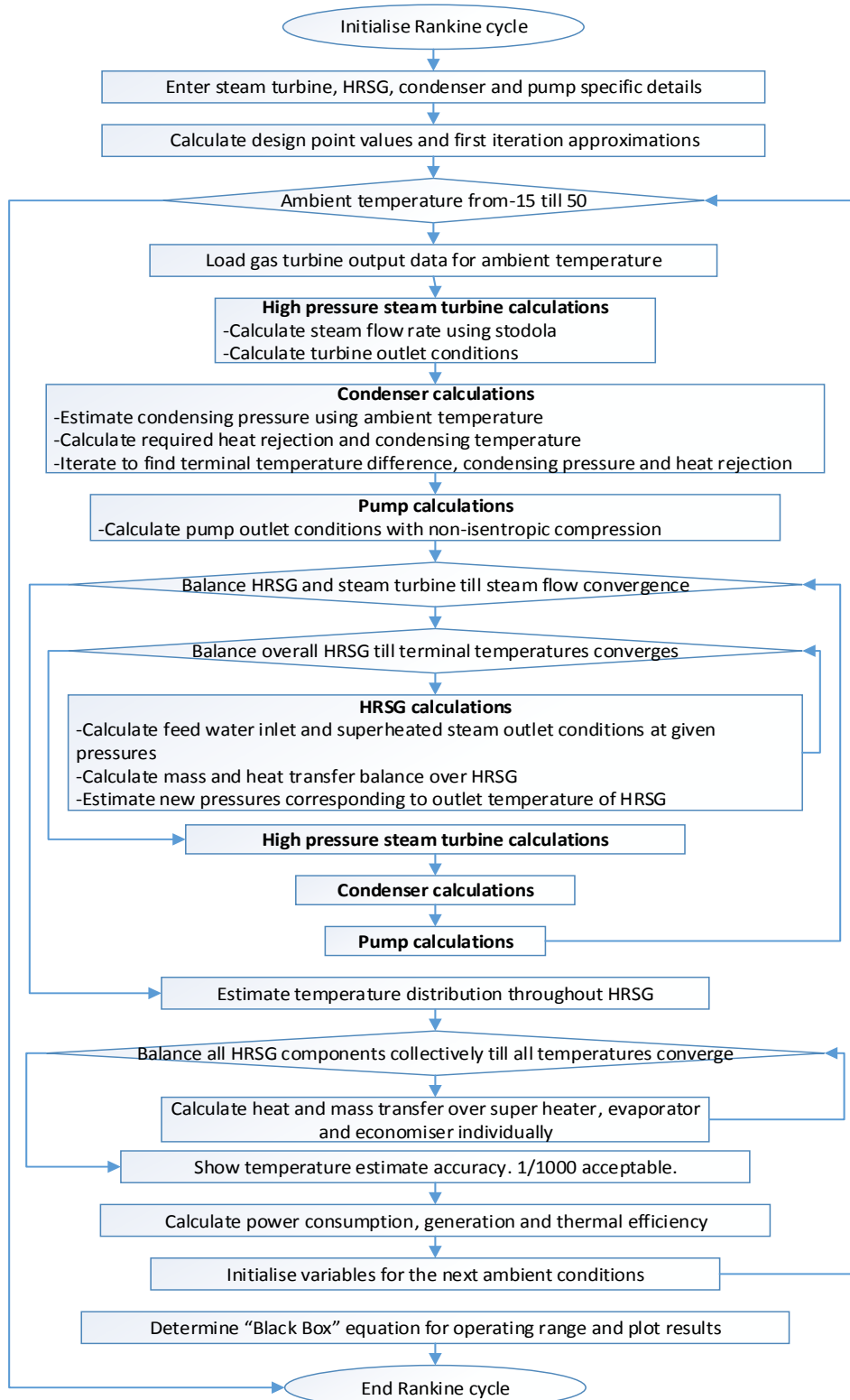


Figure 28: Flow chart of steady state Rankine cycle simulation

C.3 Annual simulation

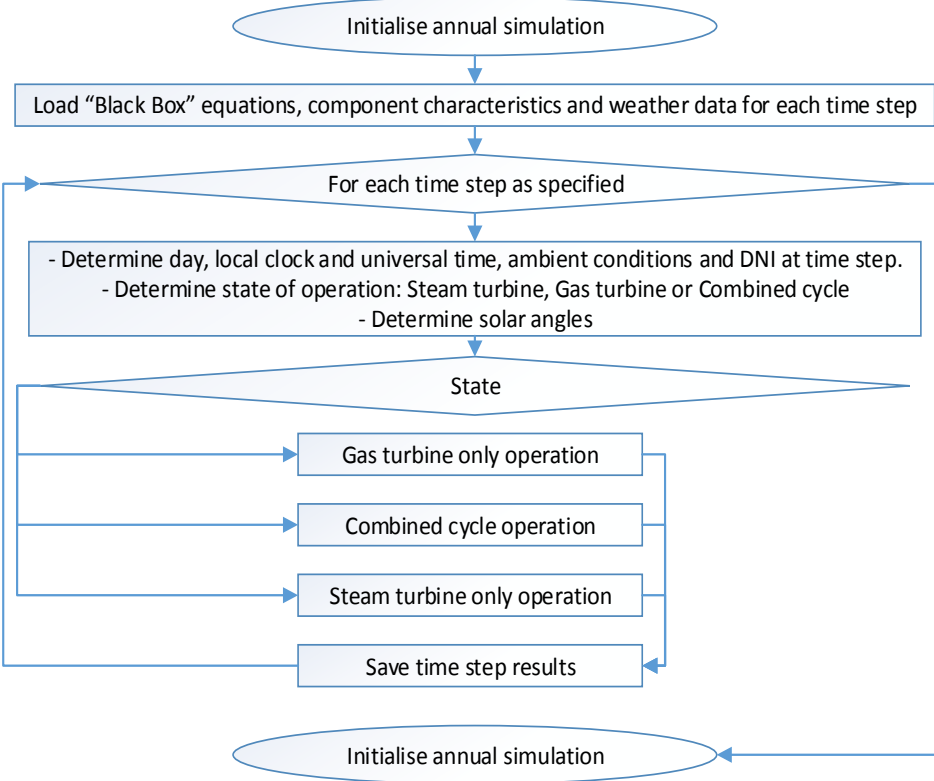


Figure 29: Flow chart of annual plant simulation

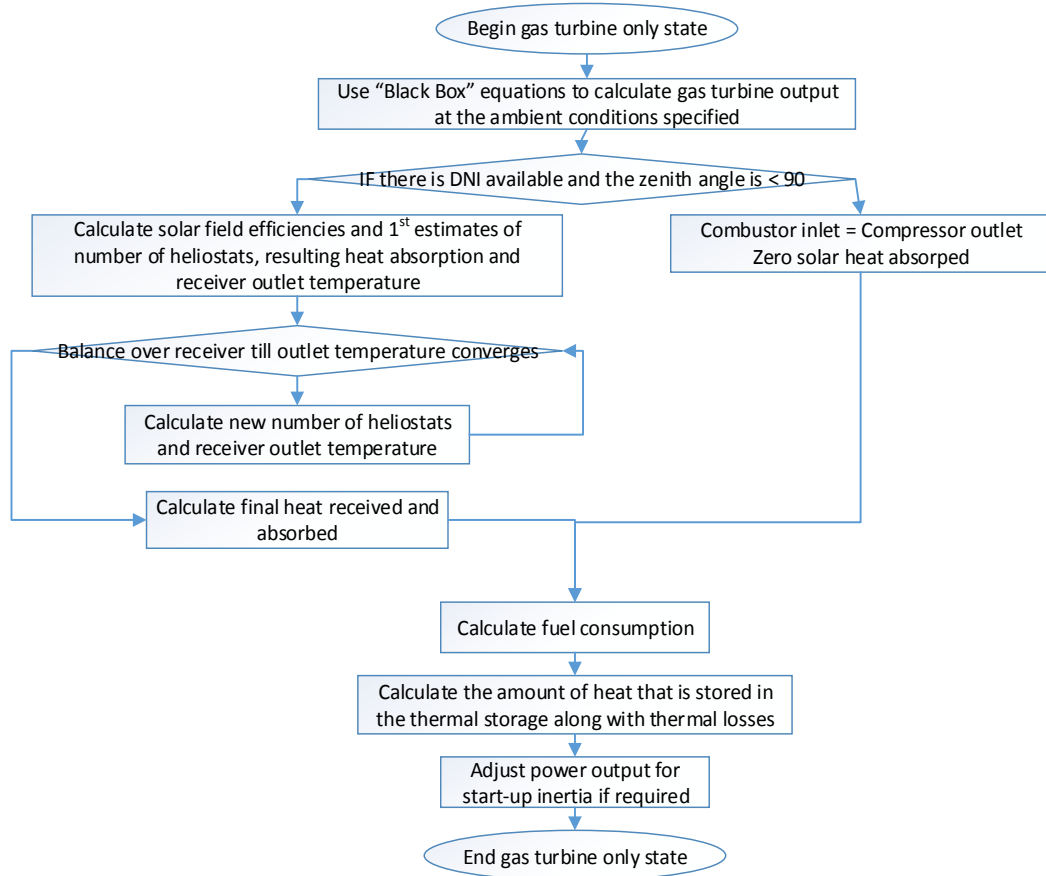


Figure 30: Flowchart representing the gas turbine only state of operation

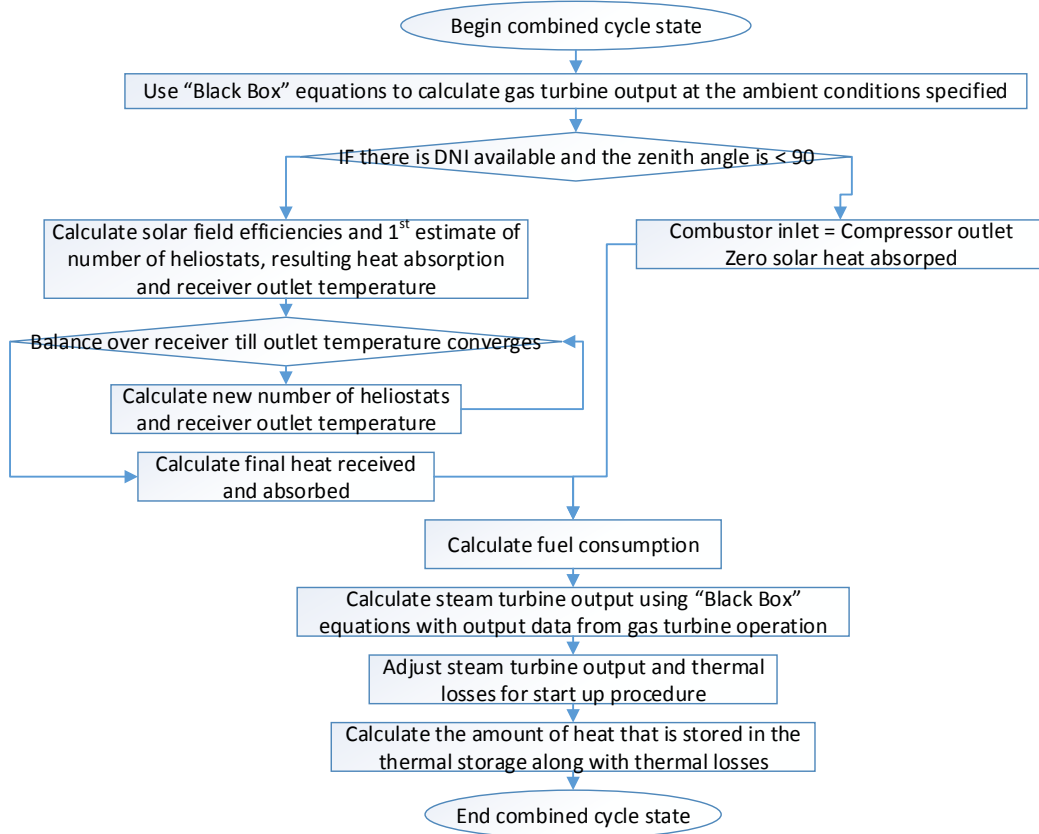


Figure 31: Flowchart representing the combined cycle state of operation

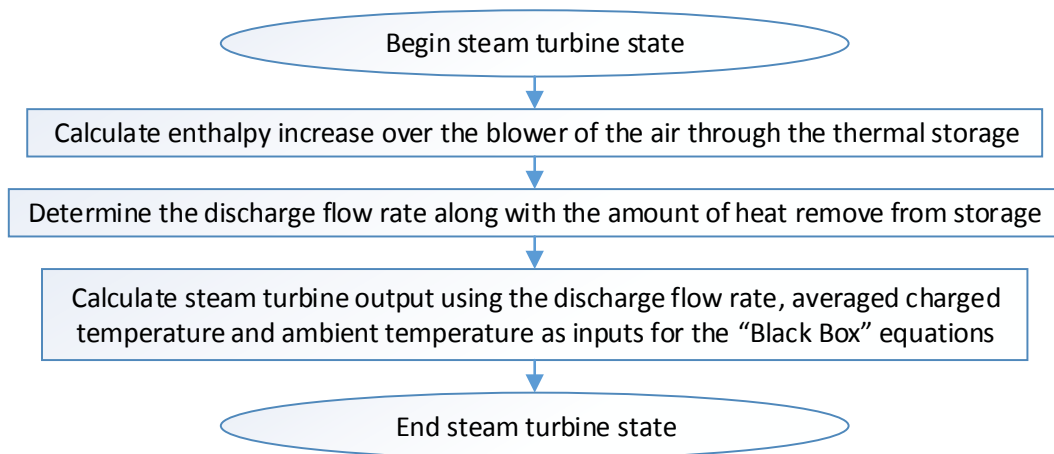


Figure 32: Flowchart representing the steam turbine only state of operation

Appendix D: Solar multiple selection

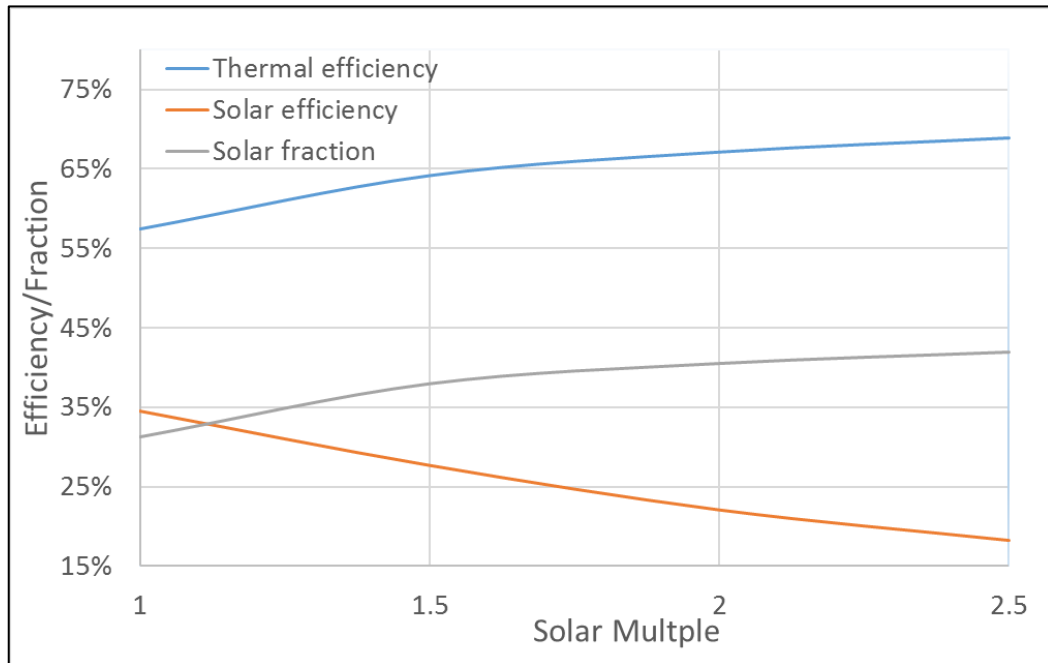


Figure 33: Solar multiple evaluation for SUNSPOT cycle

Appendix E: Operating strategy

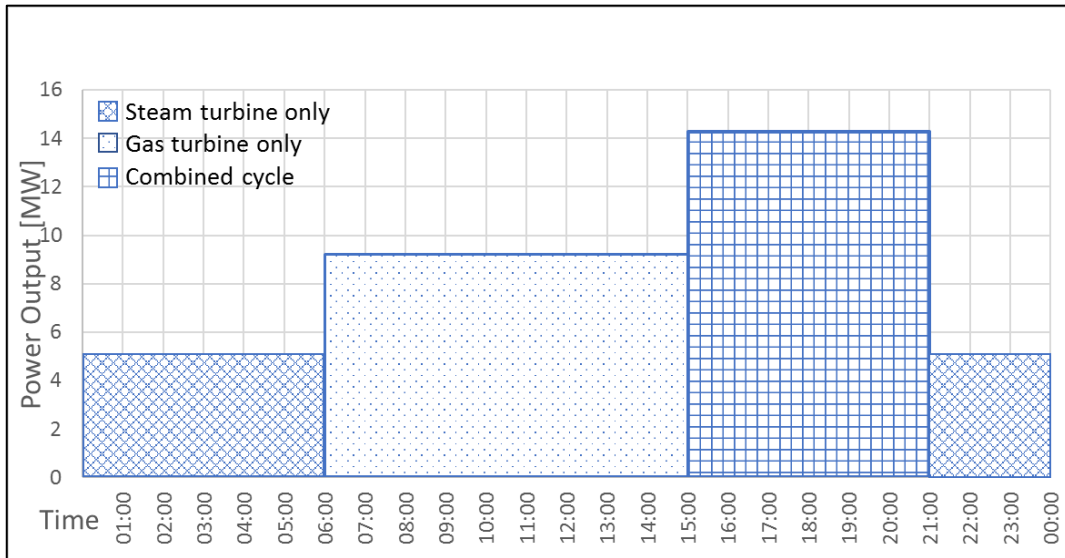


Figure 34: Operating strategy of the SUNSPOT cycle

Appendix F: Thermal efficiency of combined cycle

The following equations are deduced from simple thermal efficiency calculations and the results are used to validate the efficiency resulting from the transient simulations. The Equations correlate with the given schematic in Figure 35.

$$\eta_{cc} = \frac{Q_{in} - Q_1 + (Q_1 - Q_{exh} - Q_{out})}{Q_{in}}$$

$$\eta_{cc} = \frac{Q_{in} - Q_1}{Q_{in}} + \frac{Q_1 - Q_{out} - Q_{exh}}{Q_{in}}$$

$$\eta_{cc} = \frac{Q_{in} - Q_1}{Q_{in}} + \frac{Q_1}{Q_{in}} \left(1 - \frac{Q_{exh}}{Q_1} - \frac{Q_{out}}{Q_1} \right)$$

$$\eta_{BR} = 1 - \frac{Q_1}{Q_{in}}$$

$$\eta_{HRSG} = 1 - \frac{Q_{exh}}{Q_1}$$

$$\eta_{RC} = 1 - \frac{Q_{out}}{\eta_{HRSG} Q_1}$$

$$\eta_{cc} = \eta_{BC} + (1 - \eta_{BC}) \left(\eta_{HRSG} - \eta_{HRSG} \left(\frac{Q_{out}}{\eta_{HRSG} Q_1} \right) \right)$$

$$\eta_{cc} = \eta_{BC} + (1 - \eta_{BC}) \eta_{HRSG} (1 - (1 - \eta_{RC}))$$

$$\eta_{cc} = \eta_{BC} + (1 - \eta_{BC}) \eta_{HRSG} (\eta_{RC})$$

$$\eta_{cc} = 0.247 + (1 - 0.247)(0.8)(0.275) = 0.41266$$

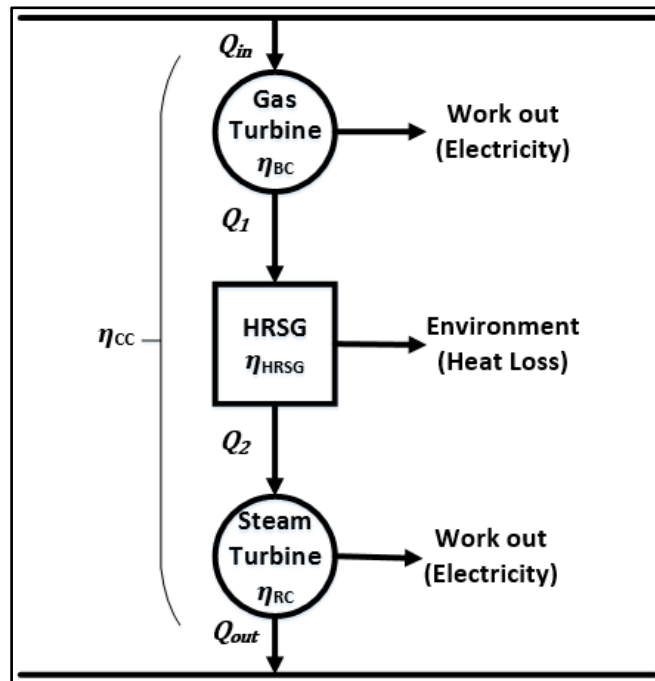


Figure 35: Thermal efficiency of combined cycle

Appendix G: Typical outputs

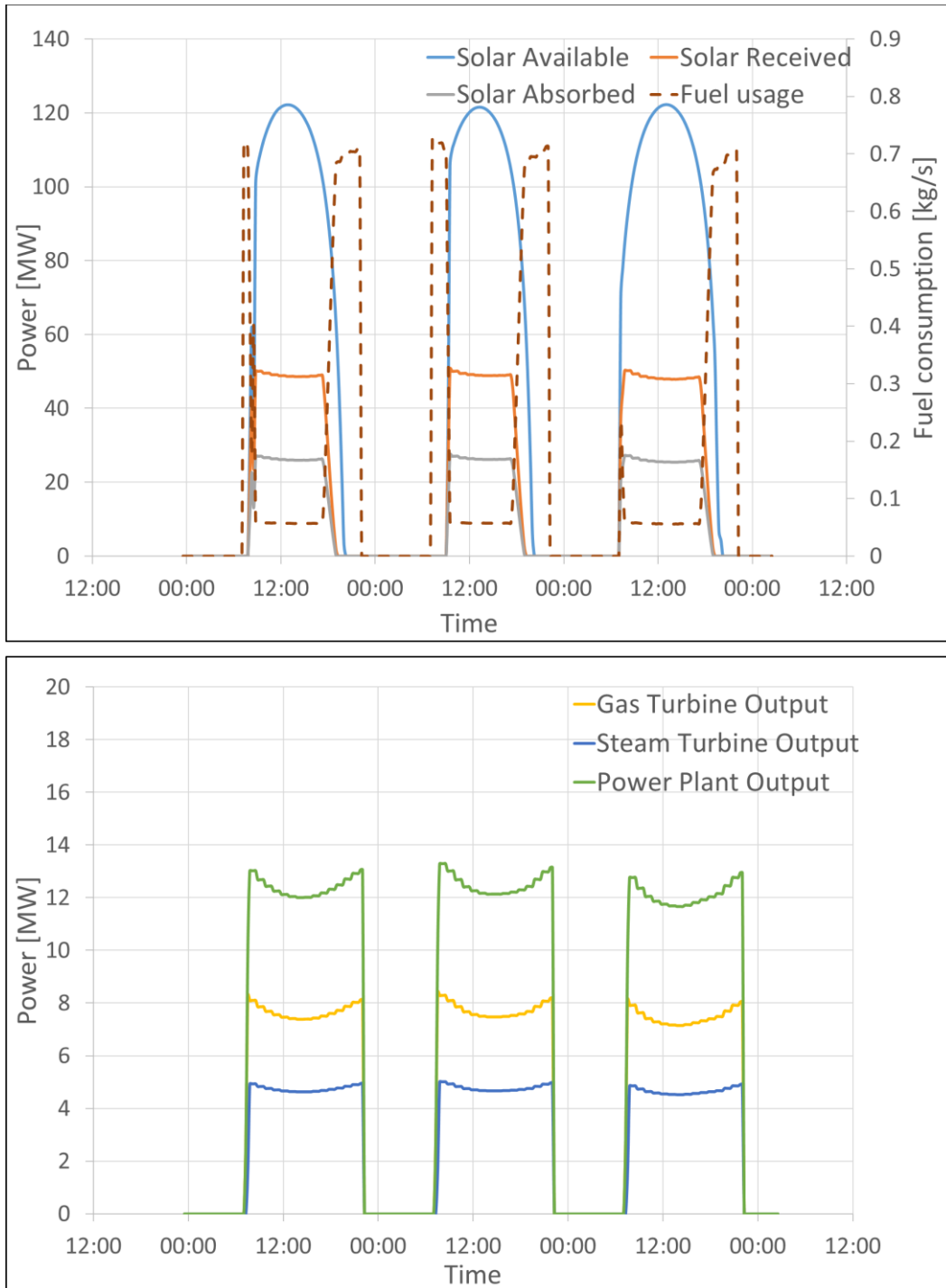


Figure 36: A typical three-day summer output for the solar hybrid combined cycle

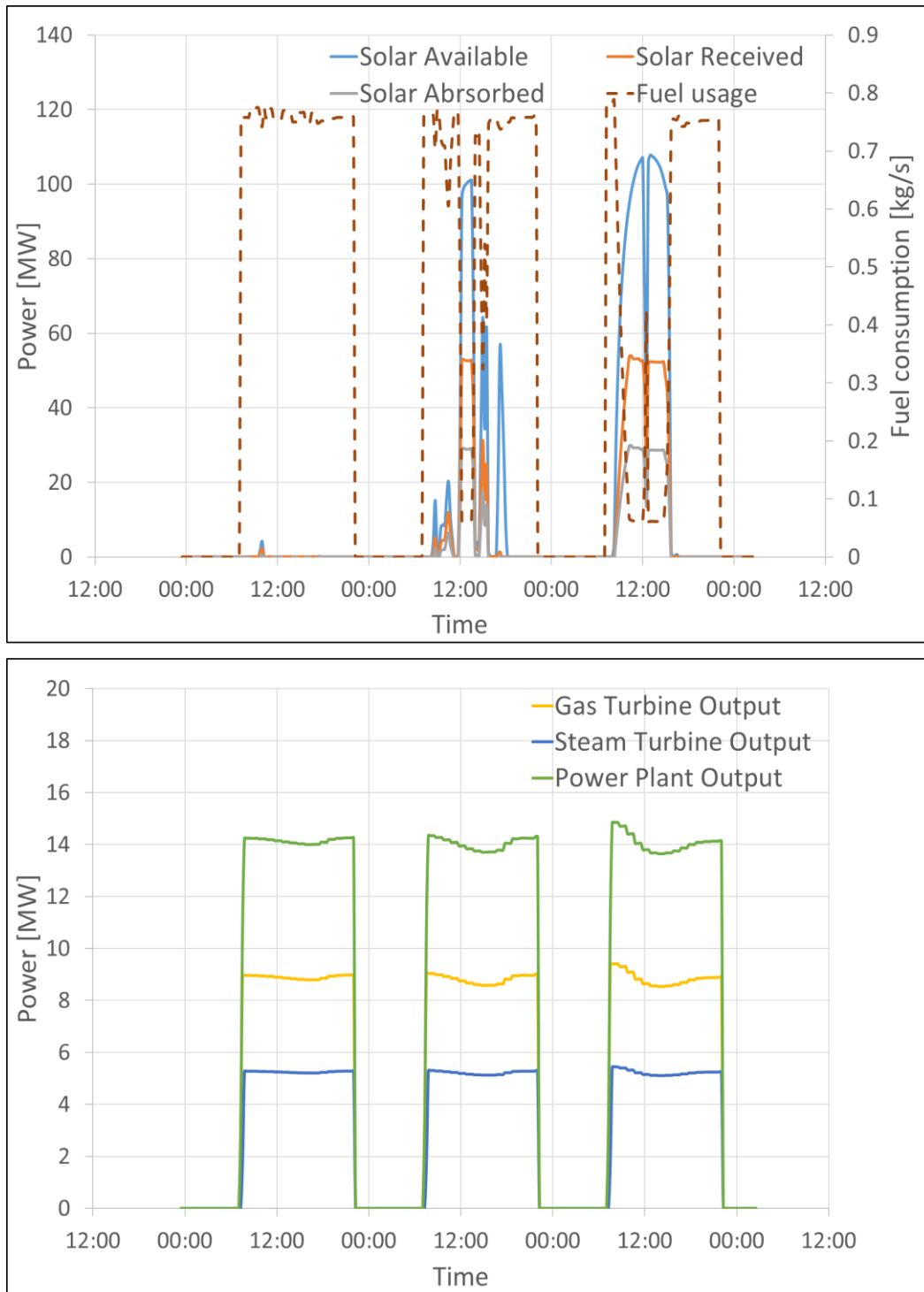


Figure 37: A typical three-day winter output for the solar hybrid combined cycle

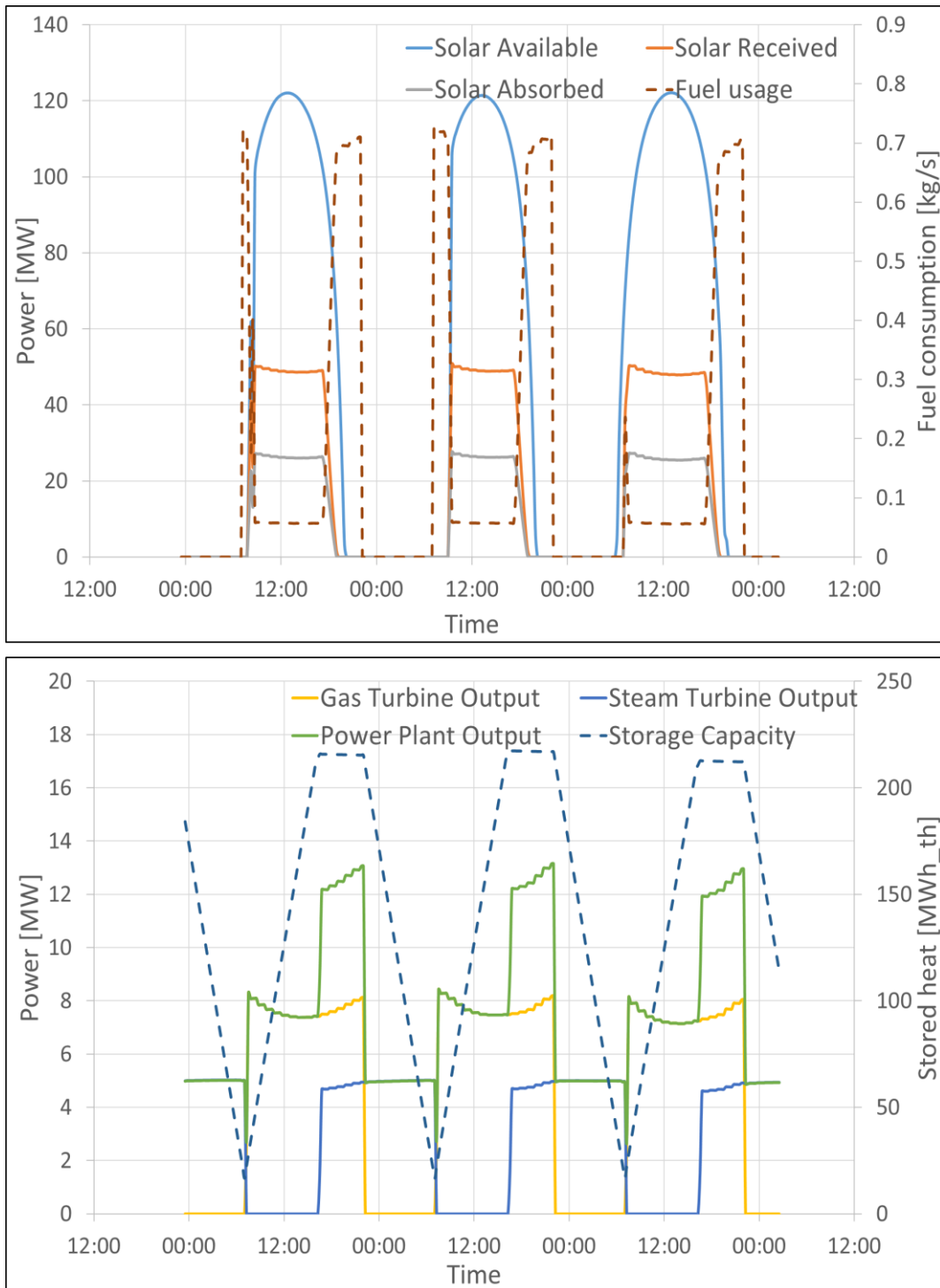


Figure 38: A typical three-day summer output for the SUNSPOT cycle

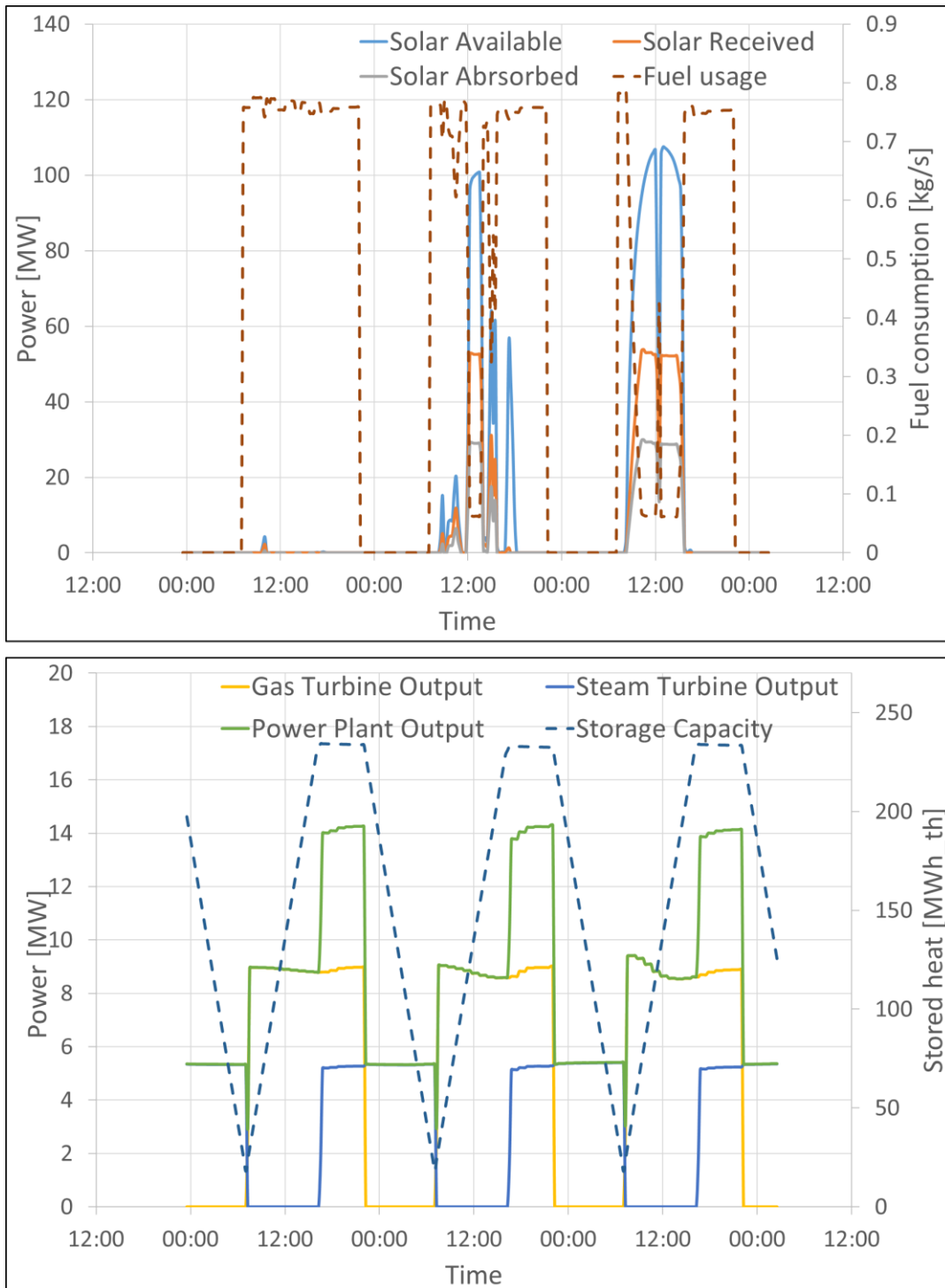


Figure 39: A typical three-day winter output for the SUNSPOT cycle

Appendix H: CAPEX composition of different configurations

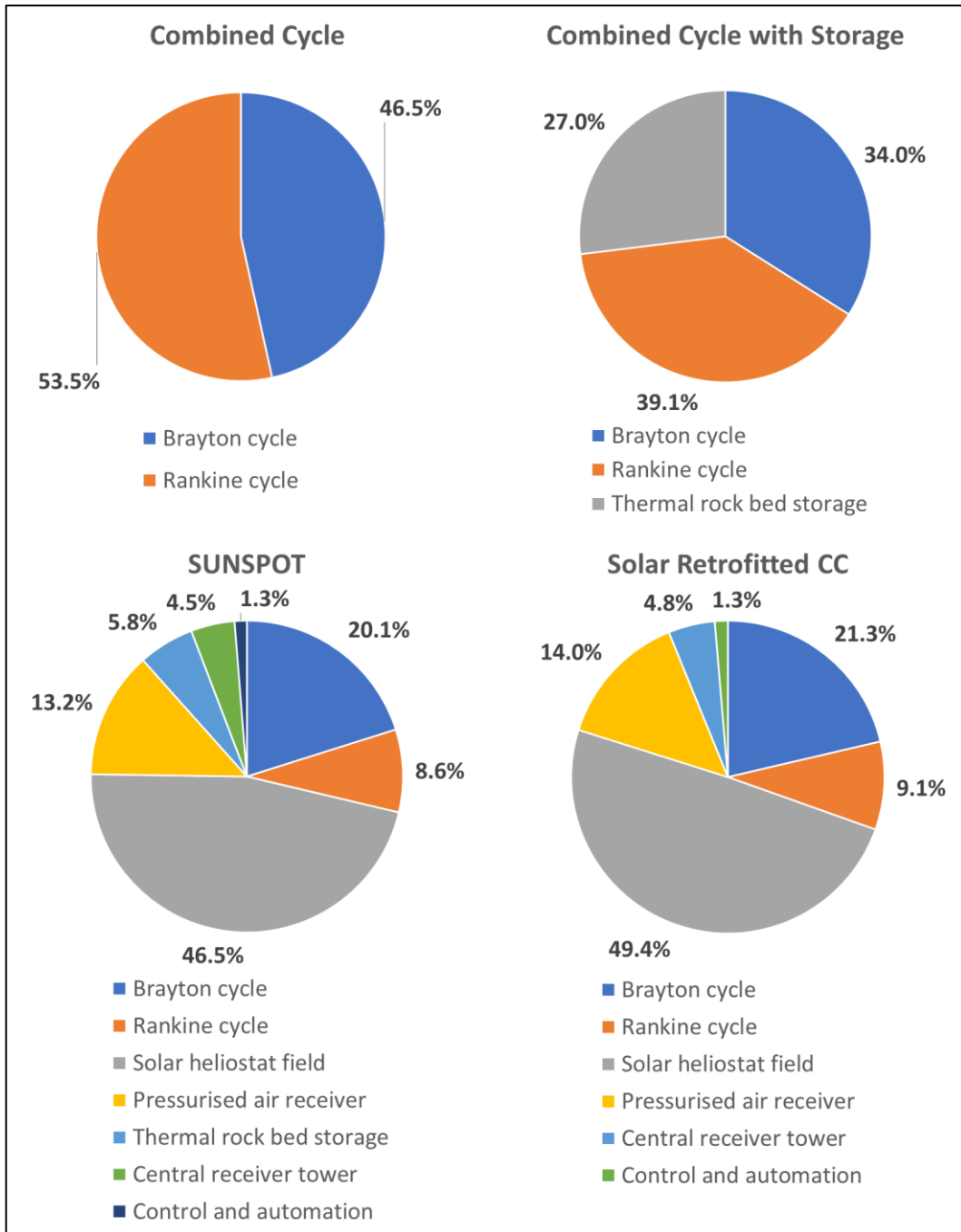


Figure 40: CAPEX breakdown of each plant